


**An Attitude Compensation Technique  
for a MEMS Motion Sensor Based  
Digital Writing Instrument**

LUO Yilun



A Thesis Submitted in Partial Fulfillment  
of the Requirements for the Degree of  
Master of Philosophy  
in  
Automation and Computer-Aided Engineering

©The Chinese University of Hong Kong

September 2006

The Chinese University of Hong Kong holds the copyright of this thesis. Any person(s) intending to use a part or the whole of the materials in this thesis in a proposed publication must seek copyright release from the Dean of the Graduate School.

An Article Comparison Tool  
for a Manuscript Review Phase  
Digital Writing Laboratory



Article submitted to the Journal of  
the Department for the Study of  
Literature and Linguistics

Authorship and Copyright Reserved

The Chinese University of Hong Kong

Library

The Chinese University of Hong Kong  
Library (any person) is hereby notified that  
in this there is a provision which states that  
the Chinese University of Hong Kong

## Thesis/Assessment Committee

Professor Yeung Yam (Chair)

Professor Wen Jung Li (Thesis Supervisor)

Professor Yun-hui Liu (Committee Member)

Professor Xiaoping Yun (External Examiner)



# **An Attitude Compensation Technique for a MEMS Motion Sensor Based Digital Writing Instrument**

submitted by

LUO Yilun

for the degree of Master of Philosophy  
at The Chinese University of Hong Kong

## **Abstract**

A MAG- $\mu$ IMU which is based on MEMS gyroscopes, accelerometers, and magnetometers is developed for real-time estimation of human hand motions. Appropriate filtering, transformation and sensor fusion techniques are combined in the Ubiquitous Digital Writing Instrument to record handwriting on any surface. In this thesis, we discuss the design of an extended Kalman filter (EKF) based on MAG- $\mu$ IMU (Micro Inertial Measurement Unit with Magnetometers) for real-time attitude tracking and the implement to record handwriting. In classical IMU applications, the Kalman filter utilizes the gyroscope propagation for transient updates and correction by reference field sensors, such as gravity sensors, magnetometers or star trackers. A process model is derived to separate sensor bias and to minimize wide-band noise. The attitude calculation is based on quaternion which, when compared to Euler angles, has no singularity problem. According to this filter framework, a Complementary Attitude EKF is designed by integrating the measurement updates from accelerometers and magnetometers alternatively, in order to compensate the attitude observation error due to sensor limitations, such as inertial accelerations, magnetic field distortion, and attitude ambiguity along each reference field. Testing with synthetic data and actual sensor data proved the filter will rapidly converge and accurately track the rigid-body attitude. The pen-tip trajectory in space can be calculated in real-time based on the real-time attitude estimation. Our goal is to implement this algorithm for motion recognition of a 3D ubiquitous digital pen.



# 基於MEMS慣性數碼筆的姿態補償技術

羅一倫

香港中文大學  
自動化與電腦輔助工程學課程  
哲學碩士論文

2006年9月

## 摘要

採用微米工藝的微機電系統(MEMS)技術,結合了機械感測結構與微電子技術,使得高精度感測器的成本降低,尺寸微型化。本文提出了集成磁力計以及MEMS加速度計、陀螺儀的捷連式微型慣性測量單元(MAG- $\mu$ IMU)的設計方案,應用於實時測量、記錄三維運動信息。通過多感測器融合技術,無源慣性制導技術,數字濾波算法,基於MAG- $\mu$ IMU的新型數碼書寫系統(Ubiquitous Digital Writing Instrument)能夠實時地跟蹤、記錄三維運動筆跡,而無需額外感測器的輔助。

本文研習了剛體的三維姿態測量方法,及其對於空間位置跟蹤的應用,並設計了用於實時姿態跟蹤的擴展卡爾曼濾波器(Extended Kalman filter)。擴展卡爾曼濾波器是一種針對隨機雜訊的高效自回歸非線性數字濾波器。通過預測過程(Time update)中對陀螺儀測得的角速度進行姿態積分;以及在更新過程(Measurement update)中,採用磁力計測得的地磁場為參考進行姿態修正,濾波器能夠即時地預測並分離出陀螺儀的輸出偏壓,濾除隨機雜訊,從而得出空間姿態的最優估計。濾波器的姿態運算全部採用四元數(Quaternion)進行,避免了採用歐拉角運算中的奇異問題。更新過程的數學模型亦適用於重力加速度計、星象跟蹤儀及其組合反饋,且無需四元數的歸一化運算。基於此濾波器的數學模型,本文提出了互補型姿態濾波器,即在更新過程中交替地採用加速度計和磁力計作為姿態測量反饋,用以相互補償各自沿重力場和磁場方向的姿態盲区;測得磁場中的電磁幹擾;以及慣性加速度對重力場姿態測量的誤差。仿真模擬及書寫實驗數據驗證本演算法能夠快速、穩定、實時地跟蹤數碼筆的空間姿態,完成對人手書寫動作的數碼記錄。

# Acknowledgments

This thesis would not be completed without the help of many people.

I would like to express my first and foremost gratitude to my Master Degree supervisor, Professor Li Wen Jung, for his tireless guidance in the past two years. He provides me creative ideas for my research work and led me working towards the ITF Digital Writing Instrument System (DWIS) project.

I would like to thank Professor Leong Heng Wai Philip who is the PI of the ITF Digital Writing Instrument System project. A number of discussions with him gave me valuable suggestions and comments for improving this work.

I also want to thank Dr Zhang Guang Lie, who has been the team manager of the DWIS project. I have learned so much from the expertise in hardware development and benefited from his selfless and inspiring advice. The years that we spent building the instrument from ground up, part by part, code by code, will always be remembered for many years to come.

I would like to give special thanks to my team members, Mr Shi Guang Yi for prototype development, Mr Tsang Chi Chiu for software design, Mr Dong Zhu Xin for testing and experiment, Miss Kwok Sze Yin for hardware packaging design, Miss Wong Yee Yan for marketing analysis, to our great teamwork and invaluable discussion.

I also be grateful to my colleagues, Mr Chung Chor Fung, Mr Chow Chun Tak, Miss Mandy Sin, Mr Chan Cheung Shing, Miss Chow Wing Yin, Mr Xiao Peng, Miss Amy Hiew, for their support to my research and bring me a comfortable working atmosphere.

Last but not least, I would like to thank my family, my relatives in Hong Kong, and especially my parents for all their trust, love, and care.



# Content

1.	Introduction.....	1
1.1.	Organization .....	3
2.	Architecture of MAG- $\mu$ IMU .....	5
2.1.	Hardware for Attitude Filter .....	5
2.2.	Handwriting Recording for a Digital Writing Instrument .....	7
3.	Inertial Tracking for Handwriting.....	9
3.1.	Spatial Descriptions and Transformations.....	9
3.1.1.	Vector Description and Position of a Frame .....	9
3.1.2.	Coordinate Transformation and Orientation of a Frame.....	10
3.1.3.	Kinematics for Digital Writing Instruments .....	12
3.1.4.	Vector Rotation .....	16
3.2.	Euler Angles for Rotation in Space .....	17
3.3.	Euler Angles Attitude Kinematics .....	19
3.4.	Singular Problem.....	19
4.	Attitude in Quaternion .....	22
4.1.	Quaternion Operations .....	22
4.1.1.	Quaternion Conjugate .....	23
4.1.2.	Quaternion Norm .....	24
4.1.3.	Quaternion Inverse.....	24
4.2.	Orientation Description in Quaternion .....	24
4.3.	Attitude Kinematics in Quaternion.....	25
5.	Kalman Filter .....	27
5.1.	Time Update .....	28
5.2.	Measurement Update.....	29
5.2.1.	Maximum a Posterior Probability .....	29
5.2.2.	Batch Least-Square Estimation.....	31
5.2.3.	Measurement Update in Kalman Filter.....	34
5.3.	Kalman Filter Summary .....	36
6.	Extended Kalman Filter .....	38
7.	Attitude Extended Kalman Filter .....	41
7.1.	Time Update Model.....	41
7.1.1.	Attitude Strapdown Theory for a Quaternion .....	41
7.1.2.	Error Model for Time Update .....	42
7.2.	Measurement Update Model .....	43
7.2.1.	Error Model for the Measurement Update.....	45
7.3.	Summary .....	46
8.	Experiment Results .....	47
8.1.	Experiment for Attitude EKF based on MAG- $\mu$ IMU .....	47
8.1.1.	Simulation Test .....	48
8.1.2.	Experiment Test .....	49
8.2.	Writing Application based on Attitude EKF Compensation .....	52



8.2.1.	Stroke Segment Kalman Filter .....	54
8.2.2.	Zero Velocity Compensation.....	58
8.2.3.	Complementary Attitude EKF for Writing Experiment.....	60
9.	Future Work .....	73
9.1.	Unscented Kalman Filter .....	73
9.1.1.	Least-square Estimator Structure .....	73
9.1.2.	Unscented Transform .....	74
9.1.3.	Unscented Kalman Filter .....	76
9.2.	Experiment Result .....	81
10.	Conclusion .....	85
10.1.	Attitude Extended Kalman Filter .....	85
10.2.	Complementary Attitude EKF .....	85
10.3.	Unscented Kalman Filter .....	86
10.4.	Future Work .....	86
	Bibliography .....	87
	Appendix A .....	92

# Lists of Figures

Figure 2.1:	Wireless MAG- $\mu$ IMU block diagram .....	5
Figure 2.2:	The Prototype of the MAG- $\mu$ IMU with Bluetooth Module .....	6
Figure 2.3:	MAG- $\mu$ IMU version 1.2 for Digital Writing Instrument application.....	6
Figure 2.4:	The MAG- $\mu$ IMU System Structure for a wireless digital writing instrument.....	7
Figure 3.1:	Position vector representation in Cascadian coordinate system .....	9
Figure 3.2:	Vector representations W.R.T different reference frames by coordinate transform, which can be considered as the reverse process for vector rotation. ....	11
Figure 3.3:	Position description for a rigid-body object in space using body-attached coordinate system. ....	13
Figure 3.4:	Rotational accelerations of rigid body in space .....	16
Figure 3.5:	Single axis rotation: the vector $OP$ is rotated about the $X$ axis for angle $\Phi$ .....	17
Figure 3.6:	The rigid body rotation in Euler angles by Roll, Pitch and Yaw rotation sequences. ....	18
Figure 3.7:	Angular velocity measured by gyroscopes in the $\mu$ IMU .....	20
Figure 3.8:	Singular problem in attitude propagation using Euler method .....	20
Figure 3.9:	Attitude propagation using quaternion method compared to Euler angles.....	21
Figure 5.1:	The real-time cycle of the discrete Kalman Filter [34].....	27
Figure 5.2:	Linear approximation for the expected posterior loss.....	30
Figure 5.3:	Block Diagram of Kalman Filter in Real Time Application [1] .....	36
Figure 7.1:	Block Diagram of Extended Kalman Filter Algorithm.....	41
Figure 8.1:	Accelerometers EKF: Attitude by Gyroscope Propagation .....	47
Figure 8.2:	Accelerometers EKF: Filter Result & Accelerometer Attitude.....	48
Figure 8.3:	Synthetic Sensor Measurement.....	49
Figure 8.4:	Simulation Attitude Comparison: Filter Result & Gyroscope Propagation .....	50
Figure 8.5:	Real Sensor Data from MAG- $\mu$ IMU .....	51
Figure 8.6:	Experiment Attitude Comparison: Filter Result & Gyroscope Propagation .....	51
Figure 8.7:	Complementary Attitude EKF Diagram .....	54
Figure 8.8:	Acceleration variance underestimates motion intensity (velocity) due to sampling error .....	56



Figure 8.9:	Kalman smoother based stroke segment for motion status detection (1) .....	57
Figure 8.10:	Kalman smoother based stroke segment for motion status detection (2) .....	58
Figure 8.11:	Zero velocity compensation diagram [51] .....	59
Figure 8.12:	Experiment setup for Digital Writing Instrument with MAG- $\mu$ IMU .....	60
Figure 8.13:	Digital Writing Instrument sensor outputs .....	61
Figure 8.14:	Nine-channel motion information W.R.T. the sensor frame .....	61
Figure 8.15:	Stroke Segment Kalman Filter as sync switch for measurement update .....	62
Figure 8.16:	Tracking result of Complementary Attitude EKF .....	62
Figure 8.17:	Accelerations W.R.T. Earth frame by Complementary Attitude EKF .....	63
Figure 8.18:	Performance comparison for the acceleration coordinate transform in X-Axis .....	63
Figure 8.19:	Performance comparison for the acceleration coordinate transform in Y-Axis .....	64
Figure 8.20:	Performance comparison for the acceleration coordinate transform in Z-Axis .....	64
Figure 8.21:	Capital letter 'A' written by Complementary Attitude EKF .....	65
Figure 8.22:	Stroke segment according to the Earth frame acceleration .....	65
Figure 8.23:	X-axis acceleration updated by Zero Velocity Compensation .....	66
Figure 8.24:	Y-axis acceleration updated by Zero Velocity Compensation .....	66
Figure 8.25:	Z-axis acceleration updated by Zero Velocity Compensation .....	67
Figure 8.26:	Velocity updated by Zero Velocity Compensation .....	67
Figure 8.27:	Writing result for 'A' by Complementary Attitude EKF and ZVC .....	68
Figure 8.28:	Handwriting result for 'A' using DWI system during the position tracking experiment .....	68
Figure 8.29:	Writing result for 'A' by gyro attitude propagation and ZVC .....	69
Figure 8.30:	Writing result for 'B' by Complementary Attitude EKF and ZVC .....	69
Figure 8.31:	Writing result for 'B' by gyro attitude propagation and ZVC .....	70
Figure 8.32:	Handwriting result for 'B' using DWI system during the position tracking experiment .....	70
Figure 8.33:	Handwriting result for 'CMNS' using DWI system during the position tracking experiment .....	71



Figure 8.34:	Writing result for 'CMNS' by Complementary Attitude EKF and ZVC.....	71
Figure 8.35:	Writing result for 'CMNS' by gyro attitude propagation and ZVC.....	72
Figure 9.1:	Approximation of a one-dimensional Gaussian distribution by three feature points.....	74
Figure 9.2:	Approximation of a two-dimensional Gaussian distribution by five feature points .....	75
Figure 9.3:	Unscented transform for mean and covariance undergo nonlinear process [46].....	76
Figure 9.4:	The real-time recursive structure of the unscented Kalman filter.....	81
Figure 9.5:	Sensor measurements for the unscented Kalman filter.....	82
Figure 9.6:	Tracking output of the unscented Kalman filter .....	82
Figure 9.7:	Tracking speed of unscented Kalman filter versus extended Kalman filter .....	83
Figure 9.8:	Tracking accuracy of unscented Kalman filter versus extended Kalman filter .....	84

# Lists of Tables

Table 5.1:	KF time update equations .....	37
Table 5.2:	KF measurement update equations .....	37
Table 6.1:	EKF time update equations .....	39
Table 6.2:	EKF measurement update equations .....	40
Table 9.1:	Unscented transform equations .....	75
Table 9.2:	UKF weighting parameters .....	77
Table 9.3:	UKF initialization equations .....	78
Table 9.4:	Unscented transform for sigma points .....	78
Table 9.5:	UKF time update equations .....	78
Table 9.6:	UKF measurement update equations .....	79



# 1. Introduction

Three-dimensional position tracking can be directly obtained successfully by some existing technologies. For instance, the Global Positioning System (GPS) is widely used in land surveying, navigation and unmanned vehicle control [2]. Supported by the timing signals broadcasted from the networked GPS satellites, the GPS receiver can accurately determine its position in longitude, latitude and altitude in any weather and anywhere on earth. In Wide-Area Augmentation System (WAAS) since August 2000, the accuracy of GPS position tracking is improved within 2 meters [3]. The precision can be further enhanced to about 1 cm by Differential GPS (DGPS) [4]. However, precise GPS receivers are bulky in size and not mobile. For example, one could not hold such receiver to track hand positions for handwriting recording. Moreover, indoor tracking applications may be very difficult to realize due to weakness of GPS signals.

On the other hand, ultrasonic and infrared positioning systems with high accuracy have been developed for tracking handwriting motions, such as the Mimio [5] and e-Beam systems [6]. The basic operating principle of these systems is that, when two transceivers are fixed on white board as the position reference and broadcast ultrasonic or infrared timing signals, the two transceivers can measure the two distances to the reflector respectively by detecting the phase difference after receiving the echo wave from the reflector on the pen-tip,. This source positioning technology is high in accuracy and quick in response. However, the system can not track multiple objects simultaneously and it requires a set of receivers and a transceiver to operate which is not convenient for users.

In this project, our overall goal is to develop a system to track handwriting motions without the need of wave sources such as ultrasonic or infrared signals. In sourceless navigation technology, such as inertial kinematics theory, accurate attitude is fundamental to determine and to keep track of the rigid-body position in space. Due to nonlinearity in the system dynamic equations, bias error and random walk noise from attitude sensors will be accumulated and magnified leading to nonlinear distortions in position tracking.



Attitude tracking is widely used in navigation, robotics, and virtual reality. Classically, the problem of distortions in position tracking is addressed by the Attitude Heading Reference System (AHRS) [7], [8]. The AHRS utilizes gyroscope propagation for transient updates and correction by reference field sensors. However, classically, the performance is ensured by extremely accurate sensors and hardware filters. Due to its expensive cost and large system size, the AHRS has been limited in applications, especially for mobile human position tracking applications.

With MEMS sensing technology, the inertial sensors could be built with low cost and small sizes. However, they suffer in accuracy when compared with bulkier sensors. Nevertheless, new reliable attitude tracking systems have been developed based on low cost gyroscope sensors and the Global Positioning System (GPS). For feedback correction, Euler angles are derived from GPS to represent spatial rotation and a Kalman filter is implemented to fuse with the attitude propagation. But GPS signals are not available for indoor applications and the GPS attitude has resolution limit for handwriting application [9].

For static applications such as the Unmanned Ground Vehicles (UGV) control [10], the MEMS accelerometers work reliable as gravity sensors. Euler angles can be derived directly [11]. However, during a dynamical situation, the accelerometer measurements for the gravitational accelerations will be interfered with the inertial accelerations, which then cannot be trusted for attitude. Further, the pitch attitude along the gravity axis cannot be determined.

Magnetometers experience no such crosstalk disturbance in both situations. However, following the same approach, attitude ambiguity occurs along the magnetic field direction and Euler angles cannot be derived directly. Furthermore, the Earth magnetic field is overlapped by random noise from electromagnetic interference (EMI).

A Ubiquitous Digital Writing Instrument has been developed by our group to capture and record human handwriting or drawing motions in real-time based on a MEMS Micro Inertial Measurement Unit ( $\mu$ IMU) [1]. However, position tracking using this  $\mu$ IMU is not accurate due to sensor measurement noise and drifts.

Thus, an extended Kalman filter is designed to improve system measurement



accuracy of an integrated gyroscopes and magnetometers device (MAG- $\mu$ IMU) [12]. For the digital writing instrument application, the MAG- $\mu$ IMU is affixed on a commercially available marker. During input hand motions, the filter tracks the real-time attitude of the pen with sensor bias separation and sensor random noise minimization. The attitude calculation is totally based on quaternion which computes faster and has no singularity problem compared to Euler angles. This filter also applies to other reference field sensors for feedback, such as accelerometers or star trackers.

Based on this filter structure, a complementary extended Kalman filter for attitude is proposed to combine the accelerometers and magnetometers in the measurement update process. During the pause phase in handwriting, the complementary filter utilizes the accelerometers as gravity tilter for attitude reference feedback. During the writing phase, the measurement model switches to the magnetometers to avoid attitude error due to the inertial accelerations in gravity sensor, by assuming the magnetic field distortion is tolerable within one stroke. This measurement mixture can compensate attitude ambiguity along the reference field direction for each other and rectify electromagnetic inference in Earth magnetic field.

## **1.1. Organization**

The remaining chapters of the dissertation are organized as follow. In Chapter 2, the design of the MAG- $\mu$ IMU system is introduced, including the hardware structure and software architecture. Chapter 3 and Chapter 4 describe the kinematics models of attitude determination and inertial position tracking. Chapter 5 reviews the details of the Kalman filter algorithm in optimization model and recursion framework. Chapter 6 introduces the extended Kalman filter as its extension in nonlinear problem. We will describe the design of the quaternion-based attitude extended Kalman filter utilizing magnetometers feedback in Chapter 7. Based on the error model for state bias, the system plant can be improved to estimate and separate the bias drift. Simulation examples and experiment results will be discussed in Chapter 8. The Complementary Attitude EKF in measurement update process is proposed to improve handwriting capture performance by precise attitude. Chapter 9 presents the design of an unscented Kalman filter for attitude tracking in quaternion, which is the future work for research.

Simulation results demonstrate the superiority of unscented Kalman filter in accuracy and response time compared to the extended Kalman filter in nonlinear estimation. Finally, we present conclusions and proposed future improvements in Chapter 10.



## 2. Architecture of MAG- $\mu$ IMU

### 2.1. Hardware for Attitude Filter

Figure 2.1 illustrates the block diagram of a wireless MAG- $\mu$ IMU with the real-time attitude filter system. The system can be divided into two parts. The first part is the hardware for the wireless sensing unit. The other part is the software for data access and 3D rotation sensing algorithms.

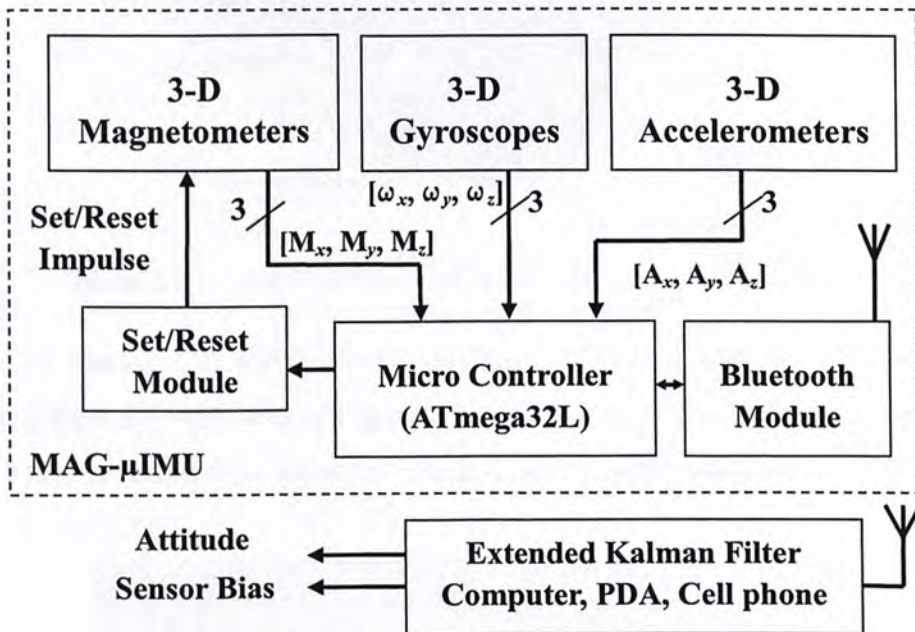


Figure 2.1: Wireless MAG- $\mu$ IMU block diagram

The MAG- $\mu$ IMU is developed for a wireless digital writing instrument and used to record human handwriting. The MAG- $\mu$ IMU is a hybrid sensing system with inertial sensors and magnetometers. The ' $\mu$ IMU' integrates the 3D accelerometers [13] and 3D gyroscopes [14] with strapdown installation [1]. The 3D magnetometers, 'MAG' sensors, are added to measure the Earth magnetic field [15], [16], [17]. The sensor unit is affixed on a commercially available marker to measure the inertial and magnetic information in the pen's body frame.

The output signals of the accelerometers  $[A_x, A_y, A_z]$  and the gyroscopes  $[\omega_x, \omega_y, \omega_z]$ , which are the body frame accelerations and the roll, pitch, yaw angular rates, respectively, are measured directly with an Atmega32L A/D converter microcontroller

[18], [19]. The serial Bluetooth transceiver is implemented via a USART connection with the MCU for wireless communications [20], [21]. The serial USB transceiver is integrated for transfer backup and hardware development [22]. The digital sample rate of the sensor unit is 200 Hz and the transmit baud rate is 57.6 Kbps via Bluetooth wireless connection, which ensures rapid response to human handwriting.

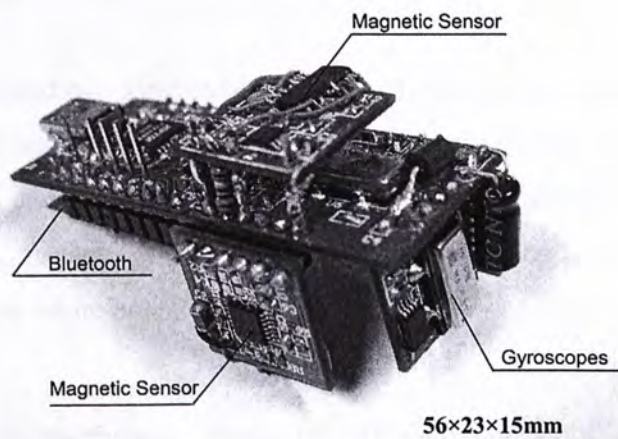


Figure 2.2: The Prototype of the MAG- $\mu$ IMU with Bluetooth Module

Figure 2.2 shows the MAG- $\mu$ IMU version 1.1 with strapdown gyroscopes and magnetometers for attitude tracking test. The sensor system utilizes four-layer printed circuit board techniques for noise reduction. The dimensions are within  $56\times 23\times 15\text{mm}$ .

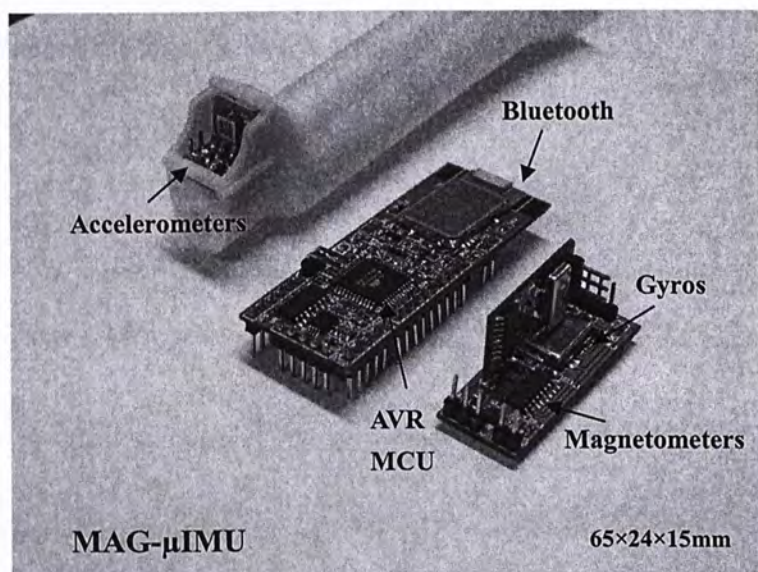


Figure 2.3: MAG- $\mu$ IMU version 1.2 for Digital Writing Instrument application

Figure 2.3 demonstrates the MAG- $\mu$ IMU version 1.2 combining accelerometers for



handwriting experiment. The sampling rate for nine-channel inertial and attitude sensors is 200 Hz. The dimensions of sensor unit are within  $65 \times 24 \times 15 \text{ mm}$ .

## 2.2. Handwriting Recording for a Digital Writing Instrument

Figure 2.4 illustrates the MAG- $\mu$ IMU sensor structure of the digital writing system for position tracking.

According to the strapdown kinematics theory [23], the body frame accelerations are transformed to the Earth frame by a Direct Cosine Matrix (DCM). After compensating for the gravitational and rotational accelerations, the translation accelerations integrate into 3D trajectories in space. Thus any 2D human handwriting is recorded in real time if the pen touches the white board plane.

$$\vec{A}_b = \vec{A}_{IMU} - \vec{A}_{Rotation}(\omega_{roll}, \omega_{pitch}, \omega_{pitch}, L) \quad (2.2.1)$$

$$\dot{\vec{V}}_e = DCM(q)_b^e \vec{A}_b - \vec{G} \quad (2.2.2)$$

$$\vec{P}_e = \iint \dot{\vec{V}}_e \quad (2.2.3)$$

Where  $\vec{A}_{IMU}$  are the body frame accelerations:  $[A_x, A_y, A_z]$ .  $q$  is the quaternion representing the pen attitude.  $\vec{G}$  is the gravity vector:  $[0, 0, -g]$ .

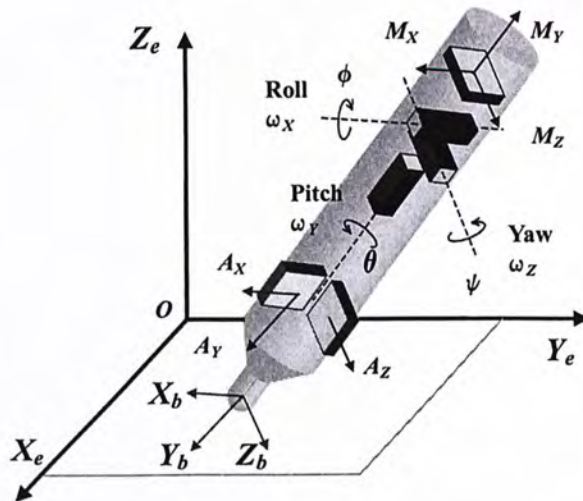


Figure 2.4: The MAG- $\mu$ IMU System Structure for a wireless digital writing instrument



According to the kinematics equations, the accelerometers are design to mount as close to the pen-tip for more sensitivity for handwriting motion and depression for the rotational accelerations. The magnetometers are fixed on the pen bottom to reduce magnetic field distortion effect by the metal white board.

# 3. Inertial Tracking for Handwriting

## 3.1. Spatial Descriptions and Transformations

In order to record the human handwriting trajectory in real time, the position representation for the pen-tip and eraser center has the requirement for precision and consistency. We establish the writing surface as the universe coordinate system to which everything we infer and deduct can be referenced. According to the handwriting conventions, the Earth coordinate system, or the Earth frame is the preferred universe coordinate system for our research. We will describe all the position and orientations with respect to the Earth coordinate system or with respect to other Cartesian coordinate systems which are defined relative to the universe system.

Consider the pen and the eraser as rigid body in space, either part of the digital writing system will move relative to the other. Assume there exists a Cartesian coordinate system or frame  $\{B\}$ ,  $\sum O-UVW$ , rigidly attached to the tracking target., the basic problem is to describe the position and orientation of the  $\vec{u}, \vec{v}, \vec{w}$  triad with respect to the reference coordinate system, the Earth frame.

### 3.1.1. Vector Description and Position of a Frame

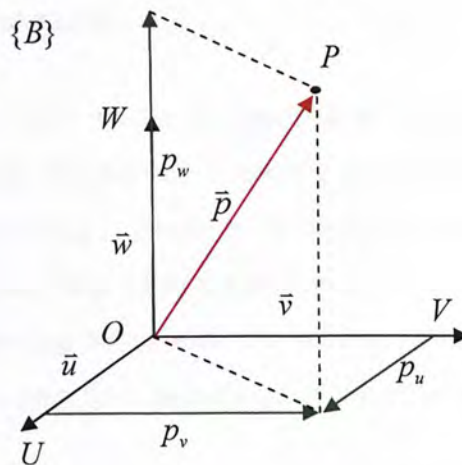


Figure 3.1: Position vector representation in Cascadian coordinate system

The body-attached coordinate system, or the body frame consists of the right handed



triad  $\vec{u}, \vec{v}, \vec{w}$  of unit vectors orthogonal to each other, such that,

$$\vec{u} \times \vec{v} = \vec{w} \quad (3.1.1)$$

A vector in a three-dimensional space,  $\vec{p} \in \mathfrak{R}^3$  is described by projecting the vector onto the corresponding unit axis of the reference coordinate system.

$$\vec{p}_B = p_u \vec{u} + p_v \vec{v} + p_w \vec{w} = [p_u, p_v, p_w] \cdot [\vec{u}, \vec{v}, \vec{w}]^T = \begin{bmatrix} \vec{p} \cdot \vec{u} \\ \vec{p} \cdot \vec{v} \\ \vec{p} \cdot \vec{w} \end{bmatrix} \quad (3.1.2)$$

In digital pen application, the vector  $\vec{p}$  could be acceleration, velocity, angular rate, and position in the three-dimensional space.

Thus the position vector of the body frame  $\vec{u}, \vec{v}, \vec{w}$  can be derived by representing the coordinate origin in respect of the Earth frame.

### 3.1.2. Coordinate Transformation and Orientation of a Frame

Because the target for observation may rotate with respect to the Earth frame, the position vector is not enough to completely describe the body frame and the vectors to be referenced. For example, if the position vector  $\vec{p}_E^{oo'}$  in Figure 3.3 is known, which locates directly between the writing frame and the sensor unit in the pen, the pen-tip position still can not be determined.

On the other hand, the same vector is required to be expressed with respect to different coordinate system for the corresponding target object. The description of a vector is different and has many alternatives. In digital pen application, the sensor unit is rigidly affixed on the pen body. Thus the inertial measurement is with respect to the body frame which is rotating along with the writing motion. However, the writing trajectory for recording is on a fixed plane surface which is defined as the Earth frame before.

Thus a mapping for coordinate transformation is required to represent a vector from one frame to another, which is very useful when the vector with respect to the

destination frame is not observable.

Figure 3.2 below demonstrates a specific example for the coordinate transformation.

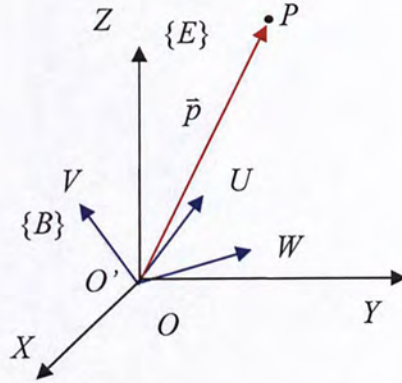


Figure 3.2: Vector representations W.R.T different reference frames by coordinate transform, which can be considered as the reverse process for vector rotation.

The orientation of the body is achieved by a description of the coordinate system  $\{B\}$  relative to  $\{E\}$ .

Define the  $\sum O-XYZ$  as the Earth frame (the reference frame) and the  $\sum O'-uvw$  as the body frame (the sensor frame). Suppose the observation  $\bar{p}_B$  W.R.T. the body frame is measured as  $[u, v, w]_B^T$ , the vector  $\bar{p}_E$  W.R.T the Earth frame:  $[x, y, z]_E^T$  can be acquired by projection along the orthogonal axis of  $\bar{x}, \bar{y}, \bar{z}$  correspondingly.

The coordinate transformation is obtained by matrix dot product for vector projection,

$$\bar{p}_E = \begin{bmatrix} x \\ y \\ z \end{bmatrix}_E = \begin{bmatrix} \bar{x} \cdot \bar{p}_B \\ \bar{y} \cdot \bar{p}_B \\ \bar{z} \cdot \bar{p}_B \end{bmatrix} = \begin{bmatrix} x_u & x_v & x_w \\ y_u & y_v & y_w \\ z_u & z_v & z_w \end{bmatrix} \begin{bmatrix} u \\ v \\ w \end{bmatrix}_B = R_B^E \bar{p}_B \quad (3.1.3)$$

Where  $R_B^E$  is the rotation matrix from the body frame to the Earth frame,

$$R_B^E = \begin{bmatrix} x_u & x_v & x_w \\ y_u & y_v & y_w \\ z_u & z_v & z_w \end{bmatrix} \quad (3.1.4)$$

And  $\bar{x}, \bar{y}, \bar{z}$  are the unit vectors representing the X, Y, Z axis W.R.T. the body frame



$\bar{u}, \bar{v}, \bar{w}$ , such that  $\bar{x} = [x_u, x_v, x_w]^T$

According to the definition of a coordinate system, the  $\bar{x}, \bar{y}, \bar{z}$  are unit vectors. As a result,

$$\|\bar{x}, \bar{x}\| = \bar{x} \cdot \bar{x} = x_u^2 + x_v^2 + x_w^2 = 1 \quad (3.1.5)$$

And  $\bar{x}, \bar{y}, \bar{z}$  are orthogonal to each other,

$$\bar{x} \cdot \bar{y} = x_u y_u + x_v y_v + x_w y_w = 0 \quad (3.1.6)$$

Thus, according to Eq. ( 3.1.5 ) and Eq. ( 3.1.6 ), the rotation matrix  $R_E^B$  is a real orthogonal matrix. The square product of  $R_E^B$  is an identity matrix  $I$  shown below:

$$R_E^B R_E^{B^T} = \begin{bmatrix} \bar{x} \cdot \bar{x} & \bar{x} \cdot \bar{y} & \bar{x} \cdot \bar{z} \\ \bar{y} \cdot \bar{x} & \bar{y} \cdot \bar{y} & \bar{y} \cdot \bar{z} \\ \bar{z} \cdot \bar{x} & \bar{z} \cdot \bar{y} & \bar{z} \cdot \bar{z} \end{bmatrix} = I \quad (3.1.7)$$

Thus,  $R_E^{B^{-1}}$ , the inverse of matrix  $R_E^B$ , which represents the orientation, or coordinate transform from the Earth frame back to the body frame, equals to the matrix transpose of itself.

$$\bar{p}_B = R_B^{E^{-1}} \bar{p}_E = R_E^B \bar{p}_E \quad (3.1.8)$$

Where,

$$R_E^B = R_B^{E^{-1}} = R_B^{E^T} \quad (3.1.9)$$

### 3.1.3. Kinematics for Digital Writing Instruments

The location of a body frame coordinate system can be specified consisting of a position vector  $\bar{p}_B^{oo'}$ ,  $\bar{p}_B^{oo'} \in \mathfrak{R}^3$  which locates its origin relative to that of the reference frame, and a rotation matrix  $R_B^E$  for the body orientation, as shown in the Figure 3.3 below [24], [25].

$$\{B\} = \{\bar{p}_E^{oo'}, R_B^E\} \quad (3.1.10)$$

Once the body frame coordinate system is established, we can locate any point in the three dimensional space with a  $3 \times 1$  position vector  $\bar{p} \in \mathfrak{R}^3$ .

$$\bar{p}_E^{op} = \bar{p}_E^{oo'} + \bar{p}_E^{o'P} \quad (3.1.11)$$

In digital pen application, the position vector W.R.T. the Earth frame, which is not directly observable, can be computed from the body frame sensor measurement and mapping by the rotation matrix by coordinate transformation:

$$\bar{p}_E^{op} = \bar{p}_E^{oo'} + R_B^E \bar{p}_B^{o'P} \quad (3.1.12)$$

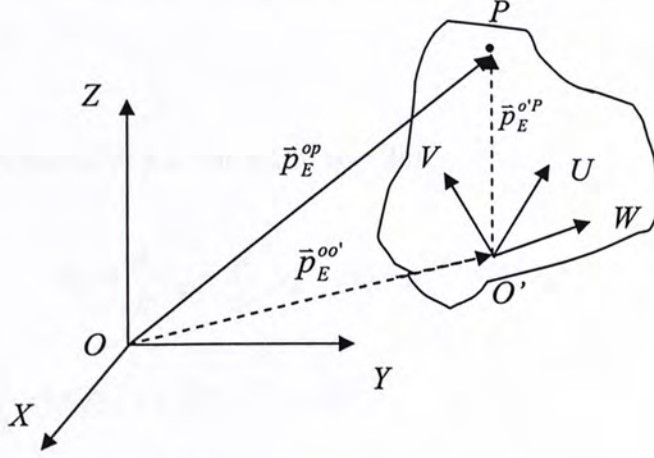


Figure 3.3: Position description for a rigid-body object in space using body-attached coordinate system.

The inertial information for motion sensors can be derived by differentiation of Eq. (3.1.12).

$$\dot{\bar{p}}_E^{op} = \dot{\bar{p}}_E^{oo'} + \dot{R}_B^E \bar{p}_B^{o'P} + R_B^E \dot{\bar{p}}_B^{o'P} \quad (3.1.13)$$

Where  $\dot{R}_B^E = \frac{d}{dt}[\bar{x}, \bar{y}, \bar{z}]^T = [\dot{\bar{x}}, \dot{\bar{y}}, \dot{\bar{z}}]^T = \bar{\omega} \times [\bar{x}, \bar{y}, \bar{z}]^T = \bar{\omega} \times R_B^E$ , (3.1.14)

$$\frac{d}{dt} \bar{x} = \bar{\omega}_x \times \bar{x} \quad (3.1.15)$$

$$\frac{d}{dt} \bar{y} = \bar{\omega}_y \times \bar{y} \quad (3.1.16)$$



$$\frac{d}{dt} \bar{z} = \bar{\omega}_z \times \bar{z} \quad (3.1.17)$$

The differentiation of  $\bar{x}, \bar{y}, \bar{z}$  denotes the changing rate for the direction of the corresponding coordinate axis by cross product. And  $\bar{\omega}_x, \bar{\omega}_y, \bar{\omega}_z$  are the angular rates about the  $X, Y, Z$  axis with respect to the body frame, respectively.

The absolute velocity of  $p$  in the Earth coordinate system is derived shown blow,

$$\bar{v}_E^{op} = \bar{v}_E^{oo'} + \bar{\omega} \times R_B^E \bar{p}_B^{o'P} + R_B^E \bar{v}_B^{o'P} \quad (3.1.18)$$

$$\bar{v}_E^{op} = \bar{v}_E^{oo'} + \bar{\omega} \times \bar{p}_E^{o'P} + \bar{v}_B^{o'P} \quad (3.1.19)$$

Where  $\bar{v}_B^{o'P}$  is the relative velocity of  $p$  W.R.T.  $\sum O'-uvw$ , represented W.R.T.  $\sum O-XYZ$ .

The absolute acceleration of  $p$  in the Earth coordinate system is,

$$\bar{a}_E = \frac{d}{dt} \bar{v}_E = \frac{d}{dt} \{ \bar{v}_E^{oo'} + \bar{\omega} \times \bar{p}_E^{o'P} + R_B^E \bar{v}_B^{o'P} \} \quad (3.1.20)$$

Where,

$$\begin{aligned} \frac{d}{dt} \{ \bar{\omega} \times \bar{p}_E^{o'P} \} &= \dot{\bar{\omega}} \times \bar{p}_E^{o'P} + \bar{\omega} \times \dot{\bar{p}}_E^{o'P} \\ &= \bar{\alpha} \times \bar{p}_E^{o'P} + \bar{\omega} \times R_B^E \bar{v}_B^{o'P} + \bar{\omega} \times (\bar{\omega} \times \bar{p}_E^{o'P}) \end{aligned} \quad (3.1.21)$$

and  $\bar{\alpha}$  is the angular acceleration.

And,

$$\frac{d}{dt} \{ R_B^E \bar{v}_B^{o'P} \} = R_B^E \dot{\bar{v}}_B^{o'P} + \bar{\omega} \times R_B^E \bar{v}_B^{o'P} \quad (3.1.22)$$

Thus, the motion of the digital pen consists of the translation and the rotation. In order to record the pen tip position along to the human hand motion, the kinematics description of a rigid body include the translation acceleration:  $\bar{a}_E^{oo'} = \frac{d}{dt} \bar{v}_E^{oo'}$ , and rotation acceleration:  $\bar{a}_E^{oo'}$ .

$$\bar{a}_E^{oo'} = \bar{\alpha} \times \bar{p}_E^{o'P} + \bar{\omega} \times (\bar{\omega} \times \bar{p}_E^{o'P}) + 2\bar{\omega} \times \bar{v}_B^{o'P} + R_B^E \dot{\bar{v}}_B^{o'P} \quad (3.1.23)$$

where  $\vec{v}_{B'E}^{o'P} = \vec{\omega} \times \vec{p}_{E}^{o'P}$  denote the relative velocity between the particle and rotation system with respect to the earth frame.

Let 
$$\vec{a}_t = \vec{\alpha} \times \vec{p}_{E}^{o'P} \quad (3.1.24)$$

$\vec{a}_t$  is the tangential acceleration for the rate of change of the tangential speed, which is in the same direction of velocity in rotation frame.

$$\vec{a}_n = \vec{\omega} \times (\vec{\omega} \times \vec{p}_{E}^{o'P}) \quad (3.1.25)$$

$\vec{a}_n$  is the normal acceleration for the centrifugal force, which is tangential to the rotation cycle.

$$\vec{a}_c = 2\vec{\omega} \times \vec{v}_{B'E}^{o'P} \quad (3.1.26)$$

$\vec{a}_c$  is the Coriolis acceleration for the relative motion between the particle and the rotating body.

$$\vec{a}_R = R_B^E \dot{\vec{v}}_{B'E}^{o'P} \quad (3.1.27)$$

$\vec{a}_R$  stands for the relative acceleration between the particle and the rotating body.

In digital pen application, the distance between the pen tip and sensor unit is fixed. Thus both the  $\vec{a}_c$  and  $\vec{a}_R$  equal to zero.

In general, the rotation acceleration is combined in tangential and normal direction,

$$\begin{aligned} \vec{a}_{E'R}^{oo'} &= \vec{a}_t + \vec{a}_n \\ &= \vec{\alpha} \times \vec{p}_{E}^{o'P} + \vec{\omega} \times (\vec{\omega} \times \vec{p}_{E}^{o'P}) \end{aligned} \quad (3.1.28)$$

Figure 3.4 below demonstrate the rotation accelerations and the direction of each component described in Eq. ( 3.1.23 ) to Eq. ( 3.1.27 ). A round table in  $X$ - $Y$  plane is rotating along the  $Z$  axis about the table origin. A rectangular object is moving away from the table origin with velocity  $\vec{v}_{B'E}^{o'P}$  in the blue arrow direction. The four components of acceleration caused by rotation are in different direction according to



the definition and cross product rule. The  $\bar{a}_t$  and  $\bar{a}_n$ , also  $\bar{a}_c$  and  $\bar{a}_R$  are orthogonal to each other.

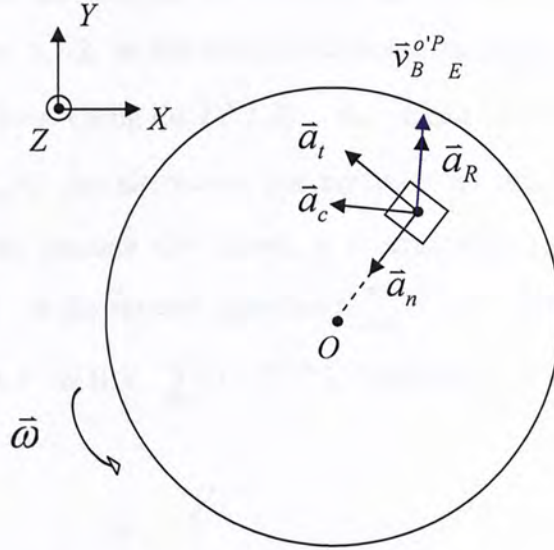


Figure 3.4: Rotational accelerations of rigid body in space

### 3.1.4. Vector Rotation

The coordinate transform is obtained by projecting the vector after the current frame is rotated to the reference frame. An alternative interpretation is that the vector is rotated in the counter direction when represented in the current frame. Similarly, in one coordinate system, the vector rotation can be specified by vector description introduced before, with respect to the coordinated system counter rotated.

As a result, the vector rotation can be achieved by rotation matrix in the same form defined by Eq. ( 3.1.3 ), in stead of the interpretation for rotation for current frame. Thus the rotation matrix of a vector  $R_B^E$  equals to  $A_E^B$ , which can be derived from Eq. ( 3.1.3 ) by the inverse or the transpose the coordinate transform matrix  $A_B^E$ .

$$R_B^E = A_B^{E-1} = A_B^{E^T} = A_E^B \quad (3.1.29)$$

The rotation about a fixed axis in matrix form is shown below,

$$\begin{bmatrix} x \\ y' \\ z' \end{bmatrix} = \begin{bmatrix} 1 & 0 & 0 \\ 0 & \cos \phi & -\sin \phi \\ 0 & \sin \phi & \cos \phi \end{bmatrix} \begin{bmatrix} x \\ y \\ z \end{bmatrix} = R(X, \phi) \begin{bmatrix} x \\ y \\ z \end{bmatrix} \quad (3.1.30)$$

Figure 3.5 illustrates the rotation for a vector and its relation with the coordinate transform in Chapter 3.1.2. In this simple example, the vector  $\bar{v}_{OP'}$  is rotated from  $P'$  to  $P$  along the  $X$  axis. Using Eq. (3.1.30), the rotated vector  $\bar{v}_{OP}$  can be obtained by  $\bar{v}_{OP'}$  and  $R(X, \phi)$ . An alternative interpretation for this rotation process is the coordinate transform: assume  $OP'$  fixed, it is equivalent to rotate the coordinate system  $\sum O-XYZ$  in the reverse direction to  $\sum O-X'Y'Z'$ . The vector  $\bar{v}_{OP}$  can still be calculated by  $P'$  W.R.T.  $\sum O-X'Y'Z'$  using Eq. (3.1.3).

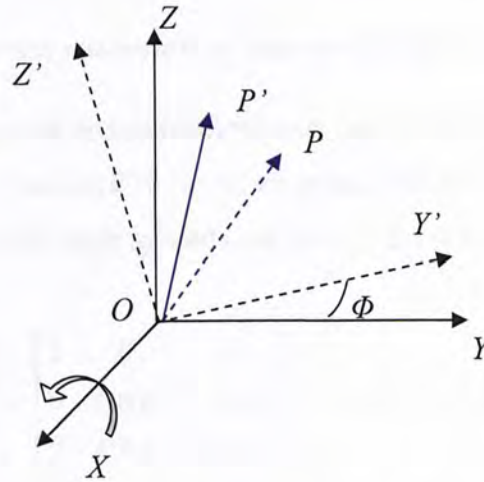


Figure 3.5: Single axis rotation: the vector  $OP$  is rotated about the  $X$  axis for angle  $\Phi$

### 3.2. Euler Angles for Rotation in Space

According to Euler's rotation theory, any orientation in space can be represented in terms of three sequential rotations along the specified axis of the body frame triad  $X, Y, Z$  individually. When using Euler angles, the type of axis should be considered according to the ordering of rotation. If the sequence of rotation is first about the  $X$  axis, then about the  $Y$  axis, and finally about the  $Z$  axis, the associated angles are signified by the reserved words "roll", "pitch" and "yaw" angle respectively. In convention, the rotation angles for "roll", "pitch" and "yaw" are designated using reserved symbols:  $\Phi, \theta, \psi$  respectively. These three angles are called Euler angles.



Figure 3.6 illustrates a specific example of Euler angles' rotation. The rotation direction is determined by the right-hand rule, which is clockwise when looking towards the origin. The Euler angles:  $\Phi$ ,  $\theta$ ,  $\psi$  describes the orientation position from the reference frame:  $X, Y, Z$  to the end frame:  $X'', Y'', Z''$ .

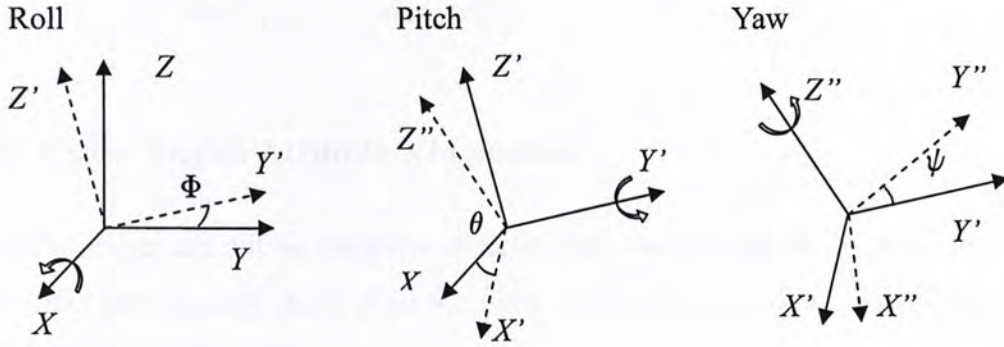


Figure 3.6: The rigid body rotation in Euler angles by Roll, Pitch and Yaw rotation sequences.

The rotation matrix for each one-axis orientation can be derived from Eq. ( 3.1.3 ) and Eq. ( 3.1.29 ). The unit vectors  $\bar{u}, \bar{v}, \bar{w}$  in coordinate transform matrix  $A$  equal to the position coordinates for the each rotated axis W.R.T. the start frame  $X, Y, Z$ .

$$\begin{bmatrix} x \\ y' \\ z' \end{bmatrix} = \begin{bmatrix} 1 & 0 & 0 \\ 0 & \cos \phi & -\sin \phi \\ 0 & \sin \phi & \cos \phi \end{bmatrix} \begin{bmatrix} x \\ y \\ z \end{bmatrix} = R(X, \phi) \begin{bmatrix} x \\ y \\ z \end{bmatrix} \quad (3.2.1)$$

$$\begin{bmatrix} x' \\ y' \\ z'' \end{bmatrix} = \begin{bmatrix} \cos \theta & 0 & \sin \theta \\ 0 & 1 & 0 \\ -\sin \theta & 0 & \cos \theta \end{bmatrix} \begin{bmatrix} x \\ y' \\ z' \end{bmatrix} = R(Y, \theta) \begin{bmatrix} x \\ y' \\ z' \end{bmatrix} \quad (3.2.2)$$

$$\begin{bmatrix} x'' \\ y'' \\ z'' \end{bmatrix} = \begin{bmatrix} \cos \psi & -\sin \psi & 0 \\ \sin \psi & \cos \psi & 0 \\ 0 & 0 & 1 \end{bmatrix} \begin{bmatrix} x' \\ y' \\ z'' \end{bmatrix} = R(Z, \psi) \begin{bmatrix} x' \\ y' \\ z'' \end{bmatrix} \quad (3.2.3)$$

Thus, combine Eq. ( 3.2.1 ), Eq. ( 3.2.2 ), and Eq. ( 3.2.3 ), the Euler angles for the rigid body orientation, which is in term of the three individual rotation sequences, can be represented by one rotation matrix: the direction cosine matrix (DCM), when the Euler angles:  $\Phi$ ,  $\theta$ ,  $\psi$  for roll, pitch, yaw are specified in Eq. ( 3.2.5 ),

$$\begin{bmatrix} u \\ v \\ w \end{bmatrix} = \begin{bmatrix} x'' \\ y'' \\ z'' \end{bmatrix} = DCM(\psi, \theta, \phi)_B^E \begin{bmatrix} x \\ y \\ z \end{bmatrix} = R(Z, \psi)R(Y, \theta)R(X, \phi) \begin{bmatrix} x \\ y \\ z \end{bmatrix} \quad (3.2.4)$$

$$DCM(\psi, \theta, \phi)_B^E = \begin{bmatrix} \cos\psi \cos\theta & \cos\psi \sin\theta \sin\phi - \sin\psi \cos\phi & \cos\psi \sin\theta \cos\phi + \sin\psi \cos\phi \\ \sin\psi \cos\theta & \cos\psi \cos\phi + \sin\psi \sin\theta \sin\phi & \sin\psi \sin\theta \cos\phi - \cos\psi \sin\phi \\ -\sin\theta & \sin\phi \cos\theta & \cos\phi \cos\theta \end{bmatrix} \quad (3.2.5)$$

### 3.3. Euler Angles Attitude Kinematics

The Euler angles can not be integrated directly from the body frame angular rates  $p$ ,  $q$ ,  $r$  since the sensing axis  $X$ ,  $Y$ ,  $Z$  in the body frame are rotated in sequence as this unique orientation description.

Thus, the body rates can be obtained from the Euler angles derivative by counter process according to the specific orientation sequence.

$$\begin{bmatrix} \omega_x \\ \omega_y \\ \omega_z \end{bmatrix}_B = R(X, -\phi)R(Y, -\theta)R(Z, -\psi) \begin{bmatrix} 0 \\ 0 \\ \dot{\psi} \end{bmatrix} + R(X, -\phi)R(Y, -\theta) \begin{bmatrix} 0 \\ \dot{\theta} \\ 0 \end{bmatrix} + R(X, -\phi) \begin{bmatrix} \dot{\phi} \\ 0 \\ 0 \end{bmatrix} \quad (3.3.1)$$

Simplify and written in a matrix form,

$$\begin{bmatrix} \dot{\phi} \\ \dot{\theta} \\ \dot{\psi} \end{bmatrix} = \begin{bmatrix} 1 & \tan\theta \sin\phi - \sin\psi \cos\phi & \tan\theta \cos\phi \\ 0 & \cos\phi & -\sin\phi \\ 0 & \sin\phi \sec\theta & \cos\phi \sec\theta \end{bmatrix} \begin{bmatrix} \omega_x \\ \omega_y \\ \omega_z \end{bmatrix}_B \quad (3.3.2)$$

### 3.4. Singular Problem

The Euler angles define an orientation motion in three successive rotations: roll, pitch, and yaw about the  $X$ ,  $Y$ , and  $Z$  axis respectively. However, the calculations of Euler angles are trigonometric functions which require costly computation time and will induce nonlinear error. This problem will be manifest since the attitude propagation matrix, defined in Eq. ( 3.3.2 ), will be singular when the pitch angle is equal to or close to 90 degrees [26].

The experimental results, shown in figures below, demonstrate the singularity



problem in attitude propagation by Euler method. In the test, the  $\mu$ IMU is speedily rotated along the yawing direction 90 degree backward and forward. Figure 3.7 below shows the angular velocity measured by the gyroscopes from the  $\mu$ IMU.

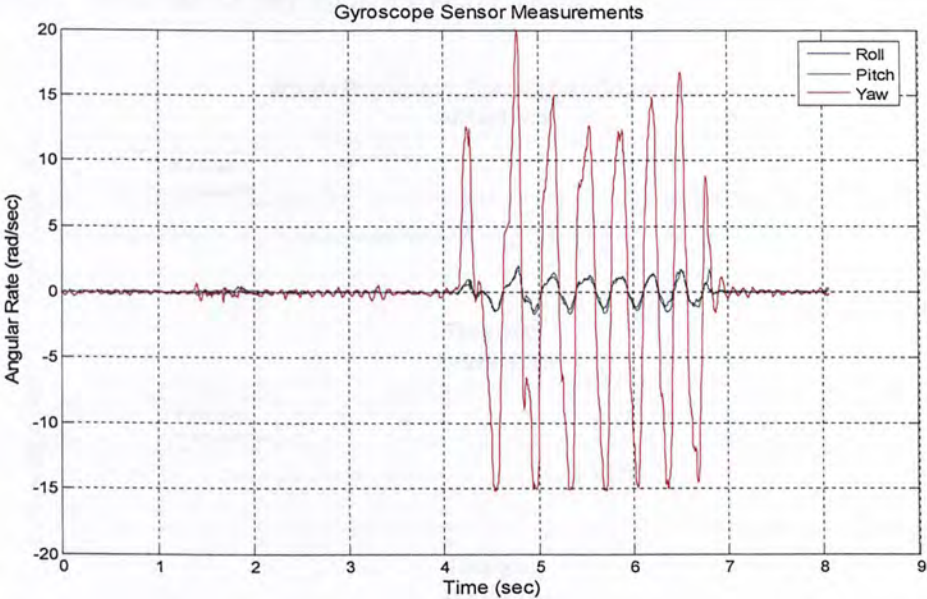


Figure 3.7: Angular velocity measured by gyroscopes in the  $\mu$ IMU

The attitude singularity occurred, as illustrated in Figure 3.8, as the yawing angle equals to or close to 90 degree because the attitude propagation matrix, defined in Eq. ( 3.3.2 ), become singular. Thus, this unexpected error can not be avoided. After the singular propagation, the attitude tracking algorithm requires recalibration and reset for initial attitude to fix the error and restart tracking.

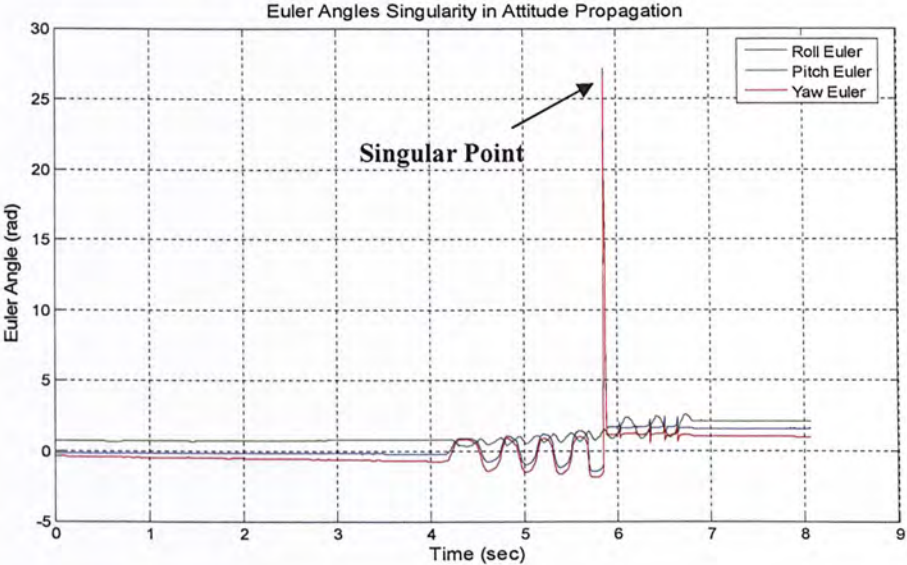


Figure 3.8: Singular problem in attitude propagation using Euler method

However, attitude propagation using quaternion method, to be introduced in the next chapter, can avoid the singularity problem. As shown in Figure 3.9, quaternion propagation, tested with the same experimental data, will not result in attitude divergence, which can be proved in the next chapter.

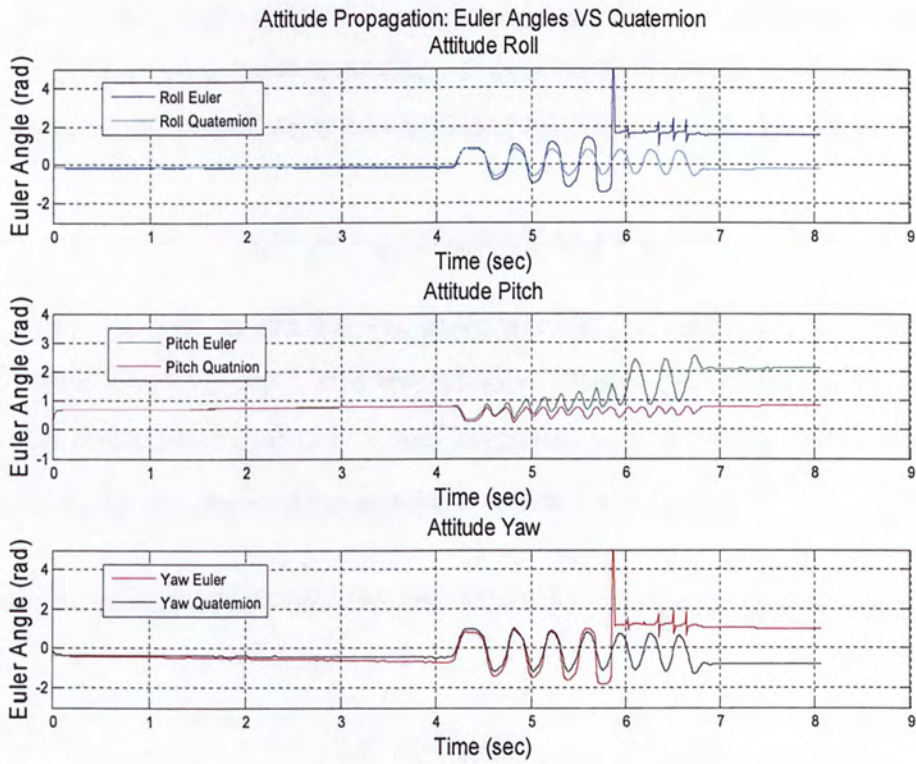


Figure 3.9: Attitude propagation using quaternion method compared to Euler angles



## 4. Attitude in Quaternion

The complex numbers are abstract quantities in the form of  $x + yi$ . With complex representation, they are useful in computation and result in physically meaningful solution. The quaternion representation of rigid body rotations leads to convenient expressions [30]. A quaternion is four-dimensional complex numbers [26], [32].

$$q = q_1i + q_2j + q_3k + q_4 = \vec{q} + q_0 \quad (3.4.1)$$

Where  $q_1, q_2, q_3,$  and  $q_4$  are the real numbers and  $i, j,$  and  $k$  are the unit vectors directed along the  $X, Y,$  and  $Z$  axis respectively. Thus, a quaternion can be described as linear combination of real part  $q_0$  and imaginary part  $\vec{q}$ , which can be denoted as the rotation angle and the rotation axis for a orientation in space.

According to the right-hand rule, the unit vector for the imaginary part has following property,

$$i^2 = j^2 = k^2 = -1 \quad (3.4.2)$$

$$ij = -ji = k \quad (3.4.3)$$

$$jk = -kj = i \quad (3.4.4)$$

$$ki = -ik = j \quad (3.4.5)$$

Thus, quaternion multiplication is not commutative.

### 4.1. Quaternion Operations

Quaternion satisfies all of the axioms in addition and multiplication in the field, except the commutative law in multiplication.

Let  $s$  be the scalar, and let,

$$q_1 = x_1i + y_1j + z_1k + r_1 \quad (4.1.1)$$

$$q_2 = x_2i + y_2j + z_2k + r_2$$

The quaternion addition is defined as Eq. ( 4.1.2 ). The quaternions are added up according to the real part, and  $i, j$  and  $k$  of the imaginary part, individually. The quaternion addition is communicative. The summation of quaternions is the same as imaginary number if we consider the normal part as the fourth imaginary number.

$$q_1 + q_2 = q_2 + q_1 = (x_1 + x_2)i + (y_1 + y_2)j + (z_1 + z_2)k + (r_1 + r_2) \quad (4.1.2)$$

The scale multiplication of a quaternion is defined as,

$$sq = s\bar{q} + sq_0 = sq_1i + sq_2j + sq_3k + sq_4 \quad (4.1.3)$$

The multiplication of two quaternions is performed the same as the complex numbers multiplications,

$$q_1q_2 = (x_1i + y_1j + z_1k + r_1)(x_2i + y_2j + z_2k + r_2) \quad (4.1.4)$$

Simplify using Eq. ( 3.4.2 ) to Eq. ( 3.4.5 ), the result is still a quaternion,

$$\begin{aligned} q_1q_2 = & (x_1r_2 + r_1x_2 - z_1y_2 + y_1z_2)i \\ & + (y_1r_2 + z_1x_2 + r_1y_2 - x_1z_2)j \\ & + (z_1r_2 - y_1x_2 + x_1y_2 + r_1z_2)k \\ & + (r_1r_2 - x_1x_2 - y_1y_2 - z_1z_2) \end{aligned} \quad (4.1.5)$$

#### 4.1.1. Quaternion Conjugate

Conjugate of a quaternion is the same as the field of complex number, which is take the opposite of the imaginary part.

$$q_1^* = -x_1i - y_2j - z_3k + r_4 \quad (4.1.6)$$

$$(q_1q_2)^* = q_2^*q_1^* \quad (4.1.7)$$



### 4.1.2. Quaternion Norm

$$N(q) = \sqrt{qq^*} = \sqrt{x^2 + y^2 + z^2 + r^2} \quad (4.1.8)$$

A quaternion can be normalized by,

$$q = \frac{q}{N(q)} \quad (4.1.9)$$

### 4.1.3. Quaternion Inverse

The inverse of a quaternion performed as,

$$q^{-1} = \frac{q^*}{(N(q))^2} \quad (4.1.10)$$

## 4.2. Orientation Description in Quaternion

After normalization for  $q$ , a unit quaternion  $n$  can be expressed in the vector and angle form:

$$n = \frac{q}{\|q, q_0\|} = (e_1i + e_2j + e_3k) \sin \frac{\theta}{2} + \cos \frac{\theta}{2} \quad (4.2.1)$$

The orientation motion of vector  $u$  from the reference frame to the destination frame can be expressed by rotation about the vector  $\bar{e}$  for  $\theta$  from the quaternion  $n$ . The rotation is performed through quaternion multiplication.

$$\bar{v} = n \otimes \bar{u} \otimes n^* \quad (4.2.2)$$

Where  $n^*$  is the quaternion conjugate which is defined as:

$$n^* = -n_1i - n_2j - n_3k + n_4 \quad (4.2.3)$$

This operation can be expressed by matrix multiplication:

$$\bar{v} = n \otimes \bar{u} \otimes n^* = R\bar{u} \quad (4.2.4)$$

$$R = \begin{bmatrix} q_1^2 - q_2^2 - q_3^2 + q_4^2 & 2(q_1q_2 + q_3q_4) & 2(q_1q_3 - q_2q_4) \\ 2(q_1q_2 - q_3q_4) & -q_1^2 + q_2^2 - q_3^2 + q_4^2 & 2(q_2q_3 + q_1q_4) \\ 2(q_1q_3 + q_2q_4) & 2(q_2q_3 - q_1q_4) & -q_1^2 - q_2^2 + q_3^2 + q_4^2 \end{bmatrix} \quad (4.2.5)$$

Furthermore, two individual rotations can be simplified in one quaternion by combining the corresponding parameters with calculation of matrix product.

$$\text{Suppose,} \quad R(q'') = R(q)R(q') \quad (4.2.6)$$

Let  $q = [q_1, q_2, q_3, q_4]^T$ , Substitute Eq. ( 4.2.5 ) directly into Eq. ( 4.2.6 ), the transform relation between  $q''$  and  $q'$  in matrix form can be derived as,

$$q'' = \begin{bmatrix} q_4 & q_3 & -q_2 & q_1 \\ -q_3 & q_4 & q_1 & q_2 \\ q_2 & -q_1 & q_4 & q_3 \\ -q_1 & -q_2 & -q_3 & q_4 \end{bmatrix} q' = T(q)q' \quad (4.2.7)$$

### 4.3. Attitude Kinematics in Quaternion

Let quaternion  $q$  represents the orientation position between the previous frame and the current frame. Assume the rotation angle  $\theta$  is small, the Eq. ( 4.2.1 ) can be simplified by,

$$q = [\cos \frac{\theta}{2}, (e_1i + e_2j + e_3k) \sin \frac{\theta}{2}] \approx [1, \bar{v} \frac{\theta}{2}] = [1, \frac{\phi}{2}, \frac{\theta}{2}, \frac{\psi}{2}] \quad (4.3.1)$$

Comparison with Eq. ( 3.2.5 ) and Eq. ( 4.2.5 ) demonstrates the approximation in small angle for the direction cosine matrix in quaternion is related to that of the Euler angles by Eq. ( 4.3.1 ). Substitute into Eq. ( 4.2.7 ),

$$\frac{dq''}{dt} = \frac{dT(q)}{dt} q' + T(q) \frac{dq'}{dt} \quad (4.3.2)$$

Consider the  $q'$  stands for the initial or previous frame attitude, which is constant.



$$\frac{dq''}{dt} = \frac{dT(q)}{dt} q' \quad (4.3.3)$$

Thus, in continuous form,

$$\dot{q}(t) = \Omega(\omega_t)q(t) \quad (4.3.4)$$

Where,

$$\Omega(\omega_t) = \frac{1}{2} \begin{bmatrix} 0 & \omega_z & -\omega_y & \omega_x \\ -\omega_z & 0 & \omega_x & \omega_y \\ \omega_y & -\omega_x & 0 & \omega_z \\ -\omega_x & -\omega_y & -\omega_z & 0 \end{bmatrix} \quad (4.3.5)$$

Thus,

$$q(t + \Delta t) = \exp\left(\int_t^{t+\Delta t} \Omega(\tau) d\tau\right) q(t) \quad (4.3.6)$$

Using the procedures by evaluating the matrix exponential, Eq. ( 4.3.6 ) can be rewritten in a more convenient way for computation.

$$q(t + \Delta t) = \left[ \cos\left(\frac{\omega\Delta t}{2}\right)I + \frac{1}{\omega/2} \sin\left(\frac{\omega\Delta t}{2}\right)\Omega \right] q(t) \quad (4.3.7)$$

Where,

$$\omega = \sqrt{\omega_x^2 + \omega_y^2 + \omega_z^2} \quad (4.3.8)$$

And  $I$  is a  $4 \times 4$  identity matrix.

# 5. Kalman Filter

Kalman filter is a recursive algorithm in discrete data linear fitting for real-time application. It is developed by R. E. Kalman in his famous paper published in 1960 [36]. Due to the advantage in digital computation and support from digital filters, the Kalman filter takes the place of the Wiener filter in analog system, and has been the subject of extensive research and application in the area of statistic learning, computer vision, and autonomous navigation.

The iterative process of the Kalman filter includes two steps. The time update step projects the current system state and its statistic information ahead in time according to system plant. The measurement update step adjusts the propagated estimate by an actual measurement based on statistic decision theory and Least-square method. Figure 5.1 below demonstrate the ongoing Kalman filtering loop.

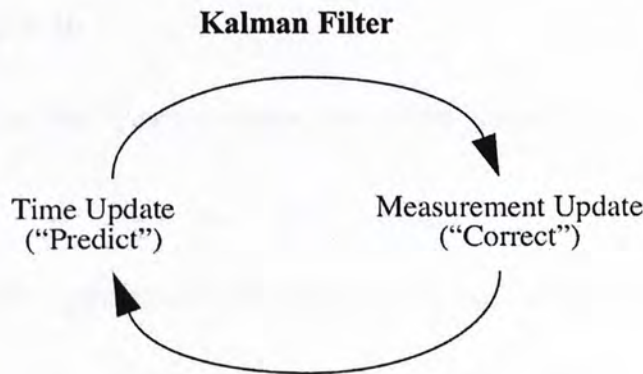


Figure 5.1: The real-time cycle of the discrete Kalman Filter [34]

The Kalman filter is developed to estimate the system state  $x \in \mathfrak{R}^m$ , of a discrete-time control process that is governed by a linear stochastic differential equation,

$$x_k = A_k x_{k-1} + B_k u_{k-1} + w_{k-1} \tag{4.3.1}$$

Where a measurement  $y \in \mathfrak{R}^n$  is referred for correction,



$$y_k = C_k x_k + v_k \quad (4.3.2)$$

In control theory,  $A$  is the system plant matrix with dimension  $m \times m$ , relating the previous state  $k - 1$  to the state at the current step  $k$ .  $A$  is defined as be separated from the process noise. The  $m \times l$  matrix  $B$  relates the optimal control input,  $u \in \mathfrak{R}^l$  to the state  $x$ . The  $n \times m$  measurement matrix  $C$  relates the measurement input,  $y \in \mathfrak{R}^n$  to the state  $x$ . In practice,  $A$ ,  $B$  and  $C$  can be constant or updated with each time step.

The random variable  $w_k$  and  $v_k$  represents the noise in propagation process and measurement respectively. Assume  $w_k$  and  $v_k$  are independent, Gaussian noise with normal probability distributions.

$$P(w) \sim N(0, Q) \quad (4.3.3)$$

$$P(v) \sim N(0, R) \quad (4.3.4)$$

## 5.1. Time Update

According to control theory and statistics, the system plant can be constructed as:

$$x_k = A_k x_{k-1} + B_k u_{k-1} \quad (5.1.1)$$

The projection of the system state covariance can be derived according to definition,

$$\text{cov}(x_k) = \text{cov}(A_k x_{k-1} + B_k u_{k-1} + w_{k-1}) \quad (5.1.2)$$

$$\begin{aligned} P_k &= \text{cov}(A_k x_{k-1}) + \text{cov}(w_{k-1}) \\ &= A_k \text{cov}(x_{k-1}) A_k^T + Q \end{aligned} \quad (5.1.3)$$

$$P_k = A_k P_{k-1} A_k^T + Q \quad (5.1.4)$$

In general, the Time update process is derived by Eq. ( 5.1.1 ) and Eq. ( 5.1.4 ).

## 5.2. Measurement Update

The measurement update in Kalman filter is achieved by Least-square estimation based on maximum a posterior probability (MAP).

Given a set of  $n$  observations taken during the time span,

$$y \equiv [y_1, y_2, \dots, y_n]^T \quad (5.2.1)$$

The statistic property of the observation measurements appears random due to the prevailing random noise mixed from sensor system, electro-magnetic interference (EMI), or uncertain misoperation in experiment. To determine the state vector  $x$ , we assume that measurement  $y$  equals to the observation vector,  $c(x, t)$ , based on the mathematical model plus additive random noise,  $v$ . Thus, for each element of  $y$ ,

$$y_i = c_i(x(t_i), t_i) + v_i \quad (5.2.2)$$

Given a priori estimate  $\hat{x}$ , and the statistical properties of  $v$ , the optimal state vector  $x$  can be achieved using Least-square method, which is to minimize the square difference (error covariance) between the observation prediction  $c(x)$  and the real observation measurement  $y$  [27].

### 5.2.1. Maximum a Posterior Probability

In statistics, maximum a posterior probability (MAP) is a kind of Bayesian estimation based on the cost function  $R(\Phi - \theta(y))$  defined as the delta function [28], [29],

$$R(\Phi, \theta(y)) = \begin{cases} 0, & \text{if } |\Phi - \theta(y)| \leq \Delta \\ 1, & \text{if } |\Phi - \theta(y)| > \Delta \end{cases} \quad (5.2.3)$$

Where  $\theta(y)$  represents the vector space expanded by the observation  $y$ , and  $\Phi$  is the true state of  $x$ . The cost is either 1 or 0, depending on whether the estimation by observation:  $\theta(y)$  is close enough to the true state  $\Phi$ . Thus, the expected posterior loss function can be derived as,



$$\begin{aligned}
E[R(\Phi, \theta(y)) | y] &= P(|\Phi - \theta(y)| > \Delta | y) \\
&= 1 - P(|\Phi - \theta(y)| \leq \Delta | y) \\
&= 1 - \int_{\theta(y)-\Delta}^{\theta(y)+\Delta} P(\Phi | y) d\Phi \\
&\approx 1 - 2\Delta P(\Phi | y) |_{\Phi=\theta(y)}
\end{aligned} \tag{5.2.4}$$

Figure 5.2 illustrates that, when  $\Delta$  is small enough, the higher order terms can be omitted, so the approximation will be accurate enough for the integration.

Eq. ( 5.2.4 ) illustrates that, in order to minimize the distance in statistics between the observations and the true state, it is the same to maximize the posterior probability  $P(\Phi | y)$ . Thus, as shown in Figure 5.2,  $\theta(y)$  should be selected as the maximum of  $P(\Phi | y)$ .

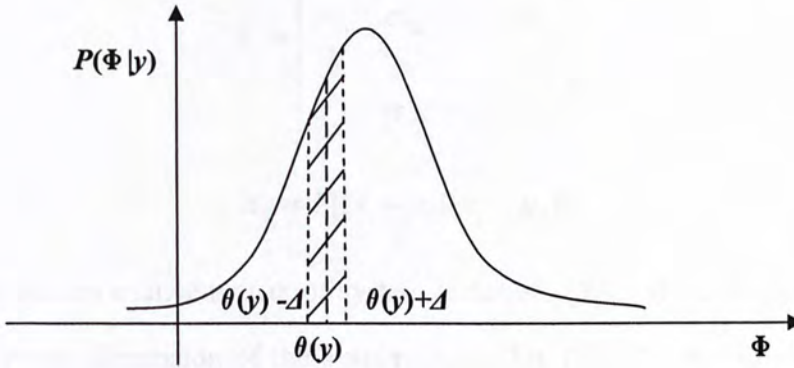


Figure 5.2: Linear approximation for the expected posterior loss

In filtering application, assume  $\Phi$  as the state vector  $x$ ,  $\theta(y)$  can be described by  $\Phi$  according to the specific measurement model. Therefore maximization of the posterior probability is equivalent to evaluation through the system state  $x$ .

$$\theta_{MAP}(y) = \arg \max_x P(x | y) \tag{5.2.5}$$

Given the Bayes' rule,  $P(x | y) = \frac{P(y | x)P(x)}{P(y)}$

And the probability of observation  $P(y)$  is independent of the state  $x$ .

$$\theta_{MAP} = \arg \max_x P(y | x)P(x) \quad (5.2.6)$$

Furthermore, to maximize Eq. ( 5.2.5 ) for  $\theta_{MAP}$ , it is equivalent to maximize,

$$\arg \max_x P(y)P(x) \quad (5.2.7)$$

### 5.2.2. Batch Least-Square Estimation

Consider an  $n$ -dimensional Gaussian classifier as,

$$P(\bar{x}) = \frac{1}{(2\pi)^{\frac{n}{2}} |\Sigma_i|^{\frac{1}{2}}} \exp\left[-\frac{1}{2}(\bar{x} - \bar{\mu})^T \Sigma_i^{-1} (\bar{x} - \bar{\mu})\right] \quad (5.2.8)$$

Where,

$$\Sigma_i = \begin{bmatrix} \sigma_{11} & \sigma_{12} & \cdots & \sigma_{1n} \\ \sigma_{21} & \sigma_{22} & \cdots & \sigma_{2n} \\ \vdots & \vdots & \ddots & \vdots \\ \sigma_{n1} & \sigma_{n2} & \cdots & \sigma_{nn} \end{bmatrix} \quad (5.2.9)$$

$$\sigma_{ij} = E[(x_i - \mu_i)(x_j - \mu_j)] \quad (5.2.10)$$

Define  $\Sigma_i$  as the covariance matrix of system state set:  $[\bar{x}_i]$ ,  $\bar{\mu}$  is the mean vector of  $[\bar{x}_i]$ , and  $n$  is the dimension of the system. Scale Eq. ( 5.2.7 ) by logarithm function and rewrite in a more convenient way for calculation.

$$\arg \max_x P(y)P(x) = \arg \max_x [\log(P(y)) + \log(P(x))] \quad (5.2.11)$$

As a result, the MAP optimization can be achieved by minimizing the loss function  $L$  defined as follows [30], [31],

$$L = \frac{1}{2}[y - c]^T R^{-1}[y - c] + \frac{1}{2}[x - \hat{x}]^T P^{-1}[x - \hat{x}] \quad (5.2.12)$$

Where  $[y - c]$  is the observation difference between the measurement set  $y$  and its predictions  $c$ .  $P$  and  $R$  are the inverse of the covariance matrix, as defined by Eq. ( 5.2.9 ) and Eq. ( 5.2.10 ), for  $x$  and  $y$ , respectively.



In probability theory, the variance of a random variable is the measure of the stochastic dispersion, which indicates the distance from its expected value. Hence, the inverse covariance matrix  $P^{-1}$  and  $R^{-1}$  works as the weighting matrix related with the contribution of each priori estimation and observation, according to their accuracy and importance.

Therefore, the evaluation for estimation will concentrate on the observations  $y_i$  with relatively small variation  $\sigma_i$  when the corresponding measurement noise is depressed. The weight matrix for state  $P^{-1}$  describes the uncertainty in the priori estimate  $\hat{x}$ . In case of inadequate observations to correct the state estimation,  $P^{-1}$  is fairly practical to utilize the information of the prior estimates.

In order to locate the minimum of the loss function  $L$  with respect to  $x$ ,  $\partial L/\partial x$  must equal to zero. Therefore,

$$\frac{\partial L}{\partial x} = -[y - c]^T R^{-1} C + [x - \hat{x}]^T P^{-1} = 0 \quad (5.2.13)$$

Where  $C$  is an  $n$  by  $m$  matrix which relates the unknown state with the observation set. The  $m$  is the dimension of vector  $x$  and  $n$  is the dimension of vector  $y$ .

$$C = \frac{\partial c}{\partial x} = \begin{bmatrix} \frac{\partial c_1}{\partial x_1} & \frac{\partial c_1}{\partial x_2} & \dots & \frac{\partial c_1}{\partial x_m} \\ \frac{\partial c_2}{\partial x_1} & \frac{\partial c_2}{\partial x_2} & \dots & \frac{\partial c_2}{\partial x_m} \\ \vdots & \vdots & \ddots & \vdots \\ \frac{\partial c_n}{\partial x_1} & \frac{\partial c_n}{\partial x_2} & \dots & \frac{\partial c_n}{\partial x_m} \end{bmatrix} \quad (5.2.14)$$

Where each element of  $\partial c_i/\partial x_j$  are computed analytically from the observation model. If the observation plant is linear, the prediction of observation can be specified by Taylor expansion at a reference point  $x_R$ .

$$c = c(x_R) + \frac{\partial c}{\partial x}(x_R)[x - x_R] \quad (5.2.15)$$

$$c = c_R + C_R x - C_R x_R \quad (5.2.16)$$

However, if the observation model is nonlinear, and the higher order terms can not be ignored, the linearization process by the Jacobian matrix will cause nonlinear distortion in the estimation result. The expected mean and variance of the state and observation will depart from its true value, which can be deformed and rotated in shape. When serious situation occurred, the filter may have difficulty to maintain convergence.

In general, each element of  $c$  can be evaluated at a different reference point with respect to the observation data block. This possibility will be useful in the later development of the sequential least-square algorithm.

Substitute the expansion from Eq. ( 5.2.16 ) to Eq. ( 5.2.13 ).

$$[P^{-1} + C_R^T R^{-1} C_R]x = P^{-1} \hat{x} + C_R^T R^{-1} [y - c_R + C_R x_R] \quad (5.2.17)$$

$$x = x_R + [P^{-1} + C_R^T R^{-1} C_R]^{-1} [C_R^T R^{-1} (y - c_R) + P^{-1} (\hat{x} - x_R)] \quad (5.2.18)$$

$$x = x_R + \frac{C_R^T R^{-1}}{P^{-1} + C_R^T R^{-1} C_R} [(y - c_R) + \frac{P^{-1}}{C_R^T R^{-1}} (\hat{x} - x_R)] \quad (5.2.19)$$

Hence, the optimal estimator based on Least-square method is obtained [33]. If the observation function  $C$  is linear, and  $x_R = \hat{x}$ , then Eq. ( 5.2.19 ) will provide the best estimation for the state  $x$ . At a fixed timespan, the state vector can be updated using prior estimations and block of measurements. When large information is available, the estimation can be supported by the entire observations if a mathematical model is available to relate the state parameters with the measurement values at each observation time. Furthermore, during every iteration step, the covariance matrix for weighting can be updated according to the priori estimates and observation data block based on stochastic analysis. Thus, the filter can be adaptive to distinct random noise with unknown probability distributions. However, the measurement data block requires large memory to store. High dimension in observation model involve more computational resources in matrix inverse and have difficulty in constructing the projection matrix  $C$  between measurement and state. Further, the filter may be lead by



early observations with large weights.

Thus a sequential estimator, Kalman filter is proposed as the real-time estimator for new incoming observations. This causes the influence of earlier data on the current estimation to fade with time so that the filter does not lose sensitivity to current observation.

### 5.2.3. Measurement Update in Kalman Filter

According to previous formula deduction, if the reference point for expansion evaluation is selected at the last optimal estimation,  $x_R \stackrel{\Delta}{=} \hat{x}_{k-1}$ , the sequential Least-Square estimator is derived from Eq. ( 5.2.19 ),

$$\hat{x}_k = \hat{x}_{k-1} + \frac{C_k^T R_k^{-1}}{P_{k-1}^{-1} + C_k^T R_k^{-1} C_k} [(y_k - c_k) + \frac{P_{k-1}^{-1}}{C_k^T R_k^{-1}} (\hat{x} - \hat{x}_{k-1})] \quad (5.2.20)$$

$$\text{As } \frac{P_{k-1}^{-1}}{R_k^{-1}} = \frac{\text{cov}(C_k \hat{x}_{k-1})}{\text{cov}(\hat{x}_{k-1})} = \frac{E[(C_k \hat{x}_{k-1})(C_k \hat{x}_{k-1})^T]}{E[\hat{x}_{k-1} \hat{x}_{k-1}^T]} = \frac{E[C_k \hat{x}_{k-1} \hat{x}_{k-1}^T C_k^T]}{E[\hat{x}_{k-1} \hat{x}_{k-1}^T]} = C_k C_k^T,$$

Rewrite Eq. ( 5.2.20 ) in a simple form,

$$\hat{x}_k = \hat{x}_{k-1} + \frac{C_k^T R_k^{-1}}{P_{k-1}^{-1} + C_k^T R_k^{-1} C_k} [(y_k - c_k) + C_k (\hat{x} - \hat{x}_{k-1})] \quad (5.2.21)$$

Where  $C_k$  and  $c_k$  are parameters associated with current observation  $k$ .

Simplify Eq. ( 5.2.21 ) to avoid matrix inverse computation for  $P$  and  $Q$ , and let  $\hat{x} = \hat{x}_{k-1}$ ,

$$\hat{x}_k = \hat{x}_{k-1} + \frac{P_{k-1} C_k^T}{R_k + C_k^T P_{k-1} C_k} (y_k - c_k) \quad (5.2.22)$$

$$\hat{x}_k = \hat{x}_{k-1} + K_k [y_k - c_k] \quad (5.2.23)$$

Where  $K_k$  is the Kalman gain, and rewritten in Eq. ( 5.2.24 ), the measurement update is shown below,

$$K_k = \frac{P_{k-1}C_k^T}{R_k + C_k P_{k-1} C_k^T} \quad (5.2.24)$$

The covariance matrix  $P_{k-1}$  can be updated from the measurement utilizing the Kalman gain in Eq. ( 5.2.24 ) from Eq. ( 5.2.23 ).

$$\text{cov}(\hat{x}_k) = \text{cov}(\hat{x}_{k-1} + K_k [y_k - c_k]) \quad (5.2.25)$$

As previous state is irrelevant with the current observation,

$$P_k = \text{cov}(\hat{x}_{k-1}) + \text{cov}(K_k [y_k - c_k]) \quad (5.2.26)$$

$$\begin{aligned} P_k &= P_{k-1} + K_k \text{cov}(-c_k) K_k^T \\ &= P_{k-1} - K_k \text{cov}(C_k x_{k-1} + v_k) \frac{C_k P_{k-1}^T}{(R_k + C_k P_{k-1} C_k^T)^T} \\ &= P_{k-1} - K_k (C_k P_{k-1} C_k^T + R_k) \frac{C_k P_{k-1}}{R_k + (C_k P_{k-1} C_k^T)^T} \\ &= P_{k-1} - K_k C_k P_{k-1} \end{aligned} \quad (5.2.27)$$

Thus, 
$$P_k = (I - K_k C_k) P_{k-1} \quad (5.2.28)$$

Because of the round off error,  $P_k$  may not maintain positive definite and therefore meaningless as covariance matrix. An alternative is to use the Joseph algorithm for the computation of  $P_k$ :

$$P_k = [I - K_k C_k] P_{k-1} [I - K_k C_k]^T + K_k R_k K_k^T \quad (5.2.29)$$

This algorithm requires more computations than Eq. ( 5.2.28 ), but can ensure that  $P_k$  will remain positive definite. The Joseph algorithm can be verified by substituting Eq. ( 5.2.24 ) to Eq. ( 5.2.28 ) as follows,

$$\begin{aligned} P_k &= (I - K_k C_k) P_{k-1} \\ &= P_{k-1} + [P_{k-1} C_k^T] K_k^T - K_k C_k P_{k-1} - P_{k-1} C_k^T K_k^T \\ &= P_{k-1} + [K_k (C_k P_{k-1} C_k^T + R_k)] K_k^T - K_k C_k P_{k-1} - P_{k-1} C_k^T K_k^T \\ &= P_{k-1} + K_k C_k P_{k-1} C_k^T K_k^T - K_k C_k P_{k-1} - P_{k-1} C_k^T K_k^T + K_k R_k K_k^T \\ &= [P_{k-1} - K_k C_k P_{k-1}] [I - C_k^T K_k^T] + K_k R_k K_k^T \\ &= [I - K_k C_k] P_{k-1} [I - K_k C_k]^T + K_k R_k K_k^T \end{aligned} \quad (5.2.30)$$



Eq. ( 5.2.30 ) indicates that the two methods are analytically equivalent for any  $K$  defined by Eq. ( 5.2.24 ).

In conclusion, Eq. ( 5.2.23 ), Eq. ( 5.2.24 ) and Eq. ( 5.2.28 ) verified the Measurement Update in the Kalman filter algorithm is optimal under Least-square optimization.

Figure 5.3 below summaries the ongoing recursive process for the discrete Kalman filtering for real-time digital computation,

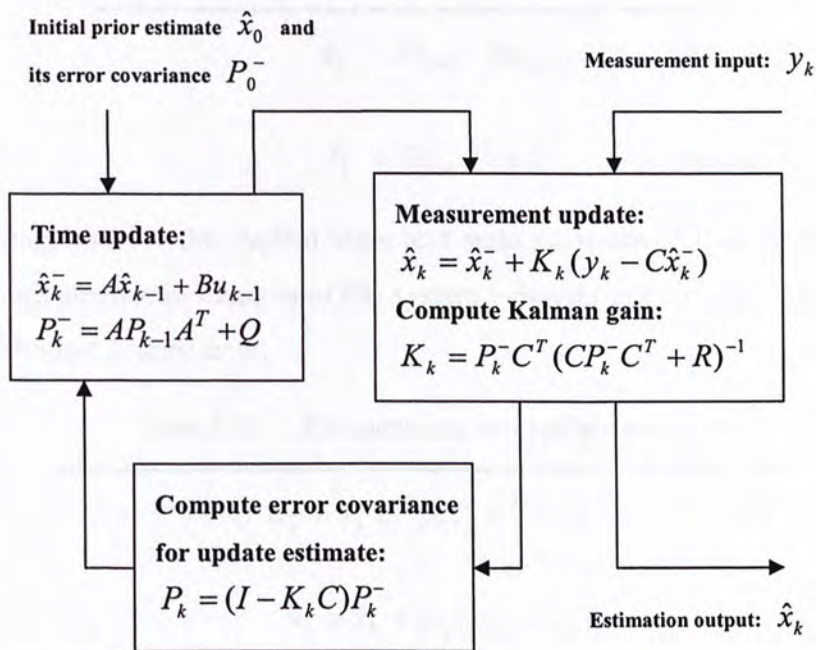


Figure 5.3: Block Diagram of Kalman Filter in Real Time Application [1]

### 5.3. Kalman Filter Summary

From the recursive estimation process, the Kalman filter estimates the state vector  $x_k$  directly based on all measurement observation up to current observation  $y_k$ . The dynamic propagation and observation models are evaluated between filter cycles. The ongoing process of Kalman filter only requires memory for the previous step estimate, compared to intensive data block for observations and priori estimates in the Batch least-square estimator. The stochastic information leading to the feedback gain in the random noise control is compressed in the mean and covariance matrix, which is updated for each measurement. Thus, Kalman filter is useful for onboard application

because the process loop does not involve the estimation results and past observations. The computation complexity only depends on updating the state transition and state noise covariance matrix. In consequence, the Kalman filter is constantly capable to estimate the current state in real time.

The complete equations of the time update and measurement update stage of the Kalman filter are listed in the Table 5.1 and Table 5.2 below. The equations in discrete model are for real-time application, which is preferable for digital systems.

Table 5.1: KF time update equations

---


$$\hat{x}_k^- = A\hat{x}_{k-1} + Bu_{k-1} \quad (5.3.1)$$

$$P_k^- = AP_{k-1}A^T + Q \quad (5.3.2)$$

After propagation for the system state and state error covariance ahead in the time update, these stochastic features of the system behavior are corrected in measurement update with least square error.

Table 5.2: KF measurement update equations

---


$$K_k = P_k^- C^T (CP_k^- C^T + R)^{-1} \quad (5.3.3)$$

$$\hat{x}_k = \hat{x}_k^- + K_k (y_k - C\hat{x}_k^-) \quad (5.3.4)$$

$$P_k = (I - K_k C)P_k^- \quad (5.3.5)$$

However, as proved in this chapter, the Kalman filter is the optimal solution to linear system. If the system plant is nonlinear, the filtering performance and estimation accuracy can not be guaranteed. Thus, the extended Kalman filter is introduced in the following chapter.



## 6. Extended Kalman Filter

Kalman filter is the optimal estimator in linear fitting problem. In applications, the linear model can not describe all real systems. In such case, the Kalman filter model will ignore nonlinearity in propagation of the state mean and covariance. As a result, this may lose accuracy in the measurement update and cause error to compute the feedback gain [35].

The nonlinear system can be linearized to summation of Taylor's expansion.

$$y = f(x) = f(\bar{x} + \delta) = f(\bar{x}) + \nabla f_{\bar{x}} \delta_x + \frac{1}{2} \nabla^2 f_{\bar{x}} \delta_x^2 + \frac{1}{3!} \nabla^3 f_{\bar{x}} \delta_x^3 + \dots \quad (5.3.1)$$

The expansion involves infinite parameters for calculation. When  $\delta_x$  is small, the Jacobian linearized approximation can be accurate enough and tolerable.

$$y \approx f(\bar{x}) + \nabla f_{\bar{x}} \delta_x \quad (5.3.2)$$

Apply the linearization method, normally first order derivative, to improve the estimation of the state mean and covariance, and combine the Least-square optimal feedback structure from Kalman filter, the nonlinear data fitting problem is addressed by the extended Kalman filter [34]. The accuracy of system approximation can improve if higher order term is considered.

Eq. ( 5.3.3 ) and Eq. ( 5.3.4) below illustrate the equations of extended Kalman filter improved from Kalman filter.

$$x_k \approx \tilde{x}_k + A(x_{k-1} - \hat{x}_{k-1}) + Ww_{k-1} \quad (5.3.3)$$

$$y_k \approx \tilde{y}_k + C(x_k - \tilde{x}_k) + Vv_k \quad (5.3.4)$$

Where  $x_k$  and  $y_k$  are the actual states,  $\tilde{x}_k$  is the approximated state and  $\tilde{y}_k$  is the measurement vector.  $\hat{x}_{k-1}$  is the optimal estimation of previous step.  $w_k$  and  $v_k$  are random variables stand for the process and measurement noise.

$A$  is the Jacobian matrix by the partial differentiation of  $f$  with respect to  $x$ .

$$A_{[i,j]} = \frac{\partial f_{[i]}}{\partial x_{[j]}}(\hat{x}_{k-1}, u_{k-1}, 0) \quad (5.3.5)$$

$W$  is the Jacobian matrix by partial differentiation of  $f$  with respect to  $w$ .

$$W_{[i,j]} = \frac{\partial f_{[i]}}{\partial w_{[j]}}(\hat{x}_{k-1}, u_{k-1}, 0) \quad (5.3.6)$$

$C$  is the Jacobian matrix by partial differentiation of  $c$  with respect to  $x$ .

$$C_{[i,j]} = \frac{\partial c_{[i]}}{\partial x_{[j]}}(\tilde{x}_k, 0) \quad (5.3.7)$$

$V$  is the Jacobian matrix by partial differentiation of  $c$  with respect to  $v$ .

$$V_{[i,j]} = \frac{\partial c_{[i]}}{\partial v_{[j]}}(\tilde{x}_k, 0) \quad (5.3.8)$$

Table 6.1 and Table 6.2 illustrate the complete equations of time update and measurement update stage of the extended Kalman filter. The error covariance propagation is enhanced by Jacobian linearization in Eq. ( 5.3.10 ).

Table 6.1: EKF time update equations

---


$$\hat{x}_k^- = f(\hat{x}_{k-1}, u_{k-1}, 0) \quad (5.3.9)$$

$$P_k^- = A_k P_{k-1} A_k^T + W_k \cdot Q_{k-1} \cdot W_k^T \quad (5.3.10)$$

By linearization to compensate the error covariance, the measurement update of extended Kalman filter improved in Kalman gain in Eq. ( 5.3.11 ).

The Eq. ( 5.3.12 ) for feedback is in the similar framework as Eq ( 5.3.4 ). in the Kalman filter. Eq. ( 5.3.13 ) could be substituted with Eq. ( 5.2.29 ) using Joseph algorithm for stable performance.



Table 6.2: EKF measurement update equations

$$K_k = P_k^- C_k^T (C_k P_k^- C_k^T + V_k R_k V_k^T)^{-1} \quad (5.3.11)$$

$$\hat{x}_k = \hat{x}_k^- + K_k (y_k - c(\hat{x}_k^-, 0)) \quad (5.3.12)$$

$$P_k = (I - K_k C_k) P_k^- \quad (5.3.13)$$

As being the linearization approximation of nonlinear system:  $\hat{x}_k^- \approx f(\hat{x}_{k-1}, u_{k-1}, 0)$ ,  $y_k \approx c(\hat{x}_k^-, 0)$ , the extended Kalman filter can be designed to operate more stably and accurately if higher order terms are analyzed, such as the Hessian matrix for the second derivative of the system [39]. However, constructing the partial derivative of a dynamic system can be difficult to implement. Furthermore, the higher order residuals of the system expansion request costly computational resource.

In [37], an effective quaternion based extended Kalman filter has been designed. A Gauss-Newton algorithm is introduced to combine observations from the accelerometers and magnetometers to estimate the attitude as observation for measurement update. The EKF is implemented to minimize the error between this attitude estimation and the propagation from the gyroscopes. The attitude quaternion as system state is normalized in system plant during each time update step.

# 7. Attitude Extended Kalman Filter

The extended Kalman filter consists of two stages. In the time update stage, the quaternion increment by the gyroscopes will propagate the attitude in time. In the measurement update stage, the difference between the estimated and the measured Earth magnetic vector is implemented as feedback to correct the propagation error [36].

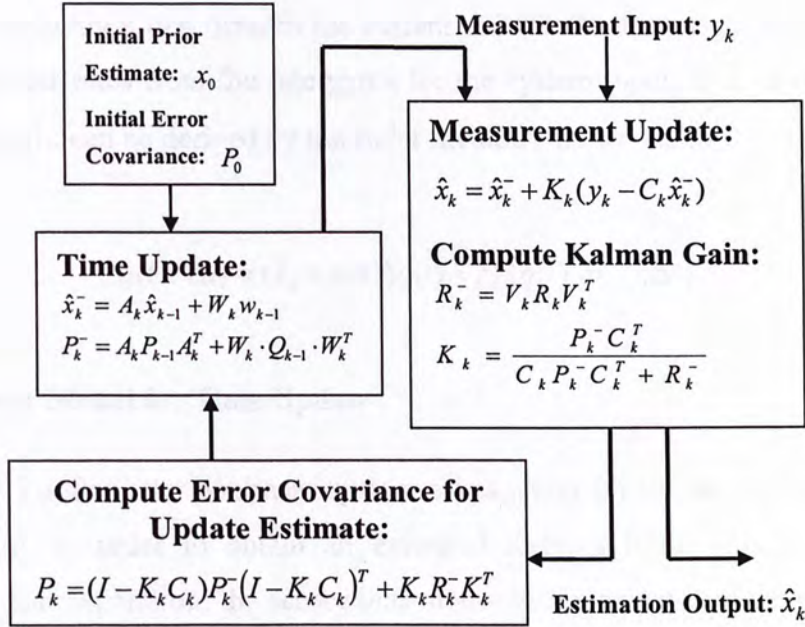


Figure 7.1: Block Diagram of Extended Kalman Filter Algorithm

Figure 7.1 demonstrates the real-time recursive process of the extended Kalman filter algorithm.

## 7.1. Time Update Model

### 7.1.1. Attitude Strapdown Theory for a Quaternion

In order to propagate the attitude in time, the quaternion kinematics equation is:

$$\dot{q}(t) = \Omega(\omega_i)q(t) \tag{7.1.1}$$



Where

$$\Omega(\omega_t) = \frac{1}{2} \begin{bmatrix} 0 & \omega_z & -\omega_y & \omega_x \\ -\omega_z & 0 & \omega_x & \omega_y \\ \omega_y & -\omega_x & 0 & \omega_z \\ -\omega_x & -\omega_y & -\omega_z & 0 \end{bmatrix} \quad (7.1.2)$$

$$q(t) = [q_1 \quad q_2 \quad q_3 \quad q_4]^T \quad (7.1.3)$$

$$\omega_t = [\omega_x \quad \omega_y \quad \omega_z]^T \quad (7.1.4)$$

$q(t)$  is the quaternion that denotes the current attitude for the system state.  $\omega_t$  are the current angular rates from the rate gyros for the system input. If  $\Delta t$  is small enough, the state matrix can be derived by the Euler method:  $\Delta t = t - t_0 \rightarrow 0$ ,

$$q(t + \Delta t) \approx (I_4 + \Delta t \Omega) q(t) = f_{\Delta t}^{\Delta}(q(t), \omega_{t+\Delta t}, \Delta t) \quad (7.1.5)$$

### 7.1.2. Error Model for Time Update

Eq. ( 7.1.5 ) defines the nonlinear system propagation for the state  $q$  and input  $\omega$  in time update. In order to obtain an extended Kalman filter with a capability of gyroscope bias separation, the sensor bias model is implemented in the state matrix by error dynamics analysis [39], [40].

We define the state error of a gyro as  $\delta\omega$ :

$$\omega_{true} = \omega_{sensor} - \delta\omega \quad (7.1.6)$$

$$\delta\omega(t) = \Delta\omega_{bias}(t) + w(t) \quad (7.1.7)$$

Where  $w(t)$  is a sensor's white noise, and  $\Delta\omega(t)$  is the gyro bias which is considered as constant since  $dt$  is small:

$$\Delta\omega(t + \Delta t) = \Delta\omega(t) \quad (7.1.8)$$

The propagation of the attitude state error,  $\delta q$  can be obtained by partial differentiation

of Eq. ( 7.1.5 ):

$$\delta q(t + \Delta t) = \frac{\partial f_{\Delta t}(t)}{\partial \omega(t)} \delta \omega(t) + \frac{\partial f_{\Delta t}(t)}{\partial q(t)} \delta q(t) \quad (7.1.9)$$

When time step  $dt$  and the previous  $\delta q$  is small, we assume:

$\frac{\partial f_{\Delta t}(t)}{\partial q(t)} \delta q(t) \approx 0$ . By Jacobian Linearization:

$$\frac{\partial f_{\Delta t}(t)}{\partial \omega(t)} = \frac{1}{2} \cdot \begin{bmatrix} q_4 & -q_3 & q_2 \\ q_3 & q_4 & -q_1 \\ -q_2 & q_1 & q_4 \\ -q_1 & -q_2 & -q_3 \end{bmatrix} \Delta t = W_k \Delta t \quad (7.1.10)$$

From Eq. ( 7.1.5 ) and Eq. ( 7.1.9 ), the gyroscope bias can be separated from the system state:

$$q_k = f_{dt}(q_{k-1}, \omega_k, dt) - \delta q_k \quad (7.1.11)$$

Thus the Discrete Time Update is:

$$q_k = q_{k-1} + \Omega(\omega_k - \Delta \omega) \cdot q_{k-1} \cdot dt + W_k \delta \omega \quad (7.1.12)$$

In the state space representation,

$$x_{k+1} = A_k x_k + W_k w_k \quad (7.1.13)$$

Where,

$$x_k = [q_k \quad \Delta \omega_k]^T \quad (7.1.14)$$

$$A_k = \begin{bmatrix} [I_4 + \Omega(\omega_k - \Delta \omega_{k-1}) \cdot dt]_k & -\frac{\partial f_{\Delta t}(t)}{\partial \omega(t)} \\ 0 & I \end{bmatrix} \quad (7.1.15)$$

## 7.2. Measurement Update Model

After extended Kalman filter estimation, the spatial magnetic field disturbance



becomes tolerable within one stroke and the Earth's magnetic field direction remains constant within the whiteboard. It can be utilized as reference for attitude in the measurement update. The three orthogonal magnetometers in the MAG- $\mu$ IMU measure the geomagnetic field with respect to (W.R.T.) the body frame. On the other hand, by coordinate transform using the propagated attitude, it can be estimated from the constant geomagnetic field WRT the Earth frame. Hence the difference between the magnetometer measurements and the transformed geomagnetic field is feedback in the measurement update of the extended Kalman filter to correct for the error in attitude propagation [41], [42].

Vector  $\bar{q}_b$ ,  $\bar{q}_e$  are introduced to represent the geomagnetic field WRT the Earth frame and the magnetometer outputs, respectively. The two vectors are expanded into quaternions:  $M_{body} = [\bar{q}_b \ 0]^T$ ,  $M_{earth} = [\bar{q}_e \ 0]^T$ .

If quaternion  $n$  denotes the current attitude, by coordinate transform from Eq. ( 4.2.2 ),

$$M_{body} = n^* \otimes M_{earth} \otimes n \quad (7.2.1)$$

Multiply the quaternion  $n$  to both sides of Eq. ( 7.2.1 ), we obtain:

$$n \otimes M_{body} - M_{earth} \otimes n = 0 \quad (7.2.2)$$

$$\begin{bmatrix} -[\bar{q}_b]_{\times} & \bar{q}_b \\ -\bar{q}_b^T & 0 \end{bmatrix} n - \begin{bmatrix} [\bar{q}_e]_{\times} & \bar{q}_e \\ -\bar{q}_e^T & 0 \end{bmatrix} n = 0 \quad (7.2.3)$$

Where  $[\bar{q}]_{\times}$  is the cross product matrix:

$$[\bar{q}]_{\times} = \begin{bmatrix} 0 & -q_3 & q_2 \\ q_3 & 0 & -q_1 \\ -q_2 & q_1 & 0 \end{bmatrix} \quad (7.2.4)$$

From Eq. ( 7.2.3 ):

$$\begin{bmatrix} -[(\bar{q}_b + \bar{q}_e)]_{\times} & \bar{q}_b - \bar{q}_e \\ -(\bar{q}_b - \bar{q}_e)^T & 0 \end{bmatrix} n = 0 \quad (7.2.5)$$

$$C = \frac{\Delta 1}{2} \begin{bmatrix} -[(\bar{q}_b + \bar{q}_e)] \times & \bar{q}_b - \bar{q}_e \\ -(\bar{q}_b - \bar{q}_e)^T & 0 \end{bmatrix} \quad (7.2.6)$$

Thus, there is no requirement for the state  $q$  to be a unit quaternion. Let  $C$  be the measurement matrix. The measurement update of the extended Kalman Filter is:

$$y = Cq \quad (7.2.7)$$

### 7.2.1. Error Model for the Measurement Update

According to error dynamics analysis [39], [40], Let:

$$\delta q_k = q_k - q_k' \quad (7.2.8)$$

$$\delta y = \frac{\partial y}{\partial q_b} \delta q_b + \frac{\partial y}{\partial q_e} \delta q_e + \frac{\partial y}{\partial q} \delta q \quad (7.2.9)$$

Where  $\frac{\partial y}{\partial q_{be}} \delta q_{be} = 0$ ,  $\frac{\partial y}{\partial q_b} \delta q_b \approx 0$  when the previous attitude state error is small.

From Eq. (7.2.7):

$$\frac{\partial y}{\partial q_b} = \frac{1}{2} \begin{bmatrix} q_4 & -q_3 & q_2 \\ q_3 & q_4 & -q_1 \\ -q_2 & q_1 & q_4 \\ -q_1 & -q_2 & -q_3 \end{bmatrix} \quad (7.2.10)$$

Thus the Discrete Measurement Update is:

$$y_k = C_k q_k - V_k \delta q_k \quad (7.2.11)$$

Where,

$$V_k = -\frac{\partial y}{\partial q_b} \quad (7.2.12)$$



### 7.3. Summary

A mathematical derivation method is introduced to derive an extended Kalman filter to minimize random noise and input bias error. The attitude calculation is totally based on a quaternion. As proved in Eq. ( 7.2.5 ), the attitude quaternion  $q$  does not need to be unified in iteration. Further, any reference field sensor, such as star sensors and accelerometers, or a combination, can be applied to this process model.

Equation 7.1.7 can be modified from Eq. ( 7.2.5 ). The gravity of the Earth is assumed to be parallel to the vertical axis in the Earth frame. Thus,

$$\frac{d}{dt} \begin{bmatrix} q_0 \\ q_1 \\ q_2 \\ q_3 \end{bmatrix} = \begin{bmatrix} -\omega_0 q_0 + \omega_1 q_1 + \omega_2 q_2 + \omega_3 q_3 \\ \omega_0 q_1 - \omega_1 q_0 + \omega_2 q_3 - \omega_3 q_2 \\ \omega_0 q_2 + \omega_1 q_3 - \omega_2 q_0 - \omega_3 q_1 \\ \omega_0 q_3 - \omega_1 q_2 + \omega_2 q_1 - \omega_3 q_0 \end{bmatrix}$$

where  $\omega = [\omega_0 \ \omega_1 \ \omega_2 \ \omega_3]^T$

However, star sensors are reliable in many more applications but are directional in their nature. Shown in Figure 8.1 and Figure 8.2 below, the experimental setup using the MATLAB/SIMULINK decomposes the inertial acceleration into a specific horizontal acceleration, which can be separated from each other in the vertical and horizontal planes. The rotation angle of the sensor is 45 degrees. Before rotation, the sensor is aligned with the vertical axis. However, during rotation, the sensor is rotated to the horizontal plane. The angle, which can be interpreted into the rotation angle of the sensor, is the rotation angle.

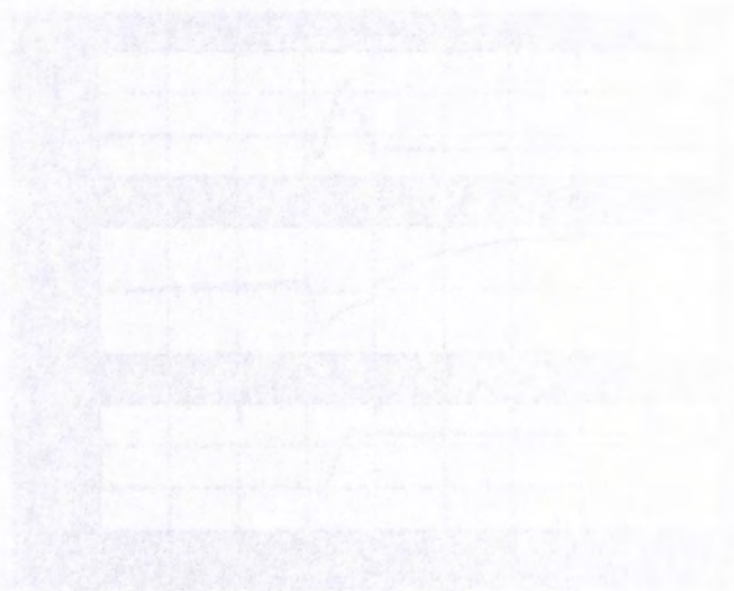


Figure 8.1 Attitude Estimation Results (45 degree rotation)

# 8. Experiment Results

## 8.1. Experiment for Attitude EKF based on MAG-μIMU

In pervious work, the attitude extended Kalman filter is implemented using accelerometers for feedback. The measurement model for accelerometer tilter based attitude EKF can be modified from Eq. ( 7.2.6 ). The gravity as reference is along the negative Z direction in the Earth frame. Thus,

$$C = \frac{\Delta}{2} \begin{bmatrix} -[(\bar{q}_b + \bar{q}_e)] \times & \bar{q}_b - \bar{q}_e \\ -(\bar{q}_b - \bar{q}_e)^T & 0 \end{bmatrix} \quad (8.1.1)$$

Where,  $\bar{q}_e = [0 \quad 0 \quad -1]^T$  (8.1.2)

However, accelerometers are reliable in motionless applications but are undependable during motion. Shown in Figure 8.1 and Figure 8.2 below, the experimental data from the MAG-μIMU demonstrates that inertial accelerations interfere with gravitational accelerations, which cannot be separated from each other. In this experiment, the pen was rotated from 0 degree to 45 degree. Before rotation and afterward, the filter tracked quickly and accurately. However, during motion, the filter was affected by the accelerometers' Euler angles, which can be interpreted into two rotations because of the acceleration and deceleration.

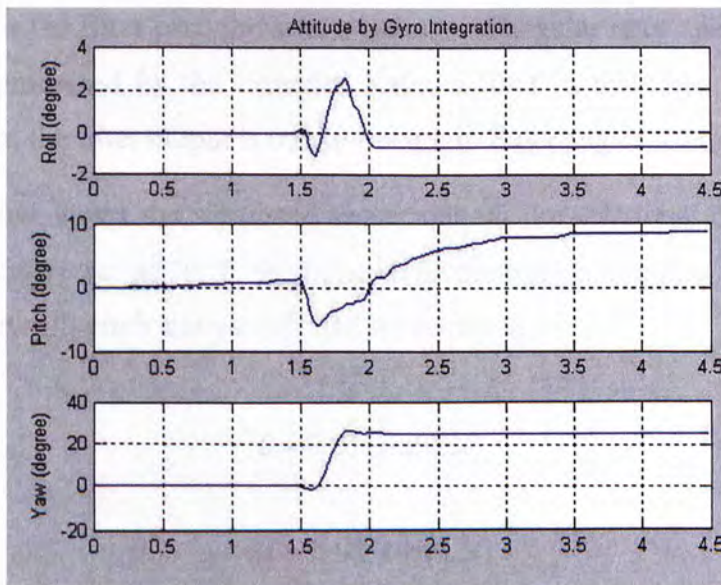


Figure 8.1: Accelerometers EKF: Attitude by Gyroscope Propagation



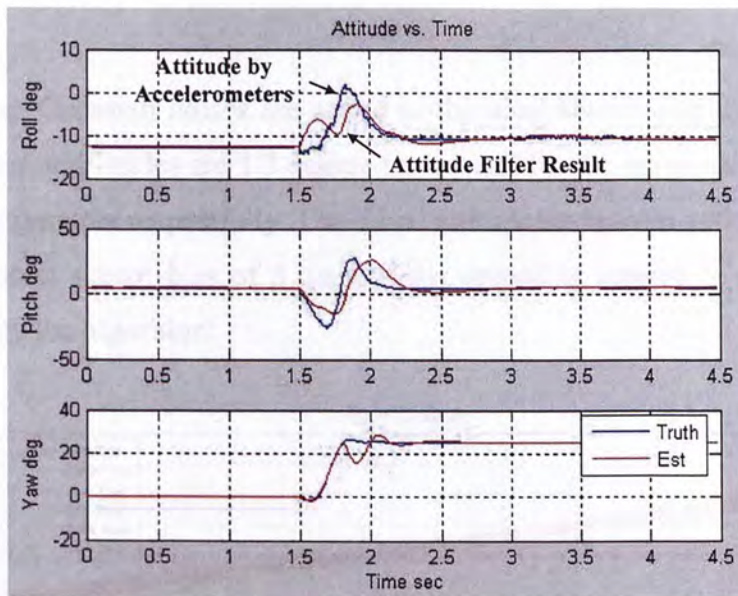


Figure 8.2: Accelerometers EKF: Filter Result & Accelerometer Attitude

### 8.1.1. Simulation Test

Extensive simulation experiments are performed to check the convergence of the MAG Extended Kalman filter. The simulation software includes two parts: the sensor output generation and the real-time filtering. In order to generate the sensor output, the digital pen's physical properties and motion are modeled by the mass, inertia matrix, input forces and torques. The kinematics and dynamics module calculates the accelerations, angular rates and magnetic field strength under ideal conditions. The sensors' outputs are synthesized by aliasing the random Gaussian noise and constant sensor bias. For the filter part, the sensor outputs of angular rates and magnetic field strengths are processed by the extended Kalman filter in real-time. The attitude-in-quaternion from the filter output is transformed into Euler angles for display.

Figure 8.3 below shows the simulated sensor output. For rotational motion analysis, the input forces are set as  $[0, 0, 0]$ . In order to simulate a complex orientation, the torque vector in roll, pitch and yaw:  $[L, M, N]$  are set as:

$$L = 0.01 \cdot \sin(0.3t) \quad (8.1.3)$$

$$M = 0.01 \cdot \cos(0.3t) \quad (8.1.4)$$

$$N = 0.01 \quad (8.1.5)$$

The zero mean Gaussian noises are added to the ideal sensor outputs. The absolute maximum error amplitudes are 1.3 degree per second for the gyros and 0.04 Oersteds for the magnetometers respectively. The initial attitude starts from 100 degrees in yaw angle. A constant sensor bias of 5 degrees per second is applied in yaw gyroscope output to verify the algorithm:

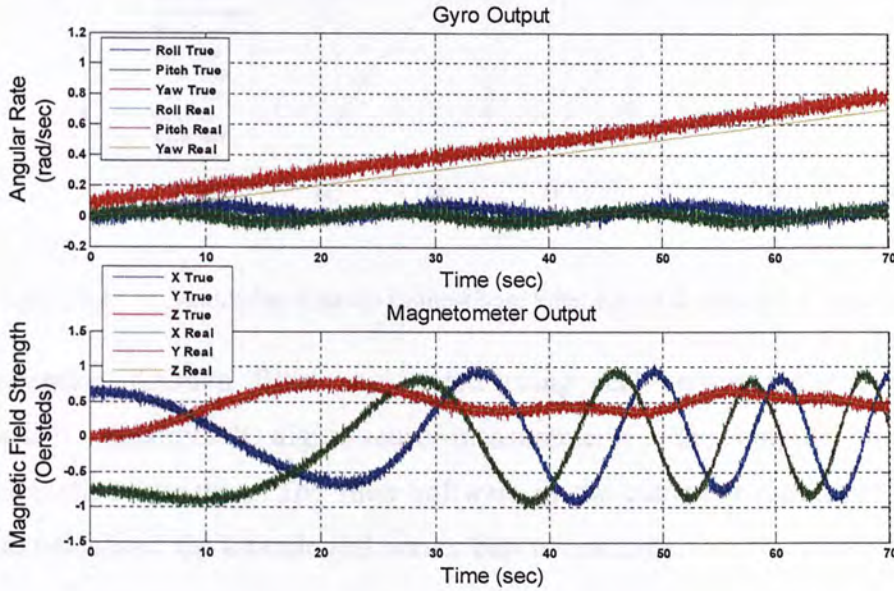


Figure 8.3: Synthetic Sensor Measurement

### 8.1.2. Experiment Test

Figure 8.4 illustrates the attitude result displayed in Euler angles. With the tracking ability of the extended Kalman filter, the initialization of the system state is simple. The attitude quaternion and gyro biases are set to zero. After iteration, the extended Kalman filter will estimate the gyro bias and remove it from the system state. According to magnetometer feedback, the filter's attitude estimation will converge and keep tracking automatically. The dash line in Figure 8.4 shows the attitude propagated by the raw output from the gyroscopes. As shown in the figure, the random noise and bias error causes a large drift in the rolling, pitching and yawing compared with the filter output.



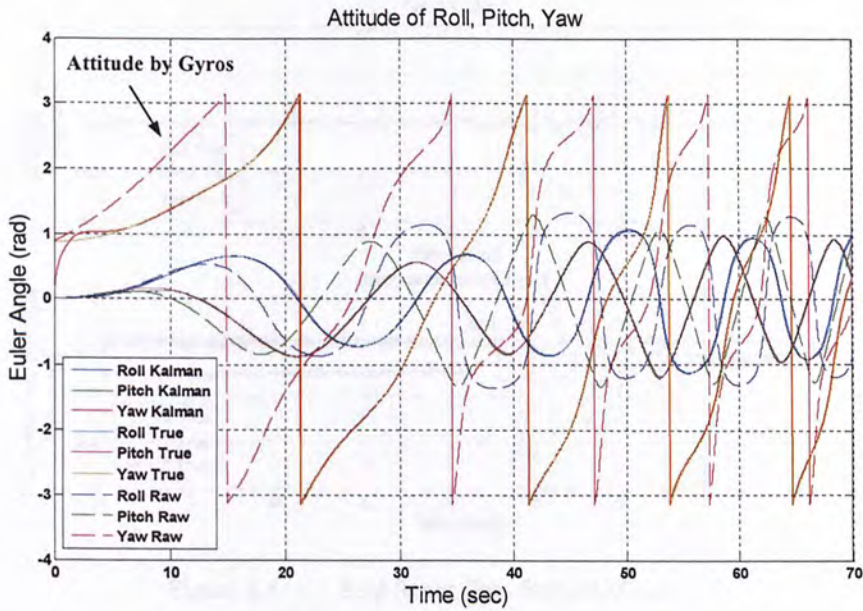


Figure 8.4: Simulation Attitude Comparison: Filter Result & Gyroscope Propagation

The extended Kalman filter was tested using real sensor measurements. The MAG- $\mu$ IMU transmits the digital sensor measurements to the computer wirelessly via the Bluetooth connection. The filter software in the computer processed the sensor data and calculated the attitude and sensor bias in real time.

The MAG- $\mu$ IMU was held still for 4 seconds. Then continuous 90 degrees rotations were performed to test the tracking performance. The sensor module was rotated counterclockwise for 90 degrees and clockwise back to 0 degrees along the sensing axis of the roll gyroscope. At the end of the 7th rotation, the MAG- $\mu$ IMU was suddenly held still again to test the convergence capability from dynamic input to static input.

Figure 8.5, Figure 8.6 below show the six raw sensor output and the estimated attitude in Euler angles. Within the first iteration, the estimated attitude converged according to the observations from the magnetometers. The dash lines show the attitude propagated by raw output from the gyroscopes. The sensor errors accumulated and caused the attitude drift.

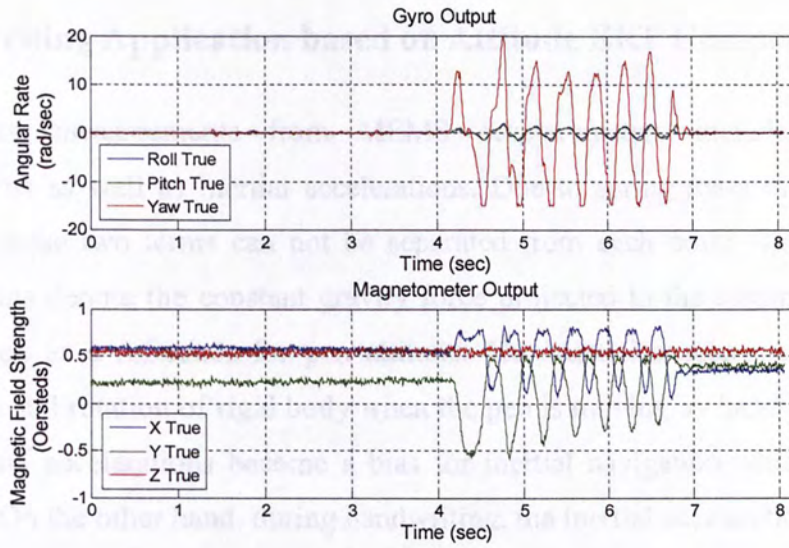


Figure 8.5: Real Sensor Data from MAG- $\mu$ IMU

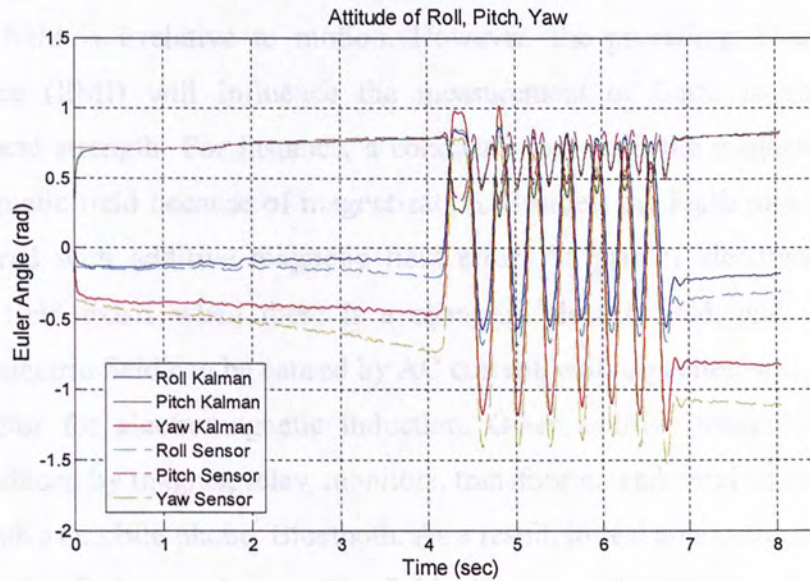


Figure 8.6: Experiment Attitude Comparison: Filter Result & Gyroscope Propagation



## 8.2. Writing Application based on Attitude EKF Compensation

The sensor measurements from MEMS accelerometers include gravitational accelerations as well as inertial accelerations. Due to spring mass model of sensor structure, these two terms can not be separated from each other. The gravitational accelerations denote the constant gravity force projected to the sensing axes, which can be used as a reference for pen attitude. The inertial accelerations specify the translation and rotation of rigid body when the pen is moving by handwriting. Hence, gravitational accelerations become a bias for inertial navigation which needs to be balanced. On the other hand, during handwriting, the inertial acceleration interfere the reference attitude calculation.

Magnetometers for attitude reference don't have such disturbance because the magnetic field is irrelative to motion. However, the prevailing Electro Magnetic Interference (EMI) will influence the measurement of Earth magnetic field in direction and strength. For instance, a conductor can bend the magnetic flux of the Earth magnetic field because of magnetization. Besides, the Earth measurement may be interfered with additive magnetic field error. As part of electromagnetic field, magnetic field exists when there is a changing electric field, and vice versa. A changing electric field can be caused by AC current, coil, capacitor, and antenna effect of conductor for electromagnetic induction. Other additive magnetic source may directly induced by magnet, relay, monitors, transformer, and wireless communication device, such as mobile phone, Bluetooth. As a result, in real applications, the direction and strength of measured magnetic field changes with different position due to complex environment.

Furthermore, attitude from the accelerometer or magnetometer has ambiguity along the reference field direction, which is in yaw and roll direction respectively.

Assume the magnetic field noise is tolerable within one stroke space for handwriting application; the tracking problem of pen attitude is addressed by a complementary filter combining the ACC-EKF and MAG-EKF. In time update, the attitude is propagated by angular rates based on quaternion model. In measurement update, during handwriting, the magnetometer model is implemented as attitude reference with no inertial noise; and in motionless stage between strokes, the estimation error



caused by EMI can be rectified by accelerometers working as gravity tilter. The measurement update from the combination of ACC-EKF and MAG-EKF is complementary to filter the reference error and compensate the attitude ambiguity for each other.

For complementary EKF, the measurement model of the attitude EKF,  $y = Cq$ , as introduced in Eq. ( 7.2.6 ).

$$C = \frac{\Delta 1}{2} \begin{bmatrix} -[(\bar{q}_b + \bar{q}_e)] \times & \bar{q}_b - \bar{q}_e \\ -(\bar{q}_b - \bar{q}_e)^T & 0 \end{bmatrix} \quad (8.2.1)$$

Where  $\bar{q}_b$  is the measurement vector for the gravitational field or magnetic field as attitude reference. The  $\bar{q}_e$  denotes the reference field vector in the Earth frame.  $\bar{q}_e = [0 \ 0 \ -1]^T$  is applied for accelerometer tilters and  $\bar{q}_e = [1 \ 0 \ 0]^T$  is for magnetometers.

However, for continuous handwriting, the magnetic field varies in direction and strength corresponding to different places such that  $\bar{q}_e \neq [1 \ 0 \ 0]$ . For the complementary attitude EKF, before switching from accelerometer attitude feedback, the magnetometer measurement should be synchronized for the magnetic reference difference. From Eq. ( 4.2.4 ) and Eq. ( 4.2.5 ), the measurement update model should be calibrated and initialized as,

$$\bar{q}_e = \text{NORM}(R(\bar{q}) \cdot \bar{q}_b) \quad (8.2.2)$$

Where

$$R(\bar{q}) = \begin{bmatrix} q_1^2 - q_2^2 - q_3^2 + q_4^2 & 2(q_1q_2 + q_3q_4) & 2(q_1q_3 - q_2q_4) \\ 2(q_1q_2 - q_3q_4) & -q_1^2 + q_2^2 - q_3^2 + q_4^2 & 2(q_2q_3 + q_1q_4) \\ 2(q_1q_3 + q_2q_4) & 2(q_2q_3 - q_1q_4) & -q_1^2 - q_2^2 + q_3^2 + q_4^2 \end{bmatrix} \quad (8.2.3)$$

The  $\bar{q}$  is latest the attitude filter tracking result and  $\bar{q}_b$  is the first magnetometer observation after the switch. The writing and pause of hand motion status for the Sync Switch can be implemented by the Stroke Segment Kalman Filter which will be introduced later. Figure 8.7 below demonstrates the diagram of the complementary attitude EKF for real-time handwriting application.



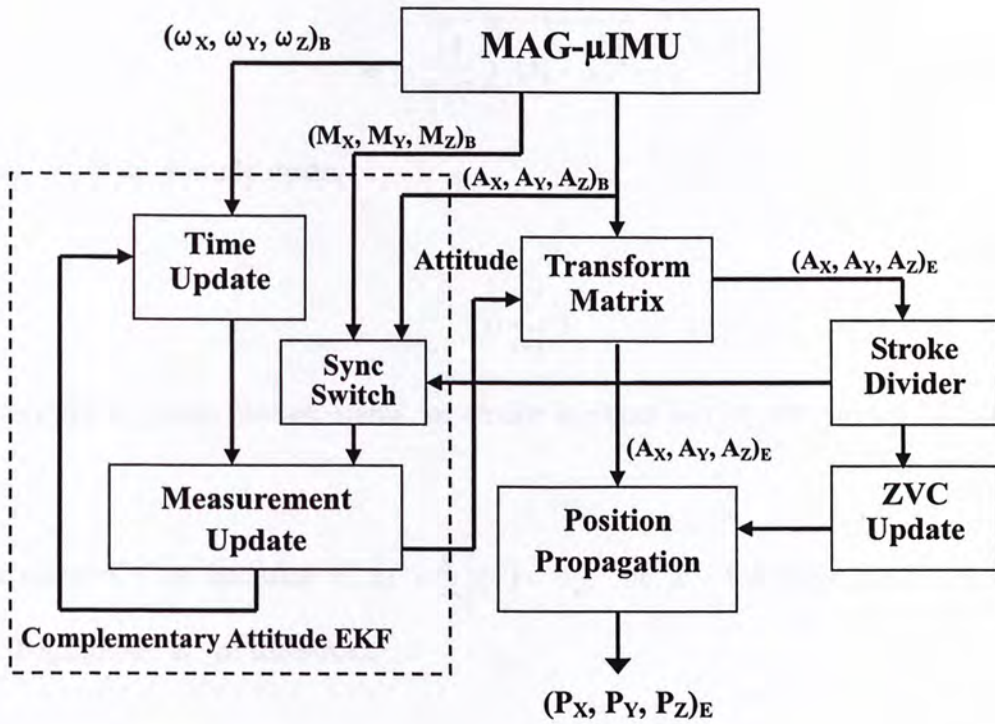


Figure 8.7: Complementary Attitude EKF Diagram

### 8.2.1. Stroke Segment Kalman Filter

The stroke segment algorithm is proposed by [51] to separate the continuous pen-tip movement of character writing into independent strokes. The velocity of the pen-tip equals to zero at the turning point between two consecutive strokes. This Motionless phase in handwriting is important to compensate the error in attitude estimation and the position integration.

In [51], the stroke segment is implemented based on the sample variance of inertial measurements. In probability theory, the variance of a random variable is a measure of the spread around its expected value. The sample variance is the approximation for variance with finite size  $N$  in real application. For the  $N$  sample set, the sample variance equals to the unbiased mean square error, which indicates the scale of values of the sample set. Hence, the intensity of handwriting motion can be described by the sample variance of corresponding acceleration sample set in real-time.

For computational efficiency, a First-in First-out (FIFO) stack is preferred to store and process the successive sample data. The sample variance with window length  $N$  can be calculated as,

$$\sigma = \sqrt{\frac{1}{N} \sum_{i=1}^N (x_i - \bar{x})^2} \quad (8.2.4)$$

Where  $\bar{x}$  is the sample mean,

$$\bar{x} = \frac{1}{N} \sum_{i=1}^N x_i \quad (8.2.5)$$

The writing or pause motion status for stroke segment can be determined as follows [51].

For a sampled time instance  $k$ , if  $\sigma_{|A_n|}^S(\kappa) < \sigma_{th}$  for  $\kappa = k, k+1, \dots, k+H$ , then  $k$  is the beginning  $k_1$  of the stroke.

For a sampled time instance  $k > k_1 + W$ , if  $\sigma_{|A_n|}^S(\kappa) > \sigma_{th}$  for  $\kappa = k, k+1, \dots, k+H$ , then  $k - S$  is the end  $k_2$  of this stroke.

Where  $\sigma_{|A_n|}^S(k)$  is a standard variance of  $|A_n|$  over  $S$  samples until  $k$ ,  $\sigma_{th}$  is a threshold of the standard deviation.  $W$  is the minimum number of samples for writing a stroke, and  $H$  is the minimum number of samples to keep  $\sigma_{|A_n|}^S(k)$  being less than  $\sigma_{th}$ .

As the unbiased motion intensity estimator of sample variance, the stroke segment algorithm does not have the concern of gravitational accelerations which is changing with pen attitude. The sample variance evaluates in stochastics from the entire sample set block. This macroscopic information can efficiently discriminate hand motions by writing or trembling. However, the  $\sigma_{th}$ ,  $W$  and  $H$  should be predefined. These parameters have to try and test in calibration. The recognition efficiency may vary with characters of different size, especially for different experimenter when the handwriting habit is different.

As the approximation to the expected variance, the error in sample variance caused in sampling may magnify to motion segment error when the sample set data are



symmetric near inflexion point as illustrated in Figure 8.8 below,

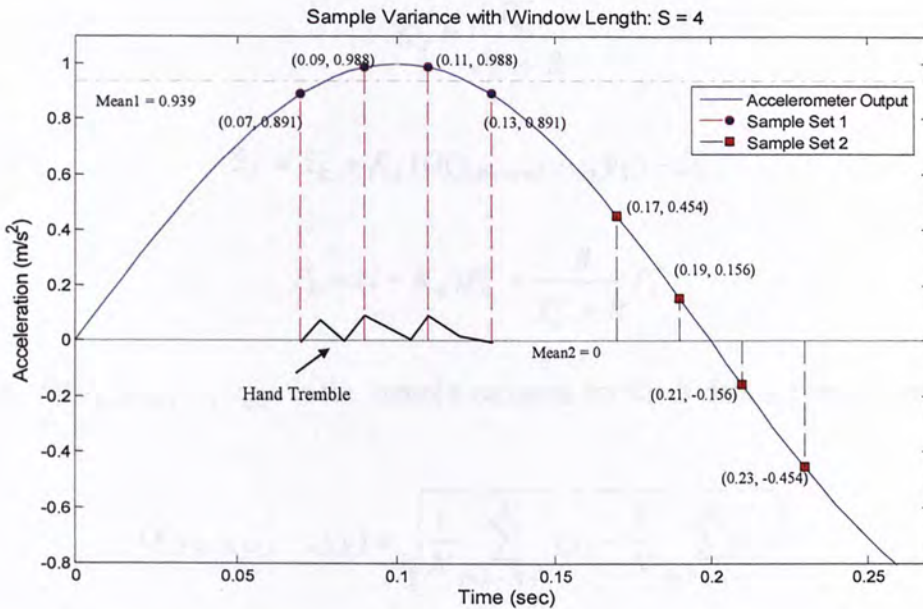


Figure 8.8: Acceleration variance underestimates motion intensity (velocity) due to sampling error

Suppose acceleration signal for handwriting is a one-interval sine wave of 2.5 Hz as demonstrated in blue curve. And the sample rate of the digital system is 50 Hz which satisfies the Nyquist sampling theorem. The window length for sample variance is 4 for quick response. The sample variance for the first sample set equals to 0.0485. On the other hand, after one measurement, the sample variance for the second sample set equals to 0.3394. A trivial hand tremble signal simulated in black line has the same sample variance as the first sample set. However, the pen-tip is accelerating during first sample set around 0.1 second until the stroke ended at 0.4 second when the velocity decelerate to zero.

Thus a Kalman filter is proposed to make use of the posterior motion information to address this problem. In time update, the variance of acceleration is propagated as the system state as follows.

$$\hat{x}_k^- = \hat{x}_{k-1} \quad (8.2.6)$$

$$P_k^- = P_{k-1} + Q \quad (8.2.7)$$

In measurement update, the estimation are updated by the sample variance

$O(y_{k-N+1}, \dots, y_k)$  as follows,

$$K_k = \frac{P_k^-}{P_k^- + R} \quad (8.2.8)$$

$$\hat{x}_k = \hat{x}_k^- + K_k (O(y_{k-N+1}, \dots, y_k) - \hat{x}_k^-) \quad (8.2.9)$$

$$P_k = (I - K_k)P_k^- = \frac{R}{P_k^- + R} P_k^- \quad (8.2.10)$$

Where  $O(y_{k-N+1}, \dots, y_k)$  is the sample variance for the  $N$  data set until current  $k$ .

$$O(y_{k-N+1}, \dots, y_k) = \sqrt{\frac{1}{N} \sum_{i=k-N+1}^k (y_i - \frac{1}{N} \sum_{j=k-N+1}^k y_j)^2} \quad (8.2.11)$$

The motion status of writing or pause can be judged by Kalman filter result for the sample variance versus a constant threshold.

Figure 8.9 below demonstrates the experiment result to verify the segment performance. A zigzag line with 13 strokes is written to verify the response and stability of the algorithm. The window length is set to:  $N = 5$ .

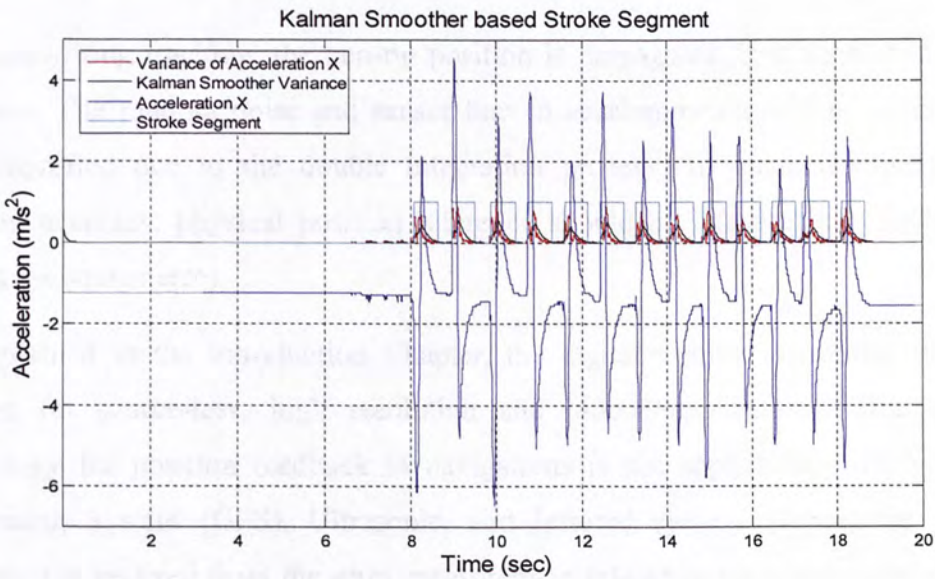


Figure 8.9: Kalman smoother based stroke segment for motion status detection (1)



The stroke segment detail is shown in Figure 8.10 below. The Kalman filter tracks the sample variance with quick reaction corresponding to the start and end of each stroke. The variance drop at symmetric sample set near max value can be compensated by previous estimation.

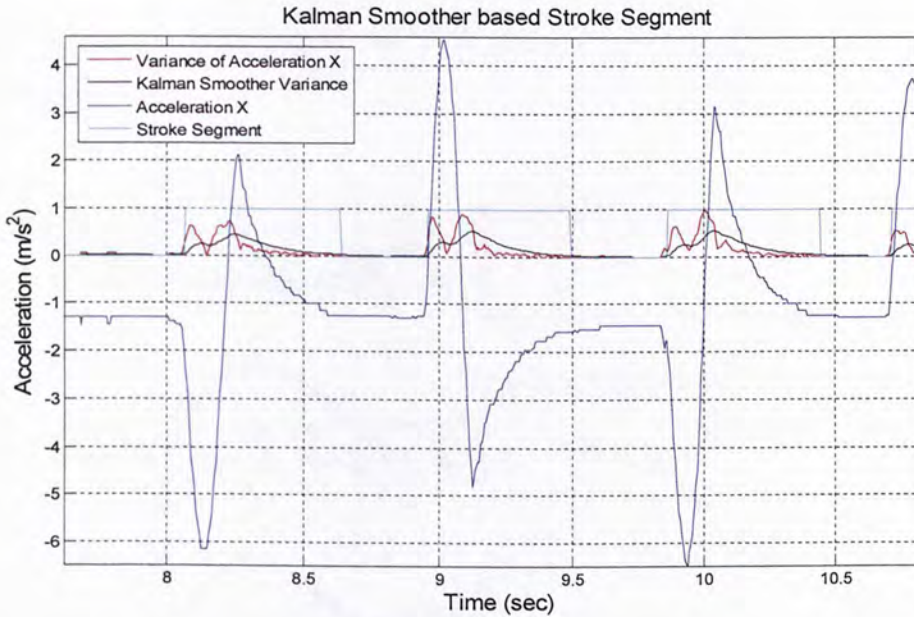


Figure 8.10: Kalman smoother based stroke segment for motion status detection (2)

### 8.2.2. Zero Velocity Compensation

For handwriting tracking, the pen-tip position is propagated from accelerometers in real-time. The random noise and sensor bias in accelerometers will be accumulated and magnified due to the double integration process. To guarantee the position tracking accuracy, physical position reference should be introduced in feedback to correct the sensor error.

As explained in the introduction Chapter, the digital writing instrument design is focused on source-less, high resolution and indoor applications. Thus popular technology for position feedback in navigations is not applicable, such as Global Positioning System (GPS), Ultrasonic, and Infrared system. Hence, the position correction is realized from the error measurement related in trajectory parameters. In [51], Zero Velocity Compensation (ZVC) algorithm is proposed based on zero velocity updates (ZUPTs).

During handwriting, the pen-tip velocity in segment between strokes equals to zero. This motionless status of hand movement can be detected by IMU based on the stroke segment algorithm. The pen-tip velocity is updated to zero and velocity difference is utilized to correct the entire acceleration during this stroke is corrected by assuming the error model for pen-tip velocity is linear when acceleration error is small.

Figure 8.11 below demonstrate the ZVC process and the algorithm flowchart for real-time application.

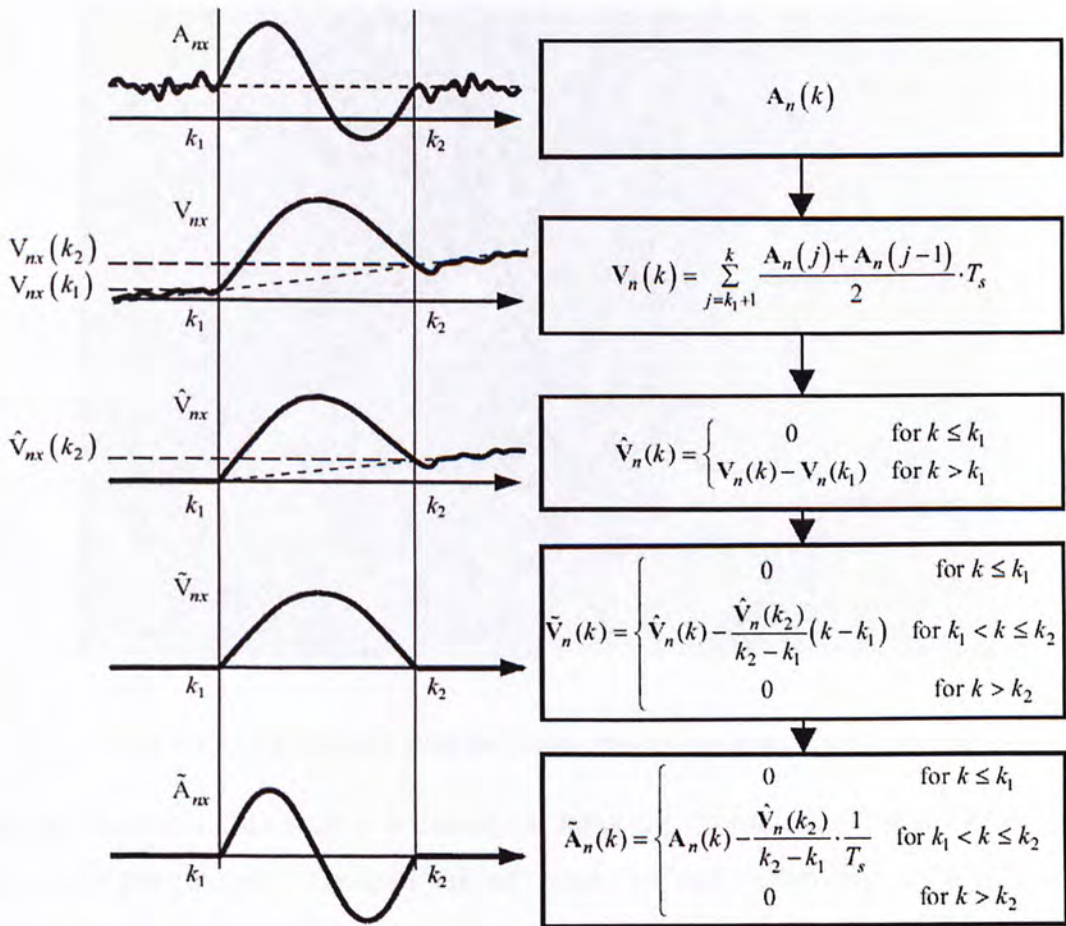


Figure 8.11: Zero velocity compensation diagram [51]

Due to high sample rate and short stroke writing, the writing experiment results demonstrate the performance for ZVC position correction. However, this algorithm is for offline process when the feedback information is available after each stroke. Thus, the error model of the accelerometer output should be analyzed and implemented for real-time application.



### 8.2.3. Complementary Attitude EKF for Writing Experiment

The handwriting experiments are performed to verify the algorithm integration for the Digital Writing Instrument system and test the performance of attitude and position tracking for handwriting recording.

Figure 8.12 below illustrates the writing experiment setup with the wireless Digital Writing Instrument based on MAG- $\mu$ IMU.



Figure 8.12: Experiment setup for Digital Writing Instrument with MAG- $\mu$ IMU

In this experiment, an 8cm  $\times$  10cm capital letter 'A' with four strokes is written on a horizontal plastic table in normal writing speed. During handwriting, the MAG- $\mu$ IMU measured the nine channel motion information of  $X$ ,  $Y$ ,  $Z$  acceleration, roll, pitch, yaw angular rate, and  $X$ ,  $Y$ ,  $Z$  magnetic field strength with 200 Hz sampling rate. After wireless transmission via Bluetooth, the Complementary Attitude EKF in computer estimated the pen attitude in real-time with dynamic switch to combine the accelerometer and the magnetometer update, controlled by Stroke Segment Kalman Filter. After coordinate transform by attitude tracking result, and Zero Velocity Compensation, the handwriting trajectory in the Earth frame was obtained stroke by stroke. Figure 8.13 below shows the nine-channel sensor output W.R.T. the body frame from the MAG- $\mu$ IMU.

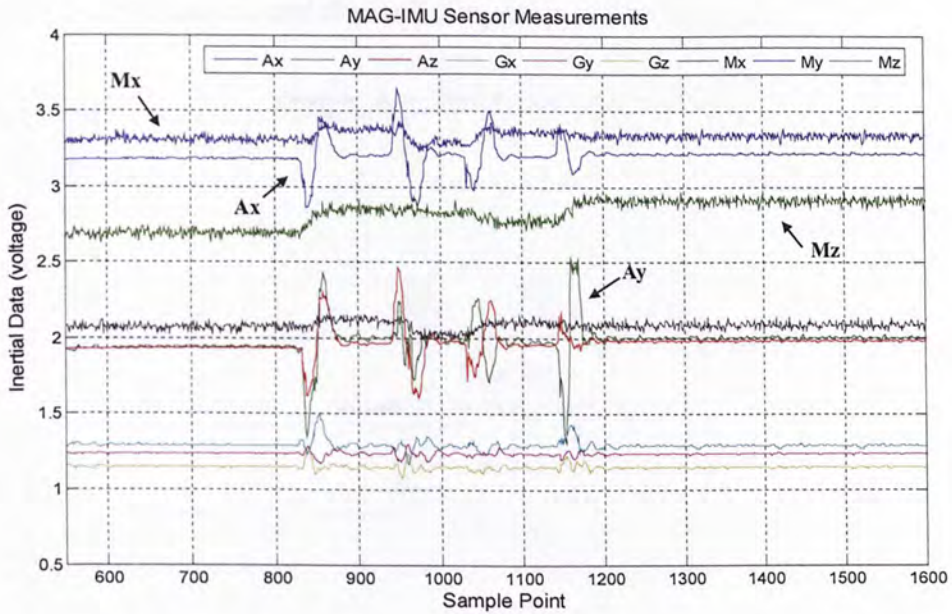


Figure 8.13: Digital Writing Instrument sensor outputs

The motion information for three-dimensional accelerations, angular rates and magnetic field strength W.R.T. the body frame are transformed after calibration experiments as shown in Figure 8.14. Random noise prevails in sensor observations.

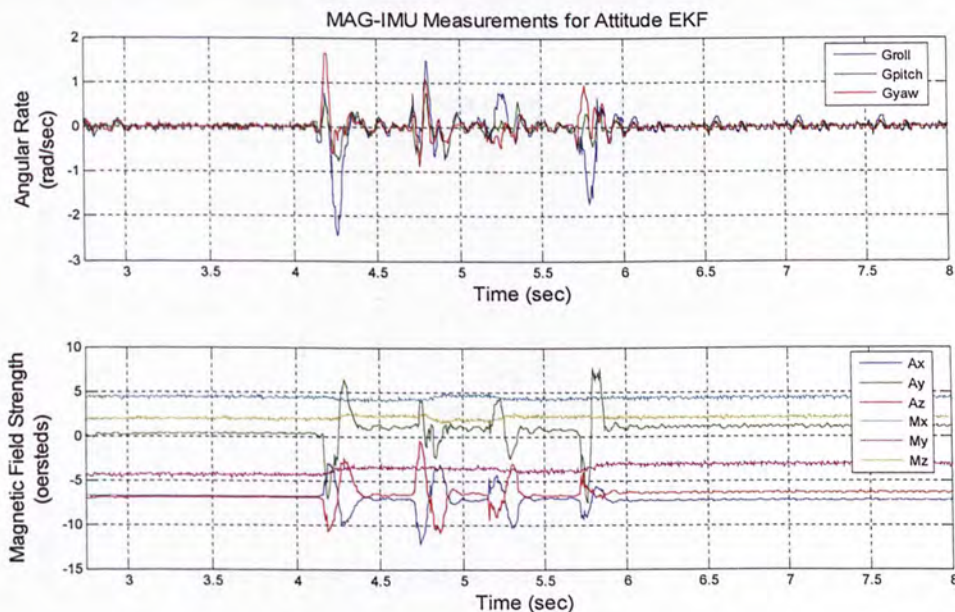


Figure 8.14: Nine-channel motion information W.R.T. the sensor frame

Meanwhile, the body frame acceleration in X-axis is utilized to detect the writing or pause of hand motion by Stroke Segment Kalman Filter in real-time. This writing



status information can control the switching in measurement update.

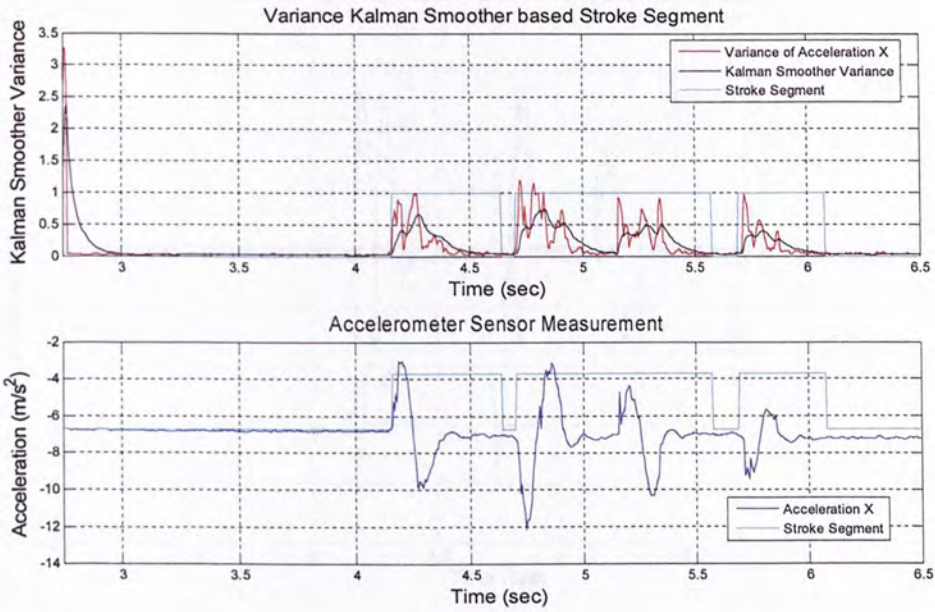


Figure 8.15: Stroke Segment Kalman Filter as sync switch for measurement update

The pen attitude in quaternion is estimated by the Complementary Attitude EKF in real-time. For comparison, the attitude is also displayed in Euler angles as shown in Figure 8.16. After 0.26 sec, the filter tracked to true attitude for 44.3 degree in roll.

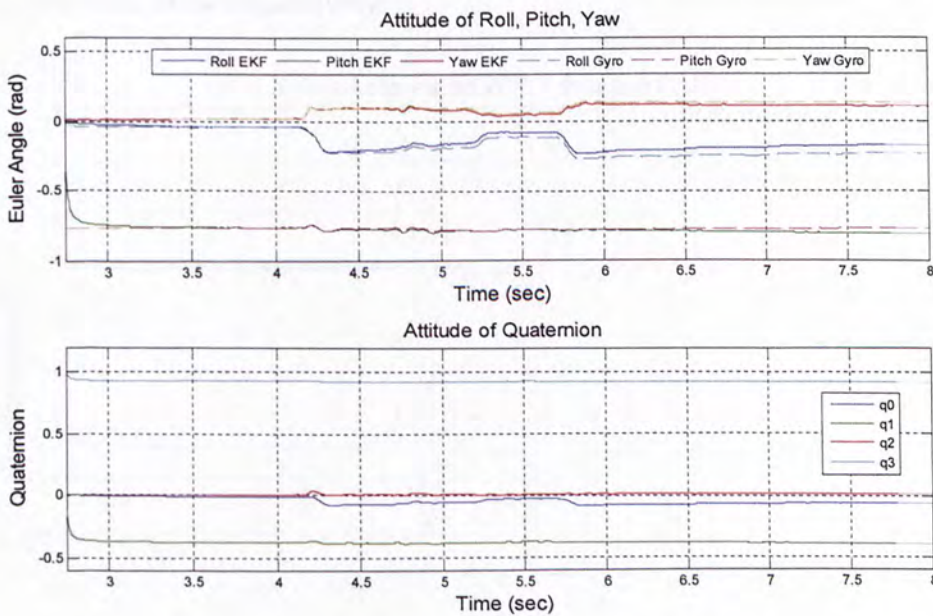


Figure 8.16: Tracking result of Complementary Attitude EKF

As shown in Figure 8.17 below, the acceleration W.R.T. the Earth frame are obtained

by coordinate transform according to the filter result for pen attitude in real-time.

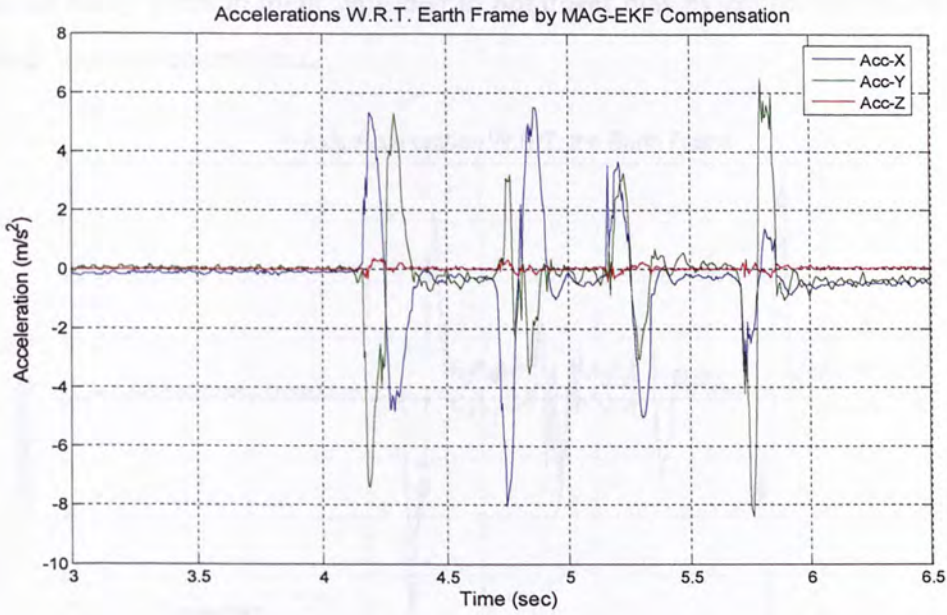


Figure 8.17: Accelerations W.R.T. Earth frame by Complementary Attitude EKF

Figure 8.18, Figure 8.19 and Figure 8.20 below demonstrate the performance for accelerations coordinate transform from the sensor frame to the writing frame by the Complementary Attitude EKF quaternion output. For comparison, the transformed acceleration by noisy gyroscope propagation and the sensor measurement are shown in green and blue lines respectively.

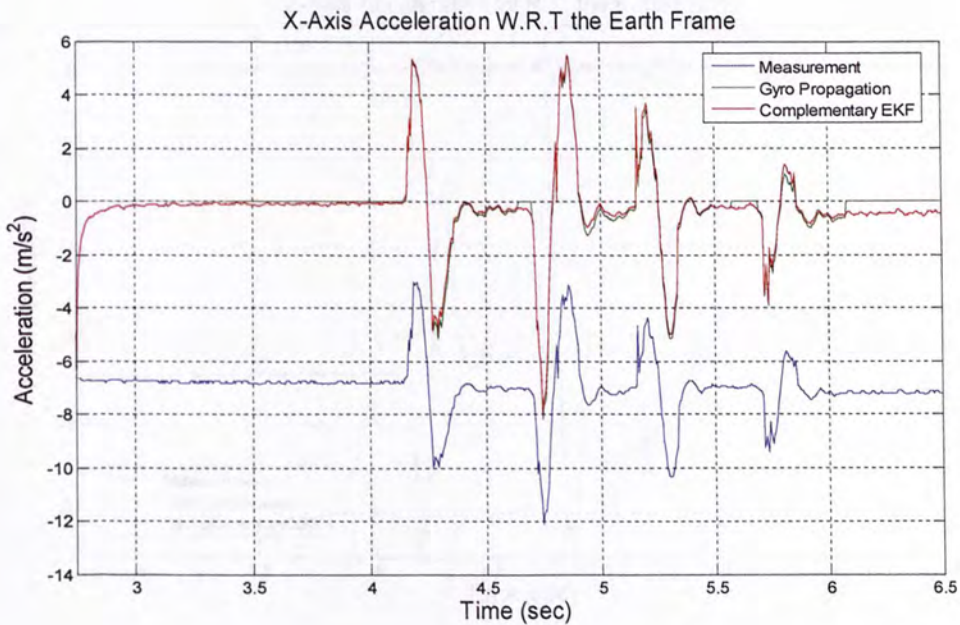


Figure 8.18: Performance comparison for the acceleration coordinate transform in X-Axis



During handwriting, the pen attitude is changing with hand motion. The attitude error caused by noisy measurement will lead to nonlinear bias by coordinate transform for the Earth frame accelerations.

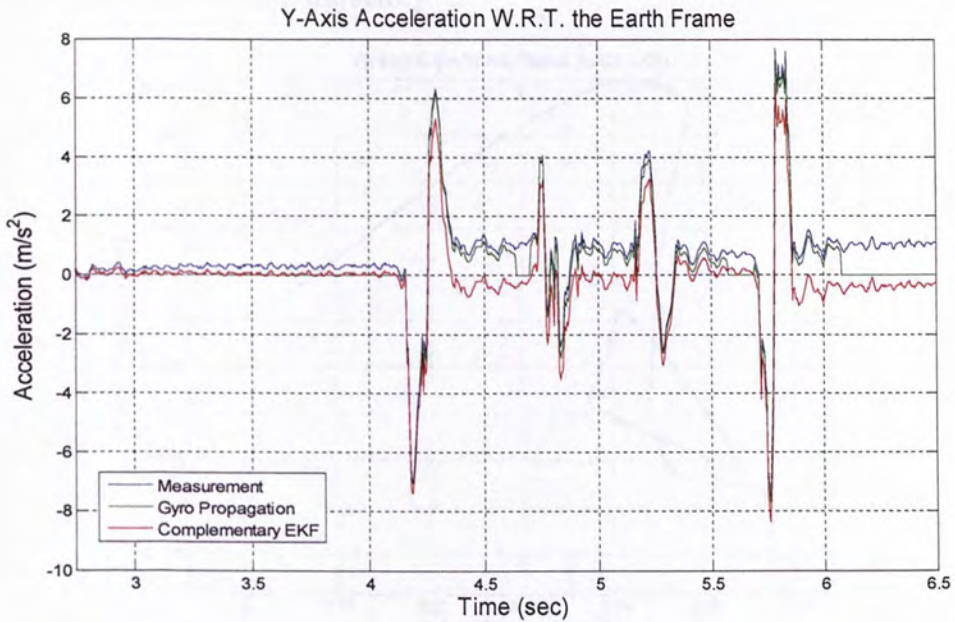


Figure 8.19: Performance comparison for the acceleration coordinate transform in Y-Axis

As the pen-tip is moving on the write board which is the X-Y plane of the Earth coordinate system, the Earth frame acceleration in Z axis should equal to zero.

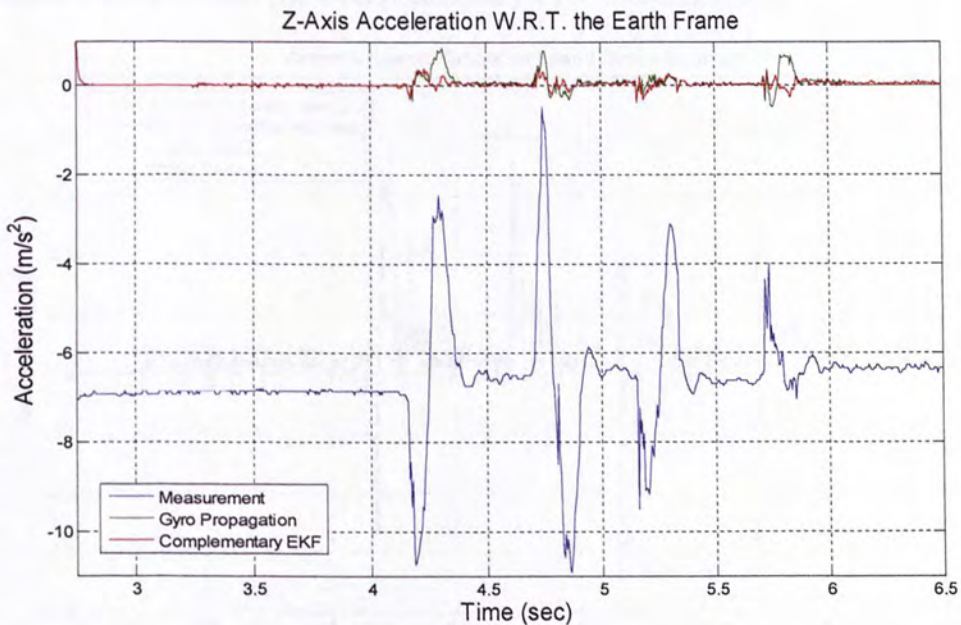


Figure 8.20: Performance comparison for the acceleration coordinate transform in Z-Axis

The real-time writing result for 'A' is shown in Figure 8.21, which started from the origin(0,0) . Due to noise and bias in the accelerometer measurements, the position error was accumulated and magnified by double integration and caused nonlinear drift and distortion in the writing trajectory.

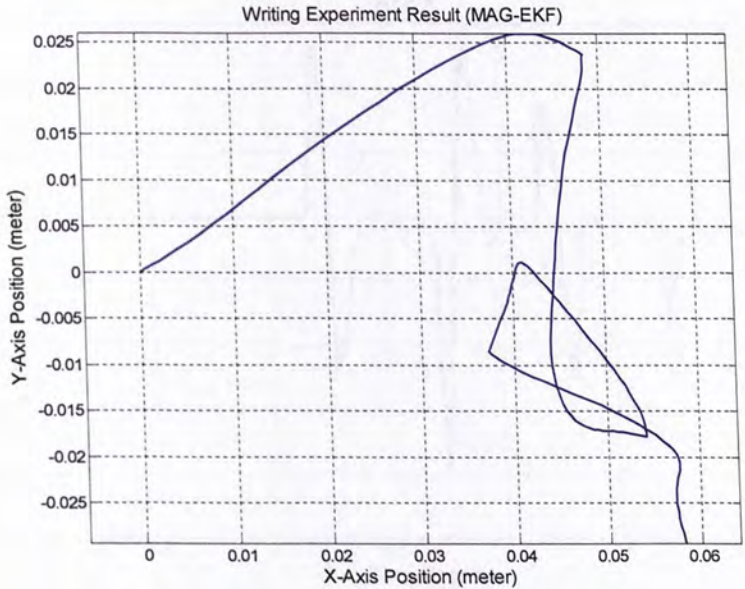


Figure 8.21: Capital letter 'A' written by Complementary Attitude EKF

Thus, the Zero Velocity Compensation is implemented to improve position accuracy [51]. The stroke segment is improved using the Z-axis acceleration in Earth frame by coordinate transform and the Complementary EKF tracking result.

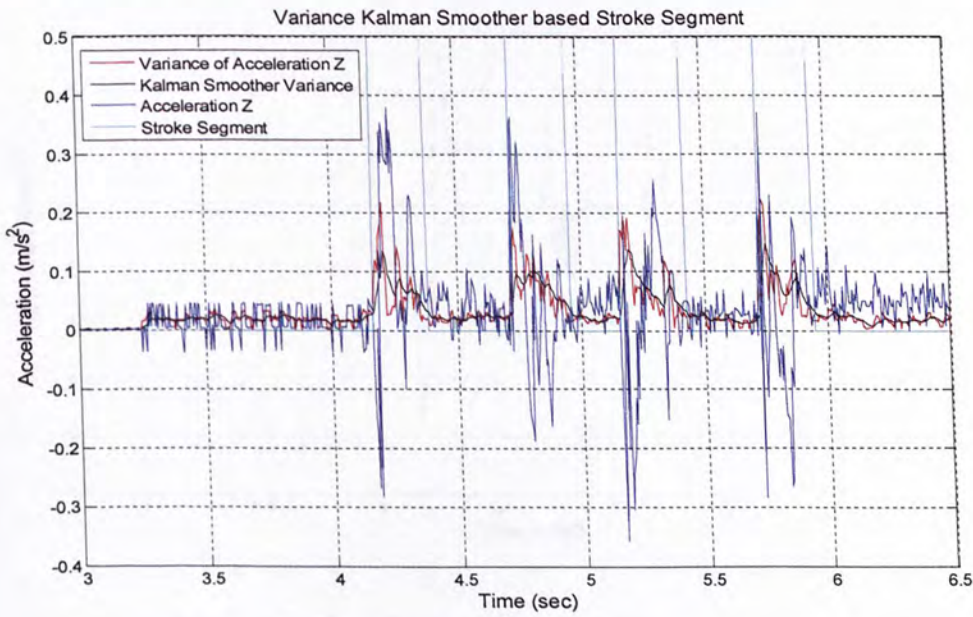


Figure 8.22: Stroke segment according to the Earth frame acceleration



Figure 8.23, Figure 8.24 and Figure 8.25 illustrate the acceleration updated by ZVC. During the pause stage of writing, the velocity was set to zero and the position remained constant to avoid position drift.

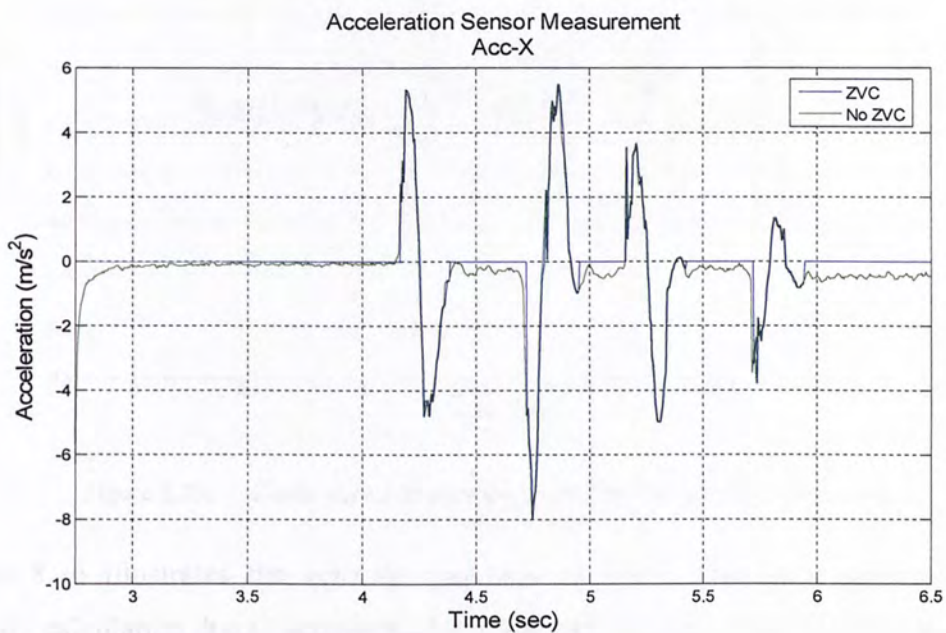


Figure 8.23: X-axis acceleration updated by Zero Velocity Compensation

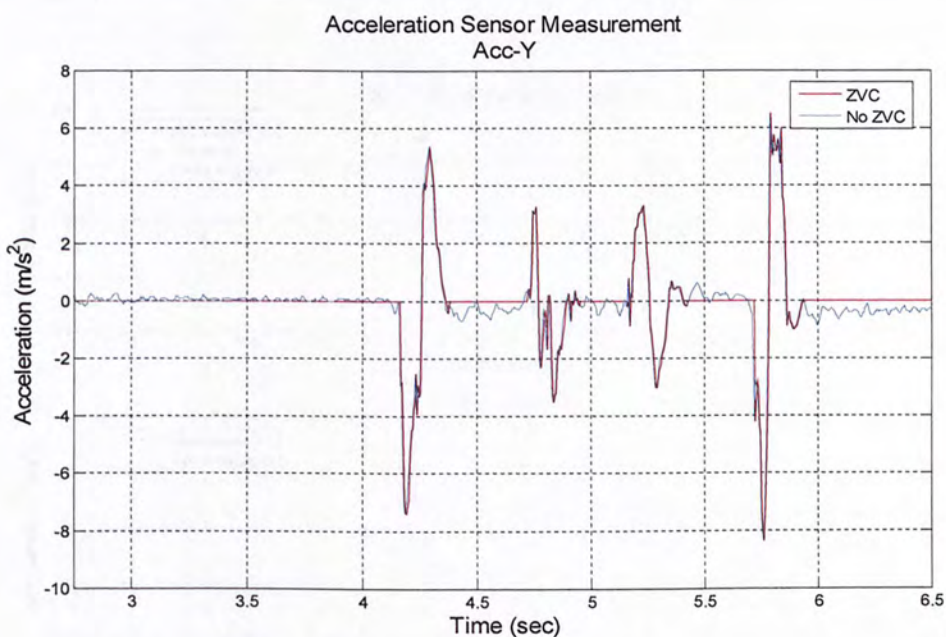


Figure 8.24: Y-axis acceleration updated by Zero Velocity Compensation

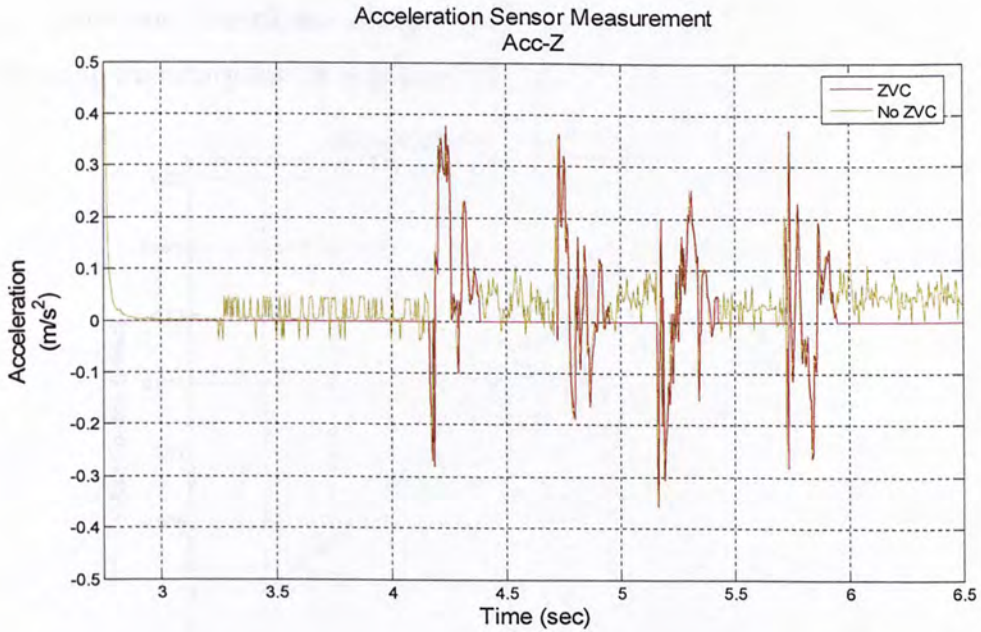


Figure 8.25: Z-axis acceleration updated by Zero Velocity Compensation

Figure 8.26 illustrates the velocity corrected by ZVC. The error accumulated in velocity calculation due to accelerometer noise and bias, and magnetic field distortion was rectified backwards after each stroke. When the sampling rate is high enough and magnetic field distortion within one stroke is tolerable, the higher order term can be omitted and the velocity error can be approximated in linear model. However, ZVC is offline algorithm. The letter should be written stroke by stroke to utilize velocity bias.

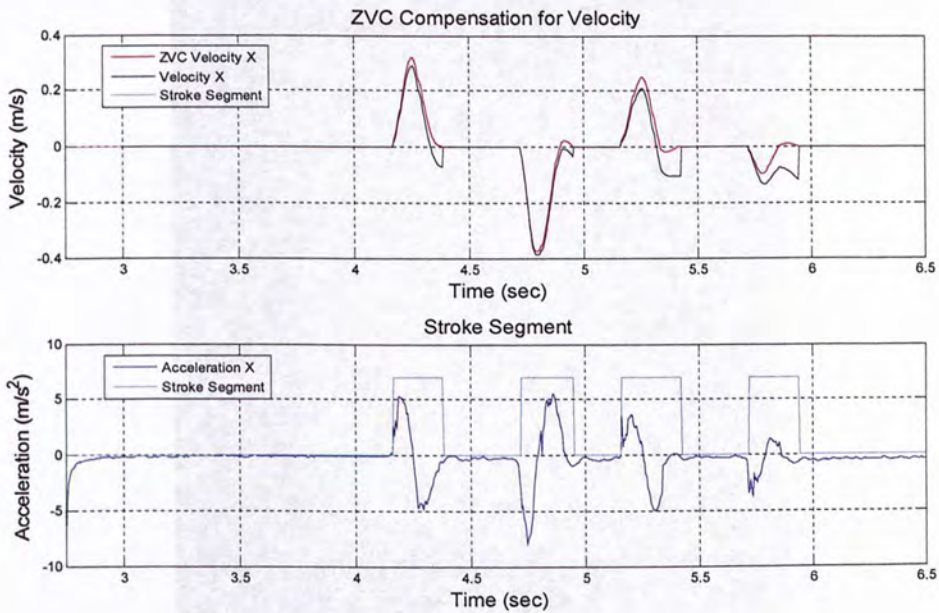


Figure 8.26: Velocity updated by Zero Velocity Compensation



After coordinate transform using Complementary EKF attitude and ZVC, the handwriting trajectory for 'A' is improved as shown in Figure 8.27.

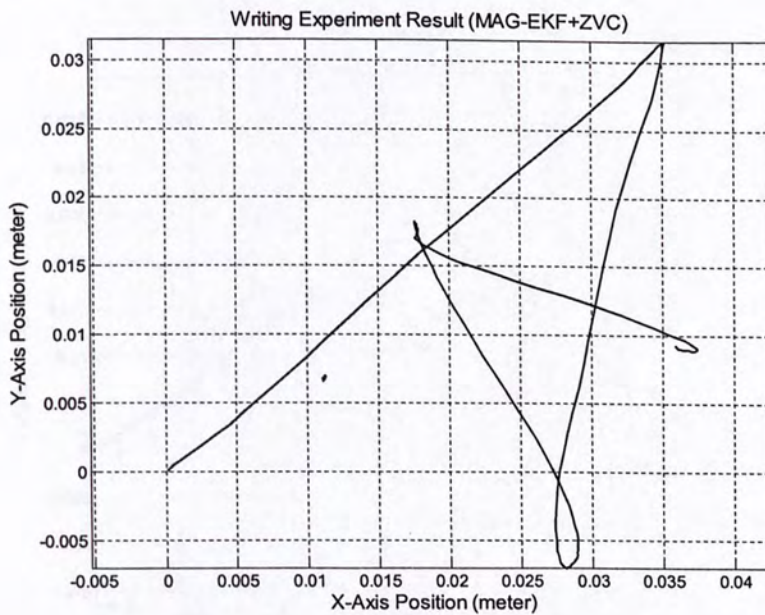


Figure 8.27: Writing result for 'A' by Complementary Attitude EKF and ZVC

Figure 8.28 below demonstrate the handwriting result during this experiment for comparison. The capitalized 'A' is written by the marker in the Digital Writing Instrument on an A4 size paper.

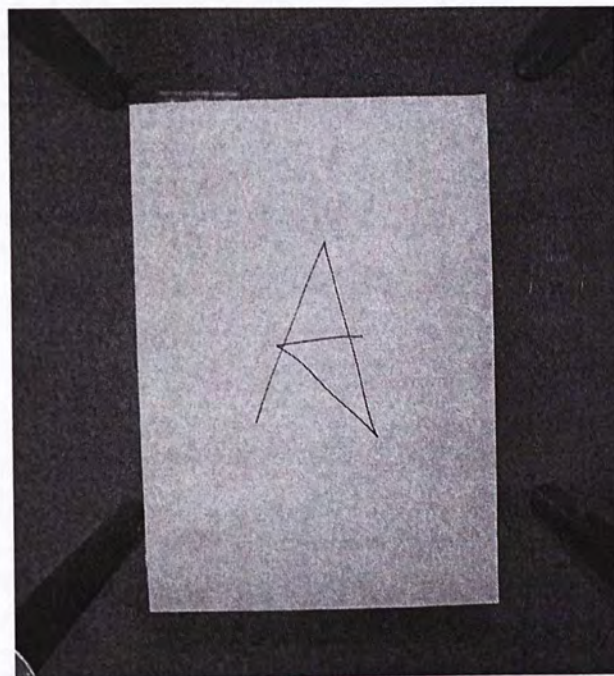


Figure 8.28: Handwriting result for 'A' using DWI system during the position tracking experiment

Compared to Figure 8.27, there is drift error and distortion in Figure 8.29 obtained by coordinate transform using gyro attitude propagation and ZVC.

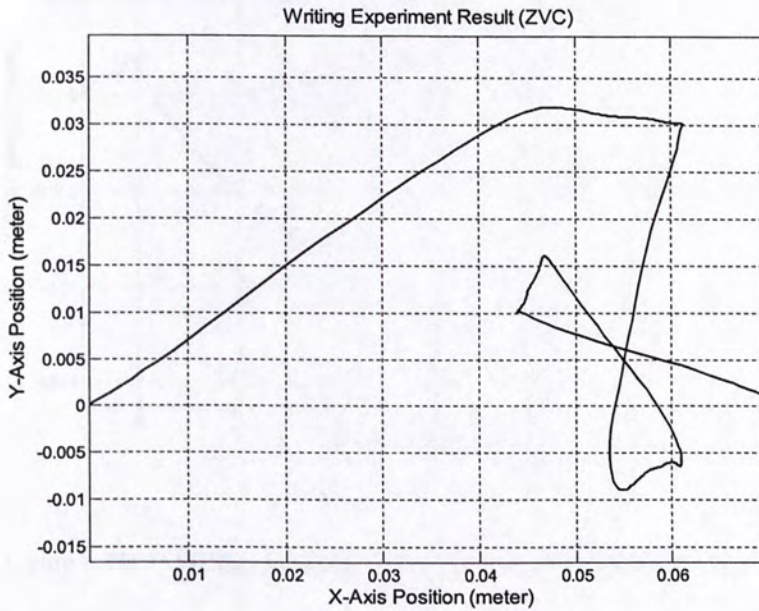


Figure 8.29: Writing result for 'A' by gyro attitude propagation and ZVC

Figure 8.30 and Figure 8.31 below illustrate the position tracking result for the pen-tip trajectory with and without Complementary Attitude EKF compensation.

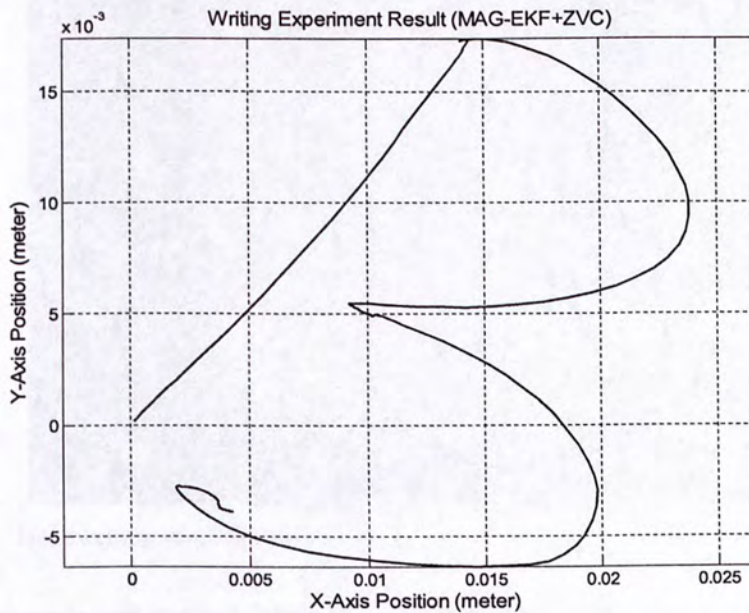


Figure 8.30: Writing result for 'B' by Complementary Attitude EKF and ZVC



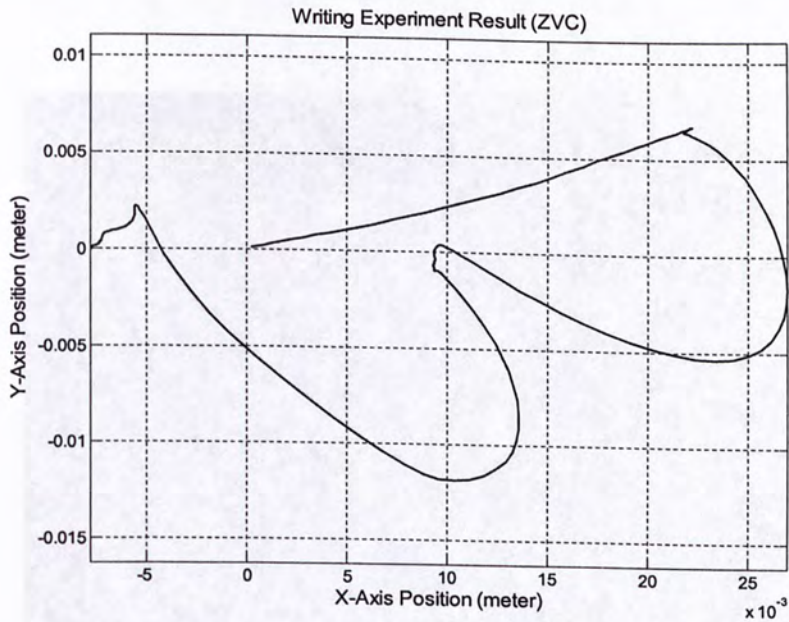


Figure 8.31: Writing result for 'B' by gyro attitude propagation and ZVC

Figure 8.32 below demonstrate the handwriting result during this experiment for position tracking comparison.

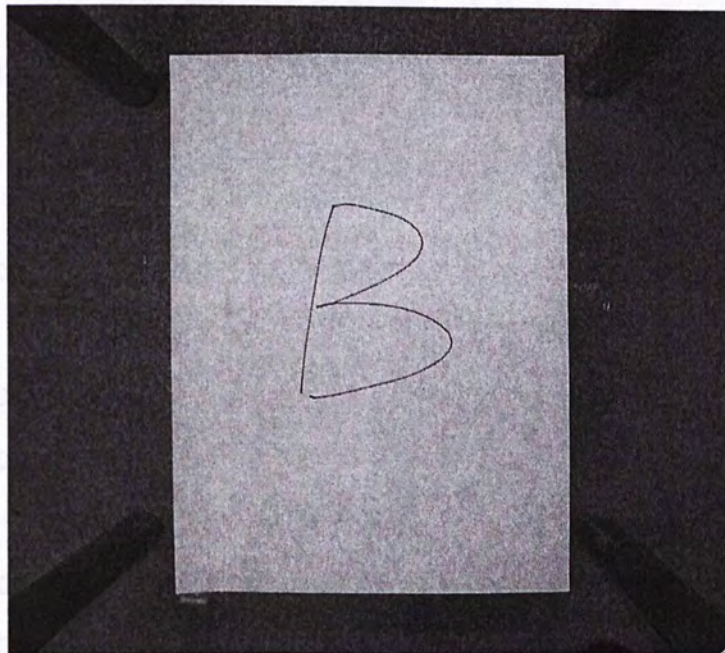


Figure 8.32: Handwriting result for 'B' using DWI system during the position tracking experiment

The writing experiment for the 'CMNS' is performed to verify the continuous attitude tracking as shown Figure 8.33. The 'CMNS' is written in normal handwriting speed with quick stop between the letters.

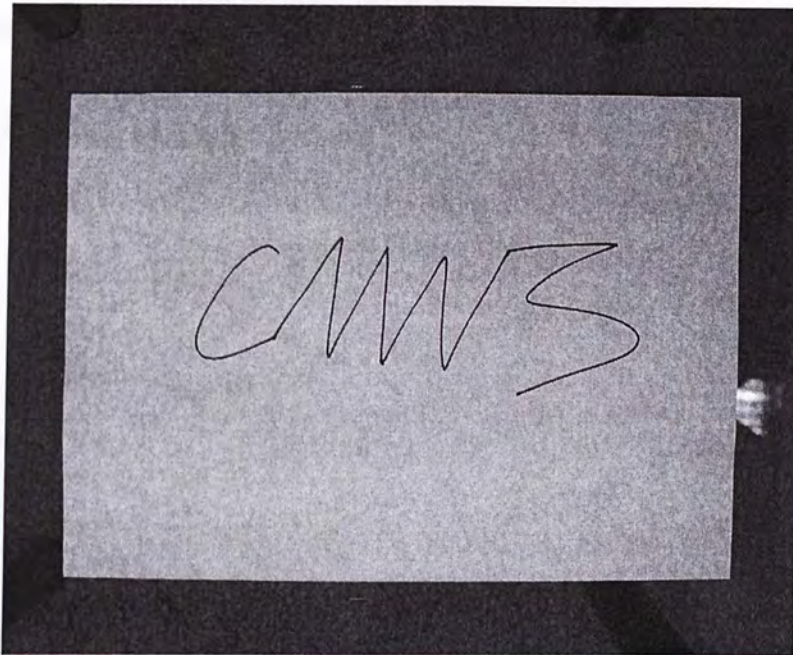


Figure 8.33: Handwriting result for 'CMNS' using DWI system during the position tracking experiment

As shown in Figure 8.34, the Complementary Attitude EKF can estimate and keep tracking the pen attitude in space for the whole word. After Zero Velocity Compensation [51], the handwriting trajectory is obtained with tolerable position tracking error.

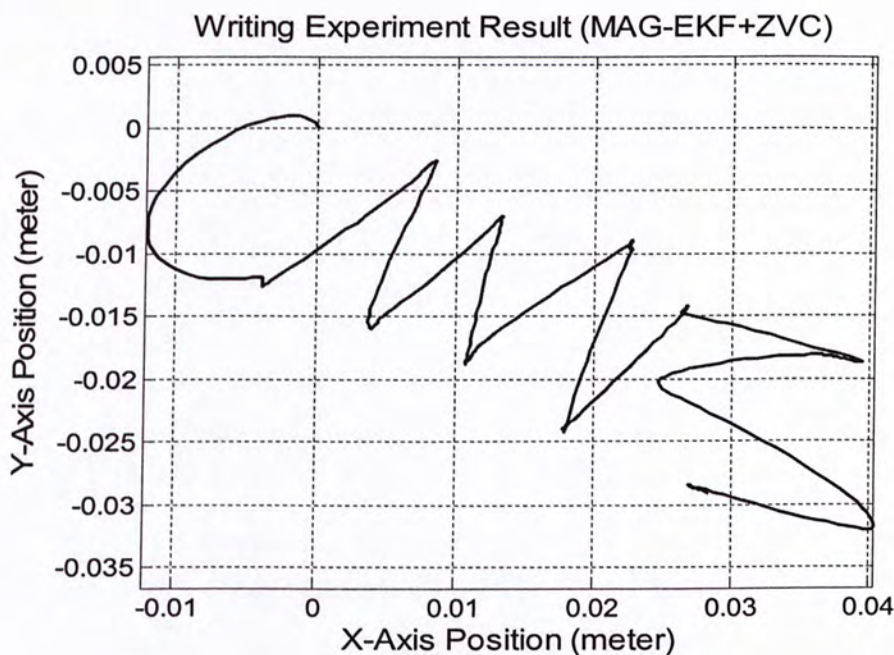


Figure 8.34: Writing result for 'CMNS' by Complementary Attitude EKF and ZVC



Figure 8.35 below demonstrates the position tracking result without Complementary Attitude EKF. Without feedback correction, the pen attitude by gyro propagation was interfered with sensor noise and bias drift. The accumulated attitude error resulted in the transformed accelerations in Earth frame and finally caused nonlinear distortions in handwriting position tracking.

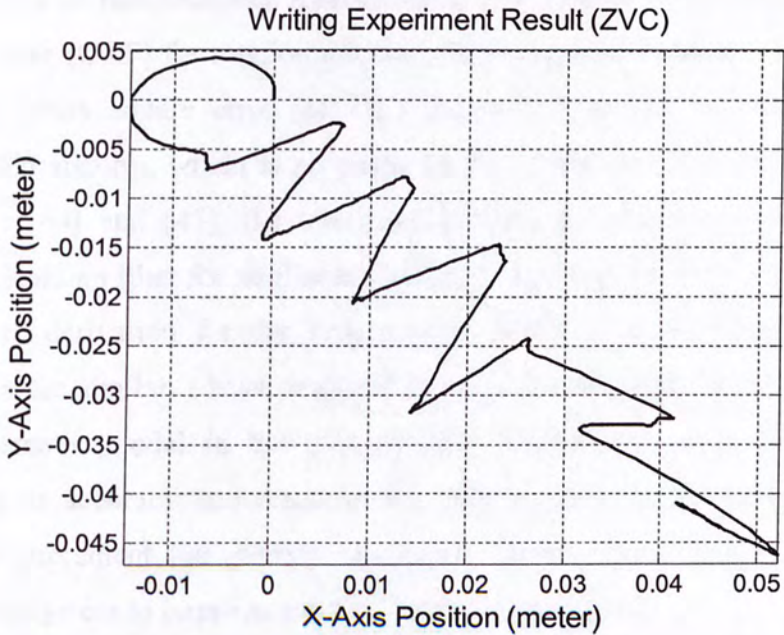


Figure 8.35: Writing result for 'CMNS' by gyro attitude propagation and ZVC

# 9. Future Work

## 9.1. Unscented Kalman Filter

Based on the attitude extended Kalman filter, I have further investigated the unscented Kalman filter (UKF) for rotation tracking. The unscented Kalman filter is a recursive minimum mean square error (MMSE) estimator based on the Kalman filter and unscented transform, which is proposed by S. J. Julier and J. K. Uhlmann [43]. As proved in [44] and [45], the unscented Kalman filter is more accurate than the extended Kalman filter for nonlinear filtering and estimation. However, the UKF does not require derivation for the system plant and the computational costs of both algorithms are similar. I have designed an attitude unscented Kalman filter based on the mathematic model in the attitude EKF. Simulation results have proved the advantage in accuracy and response for attitude tracking. In the future, I suggest others to implement the attitude unscented Kalman filter for the Digital Writing Instrument System to improve handwriting position tracking.

### 9.1.1. Least-square Estimator Structure

As proofed in Chapter 5, the Kalman filter, as Least-square estimator (LSE), is the optimal solution to the linear fitting problem as illustrated in Table 5.1 and Table 5.2. Given the observation  $y_k$  with Gaussian noise, the state  $x_k$  can be estimated by propagation iterations based on state-space framework. In nonlinear systems, the filter estimations require taking expectations of the nonlinear function for the random variables  $\hat{x}_k$ ,  $w$  and  $v$ .

$$\hat{x}_k = \hat{x}_k^- + K_k [y_k - \hat{y}_k^-] \quad (9.1.1)$$

Where,

$$\hat{x}_k^- = E[F(\hat{x}_{k-1}, w)] \quad (9.1.2)$$

$$K_k = \hat{P}_{x_k y_k} \hat{P}_{\tilde{y}_k \tilde{y}_k}^{-1} \quad (9.1.3)$$



$$\hat{y}_k^- = E[H(\hat{x}_k^-, v)] \quad (9.1.4)$$

The optimal feedback gain  $K_k$  in Eq. ( 9.1.3 ) is analytically equivalent to Eq. ( 5.2.24 ).  $K_k$  requires stochastic evaluation for the cross-covariance matrices and the posterior covariance matrices with  $\tilde{y}_k = y_k - \hat{y}_k^-$ . These calculations involve taking expectation of prior state estimates through nonlinear functions.

However, the extended Kalman filter approximates the optimal terms by linearizing the state-space model as,  $x_{k+1} \approx Ax_k + w_k$ ,  $y_k \approx Cx_k + v_k$ , usually Jacobian of first-order, and then determining the posterior covariance matrices analytically for the linear system. Consequently, this approximation will introduce large error in the true posterior mean (the estimated states) and covariance of the transformed random variable, which will incur nonlinear distortion in the filter output.

### 9.1.2. Unscented Transform

The unscented Kalman filter improves the nonlinear approximation by combining the advantages from the particle filter [50], on the other hand, making use of unscented transform in stead of random sampling of points.

The unscented transform projects the system state into stochastic feature set according to the probability characteristic. The expectations of nonlinear functions are approximated by the weighted mean approach of the transformed feature set.

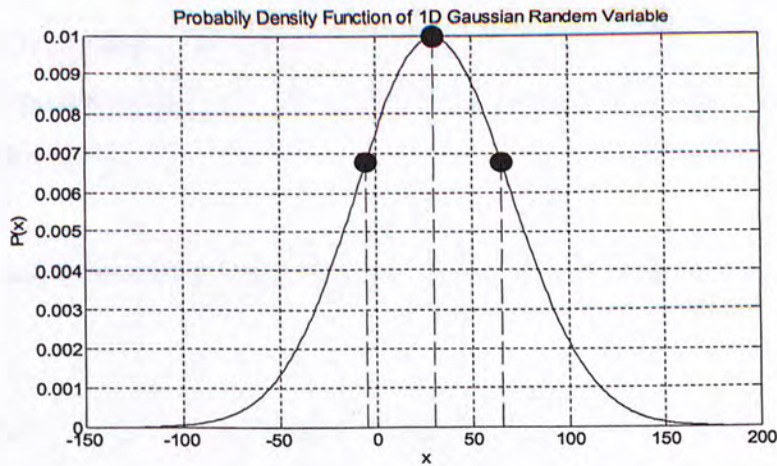


Figure 9.1: Approximation of a one-dimensional Gaussian distribution by three feature points

The Gaussian probability density function can be specified by the mean and covariance as shown in Eq. ( 5.2.8 ). In the simplest case, one-dimensional Gaussian distribution can be described uniquely by three points shown in Figure 9.1 below. The middle point stands for the mean and the other two points restrict the covariance.

Figure 9.2 below illustrate the Gaussian distribution in two-dimensional space. Consequently, the stochastic information of an  $n$ -dimensional Gaussian random variable can be described by  $2n+1$  selected sigma points. The middle point is for the mean and the others define the covariance.

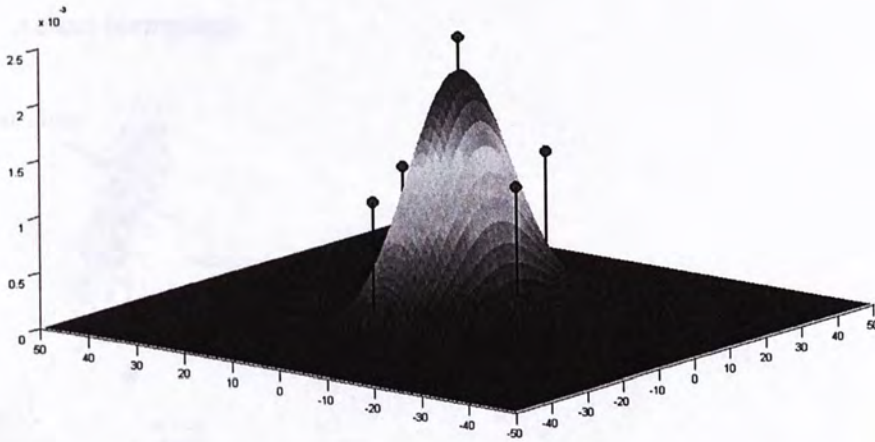


Figure 9.2: Approximation of a two-dimensional Gaussian distribution by five feature points

Given a  $n \times n$  covariance matrix  $P$ , a set of  $2n$  sigma points can be generated from the columns (or rows) of the matrices  $\pm\sqrt{(n+\lambda)P}$  (the positive and negative rows). This set of points is  $\bar{x}$  mean. The scalar  $\lambda$  is a scaling parameter to determine the spread of the sigma points around  $\bar{x}$ . The equations of unscented transform for sigma points are listed below [46].

Table 9.1: Unscented transform equations

---


$$\chi_0 = \bar{x} \tag{9.1.5}$$

$$i = 1, \dots, n, \quad \chi_i = \bar{x} + (\sqrt{(n+\lambda)P_x})_i \tag{9.1.6}$$

$$i = n+1, \dots, 2n, \quad \chi_i = \bar{x} - (\sqrt{(n+\lambda)P_x})_{i-L} \tag{9.1.7}$$



Figure 9.3 below illustrates the performance of projecting the Gaussian random variable by the unscented transform versus the extended Kalman filter. The actual sampling demonstrates the true mean and variance of the random variable after nonlinear transform. The extended Kalman filter approximates the nonlinear process to the first order accuracy. The estimated mean is shifted and the variance is rotated due to the linearization error. The unscented transform generates carefully selected sigma points. The spread of these sigma points through nonlinear dynamics is completely controlled to third order moments as proved. The distribution of the propagated random variable is refined to the stochastic features. The estimation error is much smaller than the extended Kalman filter.

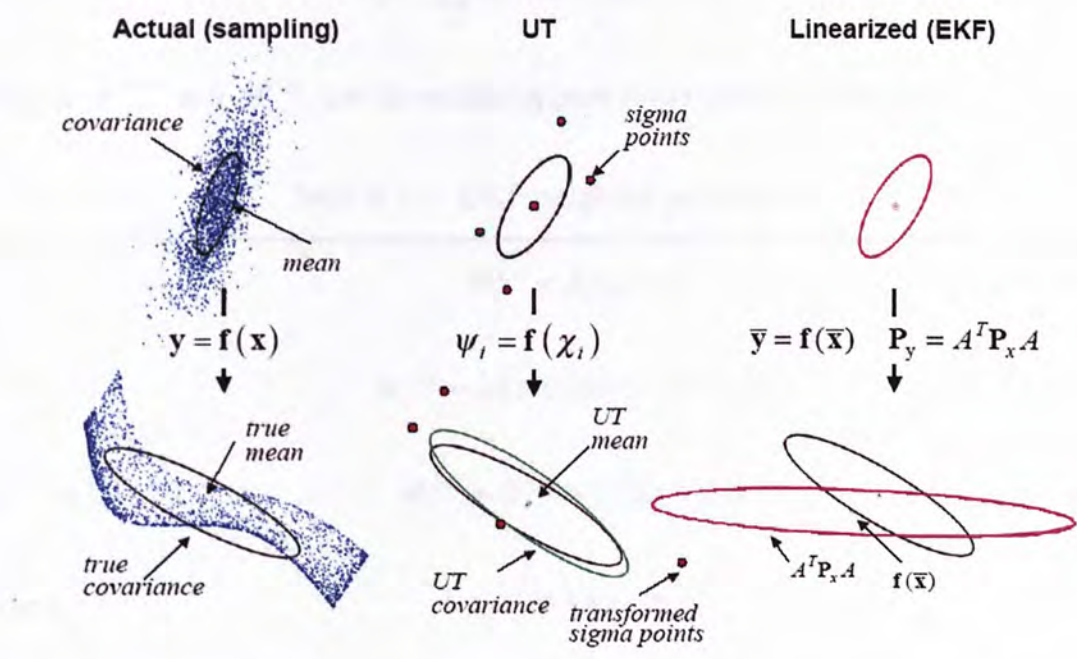


Figure 9.3: Unscented transform for mean and covariance undergo nonlinear process [46]

### 9.1.3. Unscented Kalman Filter

The  $2n+1$  generated sigma points are propagated through the nonlinear dynamic equations of the time update model in Eq. ( 9.1.8 ). The optimal estimation of the observation  $\bar{y}$  can be achieved by the weighted mean of the transformed  $2n+1$  feature set in Eq. ( 9.1.10 ). As proved by Julier and Uhlmann, to undergo nonlinear process, the propagation of mean and covariance is more accurate and feasible than the estimation of the system state [44]. The calculation of the projected mean and covariance is as accurate to the second order. However, there is no requirement for

constructing any derivatives. The unscented Kalman filter is feasible for non-differentiable system dynamics.

$$\text{For } i = 0, \dots, 2n, \quad \chi_i^- = F[\chi_i] \quad (9.1.8)$$

$$\nu_i = H[\chi_i^-] \quad (9.1.9)$$

$$\bar{y} = \sum_{i=0}^{2n} W_i^{(m)} \nu_i \quad (9.1.10)$$

$$P_{yy} = \sum_{i=0}^{2n} W_i^{(c)} [\nu_i - \bar{y}][\nu_i - \bar{y}]^T \quad (9.1.11)$$

Where  $W^{(m)}$  and  $W^{(c)}$  are the weighting parameters defined as follows,

Table 9.2: UKF weighting parameters

---


$$W_0^{(m)} = \lambda / (n + \lambda) \quad (9.1.12)$$

$$W_0^{(c)} = \lambda / (n + \lambda) + (1 - \alpha^2 + \beta) \quad (9.1.13)$$

$$\text{For } i = 1, \dots, 2n, \quad W_i^{(m)} = W_i^{(c)} = 1 / \{2(n + \lambda)\} \quad (9.1.14)$$

$$\text{Where,} \quad \lambda = \alpha^2(n + \kappa) - n \quad (9.1.15)$$

The constant parameter  $\alpha$  determine the scaling factor  $\lambda$  and is set to small positive number, typically  $10^{-4} \leq \alpha \leq 1$ .  $\kappa$  is the secondary scaling parameter which is usually set to zero.  $\beta$  is the parameter to exploit the prior knowledge of the distribution of  $x$ .  $\beta$  is set to 2 for Gaussian distribution [46].

The unscented transform preserves the first three moments of the given distribution. The scalar  $\lambda$  is a tuning factor to control the higher order moments correspond to different distribution information. For scalar system when  $n = 1$ ,  $\lambda = 2$  settles the errors in the mean and covariance to the sixth order. For higher dimensional system,  $\lambda = 3 - n$  minimizes the mean-square error up to the fourth order [44].

The Kalman gain can be updated from the mean and covariance by unscented



transform. Hence, the unscented Kalman filter has advance accuracy compared to the extended Kalman filter.

With the constant parameters defined in Table 9.2, the equations for the unscented Kalman filter (UKF) algorithm are listed in Table 9.3 to Table 9.6 below.

Table 9.3: UKF initialization equations

$$\hat{x}_0 = E[x_0] \quad (9.1.16)$$

$$P_0 = E[(x_0 - \hat{x}_0)(x_0 - \hat{x}_0)^T] \quad (9.1.17)$$

Firstly, the unscented Kalman filter is initialized by the distribution information of the initial mean and covariance matrix calculated from the training data. The  $2n+1$  sigma points are generated as follows,

Table 9.4: Unscented transform for sigma points

$$\chi_{k-1} = [\hat{x}_{k-1}, \hat{x}_{k-1} \pm \sqrt{(n+\lambda)P_{k-1}}] \quad (9.1.18)$$

The time update and measurement update structure of unscented Kalman filter is similar with the Kalman filter. However, the propagation under nonlinear dynamic equations are improved by unscented transform.

Table 9.5: UKF time update equations

$$\chi_{k|k-1} = F[\chi_{k-1}] \quad (9.1.19)$$

$$\hat{x}_k^- = \sum_{i=0}^{2n} W_i^{(m)} \chi_{i,k|k-1} \quad (9.1.20)$$

$$P_k^- = \sum_{i=0}^{2n} W_i^{(c)} [\chi_{i,k|k-1} - \hat{x}_k^-][\chi_{i,k|k-1} - \hat{x}_k^-]^T \quad (9.1.21)$$

$$v_{k|k-1} = H[\chi_{k|k-1}] \quad (9.1.22)$$

$$\hat{y}_k^- = \sum_{i=0}^{2n} W_i^{(m)} v_{i,k|k-1} \quad (9.1.23)$$

The system state is corrected by measurement update by the weighted mean approach. The updated state for mean and the covariance matrix  $\{\hat{x}_k, P_k\}$  is taken to the time update for next iteration step.

Table 9.6: UKF measurement update equations

$$P_{yy} = \sum_{i=0}^{2n} W_i^{(c)} [\nu_{i,k|k-1} - \hat{y}_k^-][\nu_{i,k|k-1} - \hat{y}_k^-]^T \quad (9.1.24)$$

$$P_{xy} = \sum_{i=0}^{2n} W_i^{(c)} [\chi_{i,k|k-1} - \hat{x}_k^-][\nu_{i,k|k-1} - \hat{y}_k^-]^T \quad (9.1.25)$$

$$K = P_{xy} P_{yy}^{-1} \quad (9.1.26)$$

$$\hat{x}_k = \hat{x}_k^- + K(y_k - \hat{y}_k^-) \quad (9.1.27)$$

$$P_k = P_k^- - K P_{yy} K^T \quad (9.1.28)$$

The unscented Kalman filter captures the mean and covariance as precise to the third order moments for any nonlinearity, while the extended Kalman filters only attain first order accuracy. On the other hand, the computational complexity of the unscented Kalman filter is in the same order of that of the extended Kalman filter.

Some successful quaternion based attitude unscented Kalman filter has been developed in [46], [47] and [48]. In [46], the process noise  $w_k$  and measurement noise  $v_k$  are implemented as additional states into the system dynamics for unscented Kalman filter process. The projected mean and variance are also updated including the random noise  $w_k$  and  $v_k$ . This approach may explore the capability of unscented transform to more complete extent. However, for the extra sigma points, the augmented filter will require twice or triple of computations compared with basic filter framework.

Quaternion does not have singularity problem in Euler angles as illustrated in Chapter 3.4. On the other hand, in sequential attitude filters, the quaternion in system state must be confined to a normalized constraint. However, the measurement model may violate this rule during feedback updates. Although brute normalization after each



recursion can still be a method, the filter does not track well when large error occurred. In [47], the UnScented QUaternion Estimator (USQUE) is developed to address this problem by introducing unconstrained quaternion error vector as system state and propagating the attitude outside the UKF. This algorithm is successful in accuracy, however cost in computations. Stated in [47], the USQUE is about 2.5 times slower than the EKF in [49].

As proofed in Chapter 7.2, the measurement model used in MAG-EKF does not require normalization during iterations. The computation is simplified by separate the quaternion rotation model into one matrix multiplication. Thus, an unscented Kalman filter based on strapdown gyroscopes and magnetometers for quaternion attitude tracking is designed as,

In this UKF, the attitude is calculated in quaternion to avoid singularity. The attitude quaternion is applied as the system state. Given current sample for angular rates from gyroscope sensors, the attitude quaternion can be updated according to the quaternion-based attitude propagation model in Eq. ( 4.3.4 ). The system state System dynamics for time update can be derived as,

$$F = [I_4 + \Omega(\omega_k - \Delta\omega_{k-1}) \cdot dt]_k \quad (9.1.29)$$

In measurement update, the three-dimensional magnetic field strengths from the magnetometer are utilized as attitude reference to correct the propagation error.

$$H = \frac{1}{2} \begin{bmatrix} -[(\bar{q}_b + \bar{q}_e)] \times & \bar{q}_b - \bar{q}_e \\ -(\bar{q}_b - \bar{q}_e)^T & 0 \end{bmatrix} \quad (9.1.30)$$

The unscented Kalman filter for real-time application with discrete data can be implemented as illustrated in the Figure 9.4 below,

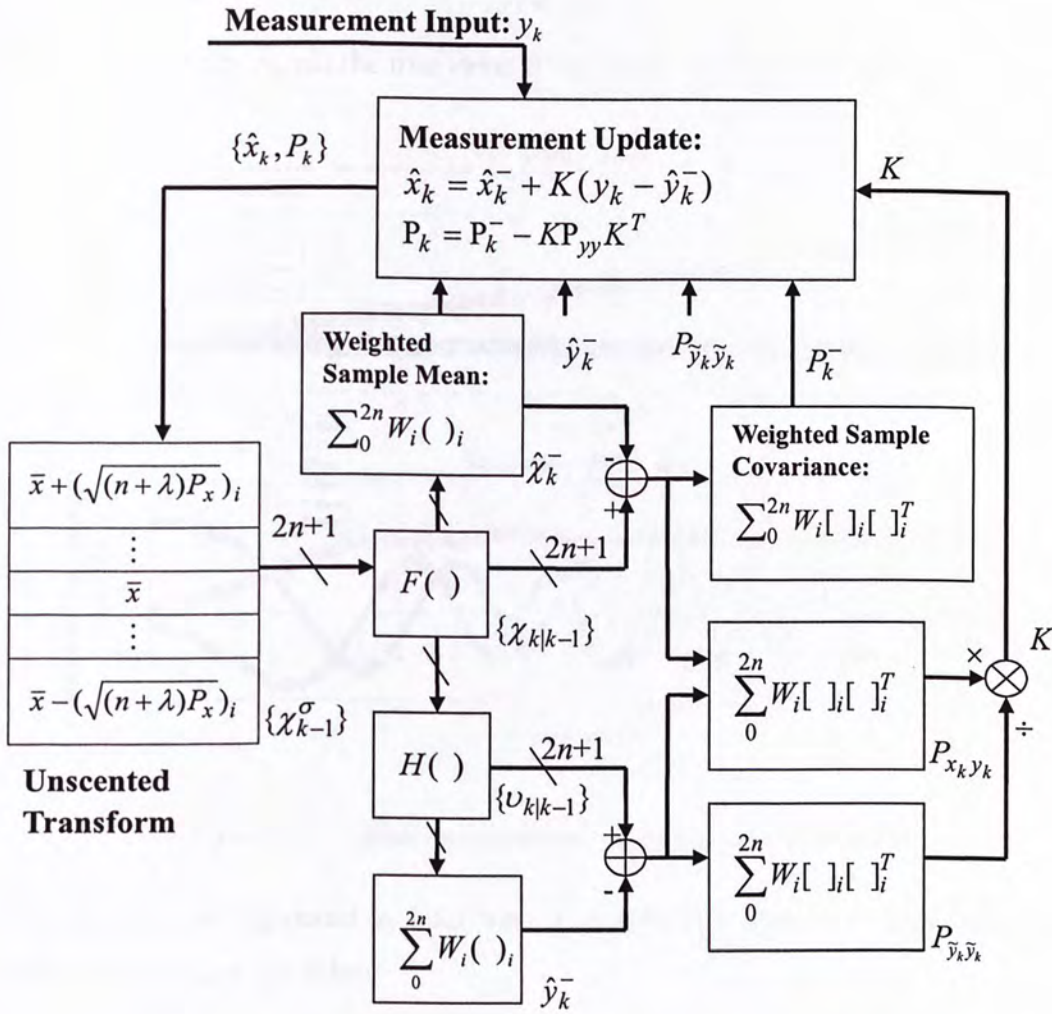


Figure 9.4: The real-time recursive structure of the unscented Kalman filter

## 9.2. Experiment Result

The performance of the unscented Kalman filter is tested under extensive simulations. The attitude quaternion is displayed in Euler angles for better comparison.

Assume the rigid object is rotated by torque  $L$ ,  $M$  and  $N$  in roll, pitch and yaw direction respectively. The angular rates from gyroscopes and magnetic field strength from magnetometers are generated according to the Newton-Euler equations with additive Gaussian random noise. The sample rate is 200 Hz.

$$L = 0.01 \cdot \sin(0.3t) \tag{9.2.1}$$

$$M = 0.01 \cdot \cos(0.3t) \tag{9.2.2}$$



$$N = 0.02$$

( 9.2.3 )

The sensor output versus the true value is displayed in Figure 9.5 below.

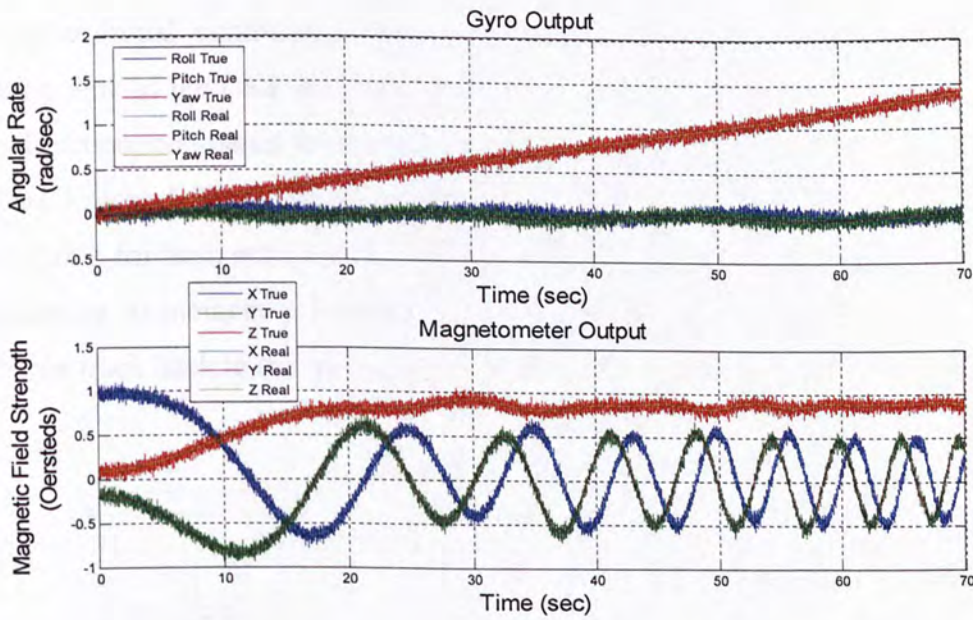


Figure 9.5: Sensor measurements for the unscented Kalman filter

The attitude tracking result by UKF versus attitude propagated by noisy gyro outputs is shown in Figure 9.6 below.

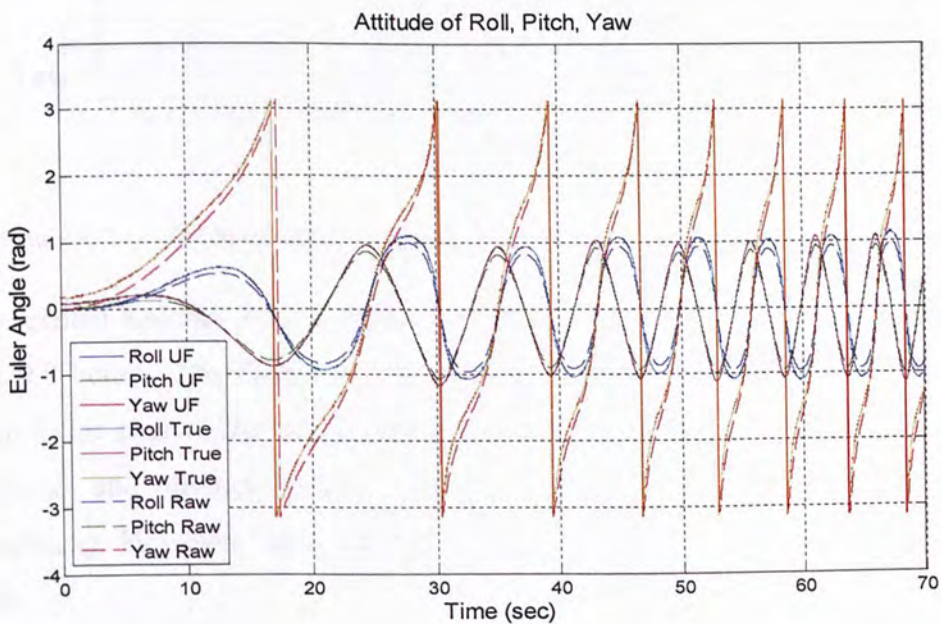


Figure 9.6: Tracking output of the unscented Kalman filter

Due to selected sigma points by unscented transform, the UKF projects the nonlinear mapping of random distribution more accurately than the linear approximation of the EKF. Thus, the unscented Kalman filter can achieve faster convergence from inaccurate initial conditions. Figure 9.7 below demonstrates the comparison for tracking time of the UKF and EKF. Given a large initial attitude error of 90 degree in Yaw direction, compared to the 0.95 second of the EKF, the tracking time for UKF is only 0.03 second. Thus, the unscented Kalman filter is more sensitive in tracking and more stable for hash environment. For onboard applications, when severe EMI cause malfunction in memory for attitude of the system state, the attitude filter based on UKF can track back to the true state in a shorter time or restart with less cost.

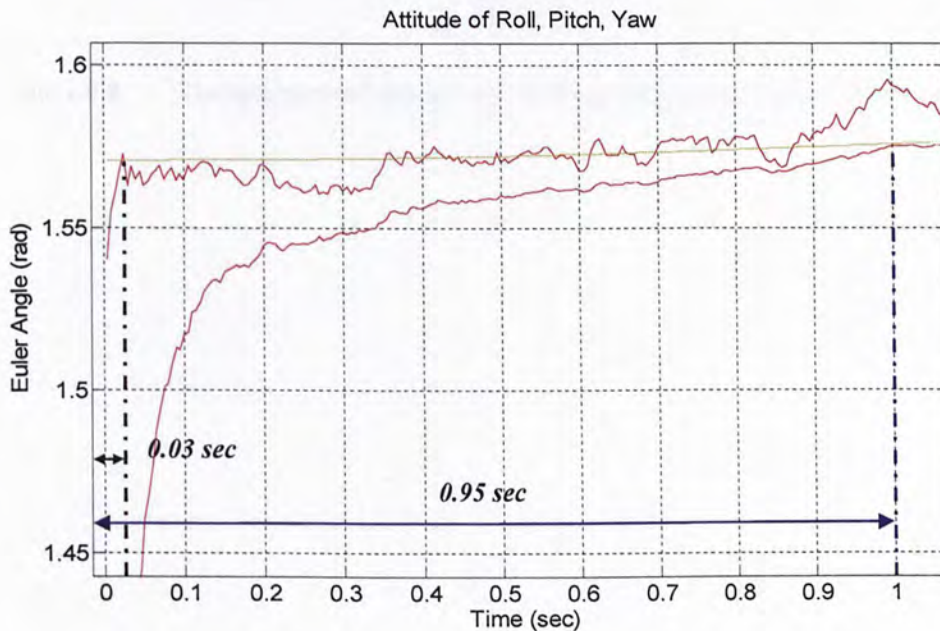


Figure 9.7: Tracking speed of unscented Kalman filter versus extended Kalman filter

The unscented Kalman filter is superior in accuracy compared with EKF as shown in Figure 9.8 below. The dash lines represent the tracking result by extended Kalman filter in Euler angles. Due to linearization error, the attitude result deviates from the true value and diverge prone to noisy measurements as the tracking error accumulating. However, the UKF maintain good performance for tracking the true attitude.



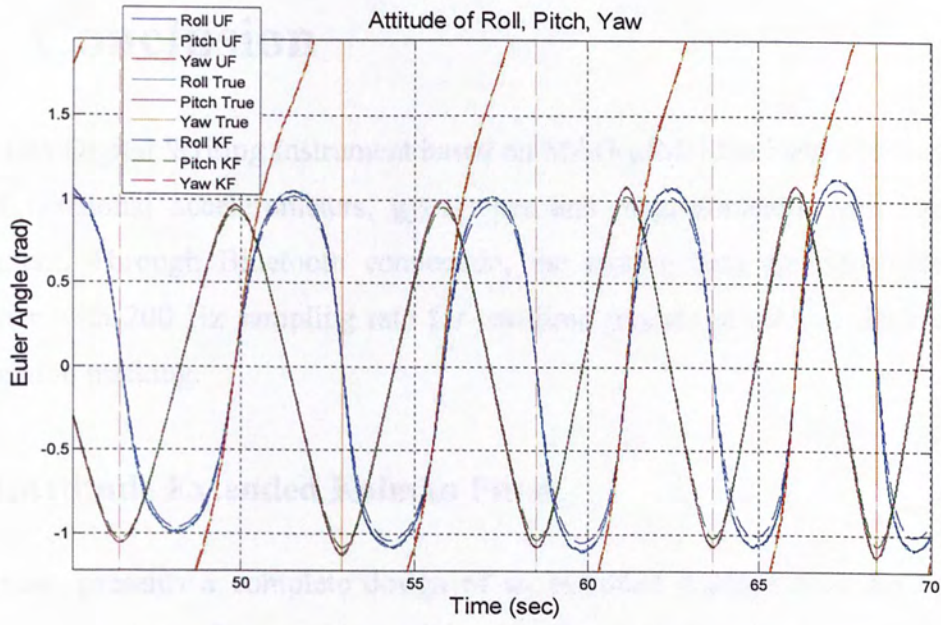


Figure 9.8: Tracking accuracy of unscented Kalman filter versus extended Kalman filter

# 10. Conclusion

A wireless Digital Writing Instrument based on MAG- $\mu$ IMU has been developed with three-dimensional accelerometers, gyroscopes and magnetometers with strapdown installment. Through Bluetooth connection, the motion data are transmitted to a computer with 200 Hz sampling rate for real-time process in attitude determination and position tracking.

## 10.1. Attitude Extended Kalman Filter

This thesis presents a complete design of an extended Kalman filter for real-time attitude estimation of a moving rigid body. We also discussed about a general approach to improve the extended Kalman filter to remove the input state's bias. The attitude representation is completely in quaternion, instead of Euler angles. The Euler angles have triangle functions which will cost more computation resources and cripple the filter due to the singularity problem. The measurement update is also applicable to other reference field sensors, such as accelerometer tilters. Further, no quaternion normalization is needed during filter iterations.

## 10.2. Complementary Attitude EKF

Base on this filter model, a Complementary Attitude EKF is designed to combine accelerometers and magnetometers in the measurement update, sensing gravity field and Earth magnetic field as reference, respectively. The measurement model is improved to synchronize the filter observation input when switching between the two sensors. During writing, the magnetometers contribute in attitude correction because the inertial acceleration measured by accelerometers will interfere for gravity attitude. When writing is paused, the filter utilizes the accelerometer in feedback to update the magnetic field distortion within the stroke. The attitude will be updated when the pen is static and the output from the accelerometers can be trusted as a gravity vector. Also, this long term correction will help eliminating magnetic field interference. The sensor sets corresponding to orthogonal attitude reference field can compensate the attitude ambiguity along the field axis for each other.



### **10.3.Unscented Kalman Filter**

The unscented Kalman filter as an advanced nonlinear estimator combines the Kalman filter and particle filter. A quaternion-based attitude unscented Kalman filter is developed based on magnetometers update. With similar computational resource cost, the performance of the unscented Kalman filter is superior compared to the extended Kalman filter in tracking accuracy and estimation response.

Extensive experiments were conducted to verify the convergence performance of the extended Kalman filter. The filter achieved good results for all tests using ideal simulation data and actual sensor data. The filter can track the pen attitude with the MAG- $\mu$ IMU installed. The filter system is stable without the singularity or normalization problem even after consecutive, rapid 90 degree rotations. The writing experiment for whole system verifies the tracking or pen-tip movement is enhanced by the Complementary Attitude Kalman Filter. Based on the inertial position tracking technology, the handwriting trajectory in space is calculated stroke by stroke in order to correct accelerometer drift.

### **10.4.Future Work**

In handwriting experiment, Zero Velocity Compensation [51] is introduced to correct drift error in MEMS accelerometers. This offline algorithm assumes the accelerometer error model is linear in velocity, and the accelerations can be updated backwards by clamping from the velocity drift at the end of each stroke. Hence, more experimental effort is required to set up precise motion stage and build motion database for MEMS accelerometer to analyze the error model. Thus the acceleration drift error in measurement can be compensated in real-time.

As demonstrated in Chapter 9, the unscented Kalman filter is an advanced estimator for nonlinear system. The quick tracking response ensures the stable performance, especially for the switching in the measurement update. Therefore, the unscented Kalman filter will be implemented in the complementary framework for real-time attitude tracking.



# Bibliography

- [1] Guanglie Zhang, G. Y. Shi, Y. L. Luo, H. Wong, Wen J. Li, Philip H. W. Leong, and Ming Yiu Wong, "Towards an Ubiquitous Wireless Digital Writing Instrument Using MEMS Motion Sensing Technology," *Proceedings AIM '2005*, IEEE/ASME, 2005, pp. 795-800.
- [2] Wikipedia Foundation Inc. Global Positioning System, 2006.  
[http://en.wikipedia.org/wiki/Global\\_Positioning\\_System](http://en.wikipedia.org/wiki/Global_Positioning_System).
- [3] Demoz Gebre-Egziabher, J, David Powell, Per Enge, "A DME Based Area Navigation Systems for GPS/WAAS Interference Mitigation In General Aviation Applications", *Position Location and Navigation Symposium*, IEEE, 2000, pp. 74-81, March, 2000.
- [4] Luís Sardinha Monteiro, Terry Moore, Chris Hill, "What is the accuracy of DGPS?", *The Journal of Navigation*, vol. 58, pp. 207-225, 2005.
- [5] Virtual Ink Corporation. mimio Studio User's Guidance, 2005.  
[http://www.mimio.com/products/documentation/mimiostudio\\_usersguide.pdf](http://www.mimio.com/products/documentation/mimiostudio_usersguide.pdf).
- [6] Lucia, Inc. eBeam Interactive Whiteboard Technology, 2006.  
<http://www.e-beam.com/downloads/files/WhatIsBeam.pdf>.
- [7] Sagem Avionics, Inc. APIRS F200-AHRS Brochure, 2006.  
<http://www.sagemavionics.com/Products/Brochures/APIRS-F200.pdf>.
- [8] Watson Industries, Inc. AHRS-E304 Manual, 2006.  
[http://www.watson-gyro.com/files/attitude\\_reference\\_AHRS-E304\\_spec.pdf](http://www.watson-gyro.com/files/attitude_reference_AHRS-E304_spec.pdf).
- [9] Roger C. Hayward, Demoz Gebre-Egziabher, Matthew Schwall, J. David Powell and John Wilson. "Inertially Aided GPS Based Attitude Heading Reference System (AHRS) for General Aviation," *Proceedings of ION GPS '97*, Kansas City, MO, September, 1997.
- [10] Alison K. Brown, "Test Results of a GPS/Inertial Navigation System Using a Low Cost MEMS IMU", 11<sup>th</sup> Annual Saint Petersburg International Conference on Integrated Navigation System, Saint Petersburg, Russia, May, 2004.
- [11] Eun-Seok Choi, W. Chang, W. C. Bang, J. Yang, S. J. Cho, J. K. Oh. J. K. Cho, and D.Y. Kim, "Development of the Gyro-free Handwriting Input Device based on Inertial Navigation System (INS) Theory," *Proceedings of SICE Annual Conference '2004*, SICE, 2004, pp. 1176-1181, vol. 2.
- [12] Yilun Luo, Chi Chiu Tsang, Guanglie Zhang, Zhuxin Dong, Wen J. Li, Philip H. W. Leong, "An Attitude Compensation Technique for a MEMS Motion Sensor Based Digital Writing Instrument", *Proceedings of IEEE NEMS*



'2006, Zhuhai, China, January 18-21, 2006.

- [13] Analog Devices, Inc. Low-Cost Ultracompact  $\pm 2g$  Dual-Axis Accelerometer ADXL311 Data Sheet (Rev. B, 01/2005), 2005.  
[http://www.analog.com/UploadedFiles/Data\\_Sheets/243920868ADXL311\\_B.pdf](http://www.analog.com/UploadedFiles/Data_Sheets/243920868ADXL311_B.pdf).
- [14] Murata Manufacturing Co., Ltd. GYROSTAR Piezoelectric Vibrating Gyroscopes Data Sheet (No. S42E, 06/2006), 2006.  
<http://www.murata.com/catalog/s42e.pdf>.
- [15] Koninklijke Philips Electronics N. V. Magnetic Field Sensor KMZ51 Data Sheet (06/2000), 2006.  
[http://www.nxp.com/acrobat\\_download/datasheets/KMZ51\\_3.pdf](http://www.nxp.com/acrobat_download/datasheets/KMZ51_3.pdf).
- [16] Koninklijke Philips Electronics N. V. Magnetic Field Sensor KMZ52 Data Sheet (06/2000), 2006.  
[http://www.nxp.com/acrobat\\_download/datasheets/KMZ52\\_1.pdf](http://www.nxp.com/acrobat_download/datasheets/KMZ52_1.pdf).
- [17] Honeywell International, Set/Reset Function for Magnetic Sensors (08/02), 2003.  
<http://www.ssec.honeywell.com/magnetic/datasheets/an213.pdf>.
- [18] Atmel Corporation. 8-bit AVR Microcontroller with 32 Bytes In-System Programmable Flash ATmega32(L) Data Sheet (Rev. I, 04/06), 2006.  
[http://www.atmel.com/dyn/resources/prod\\_documents/doc2503.pdf](http://www.atmel.com/dyn/resources/prod_documents/doc2503.pdf).
- [19] Richard H. Barnett, Sarah Cox, Larry O'Cull, *Embedded C Programming and the Atmel AVR*, Delmar, Clifton Park, NY, USA, 2003
- [20] BlueRadios, Inc. Class 1, Class 2 and 3 BR-C30 ver 1.2 Module Specification, 2006.  
<http://www.blueradios.com/BR-C30.pdf>.
- [21] IVT Corporation, BlueSoleil 2.3 Commercial Version Release Note (Ver. 2.3, 07/06), 2006.  
[http://www.bluesoleil.com/Download/files/IVT\\_BlueSoleil\\_%28Standard%29\\_Release\\_Note.pdf](http://www.bluesoleil.com/Download/files/IVT_BlueSoleil_%28Standard%29_Release_Note.pdf).
- [22] Future Technology Devices International Ltd. FT232BM USB UART (USB-Serial) I.C. Data Sheet (Ver. 1.8, 2005), 2006.  
<http://www.ftdichip.com/Documents/DataSheets/ds232b18.pdf>.
- [23] D. H. Titterton, J. L. Weston, *Strapdown Inertial Navigation Technology, 2<sup>nd</sup> Edition*, AIAA, Reston, USA, 2004.
- [24] Robot Dynamics and Control. Lecture Notes, 2005.  
<http://www2.acae.cuhk.edu.hk/~ace3130>.
- [25] John J. Craig, *Introduction to Robotics: mechanics and control, second edition*, Addison-Wesley, Reading, MA, 1989.



- [26] Jack B. Kuipers, *Quaternions and Rotation Sequences: A Primer with Applications to Orbits, Aerospace, and Virtual Reality*, Princeton University Press, Princeton, N. J. , 1999
- [27] H. W. Sorenson, "Least-squares Estimation: from Guass to Kalman," *IEEE Spectrum*, vol. 7, pp. 63-68, July 1970.
- [28] Sergios Theodoridis, Konstantinos Koutroumbas, *Pattern Recognition, 2<sup>nd</sup> edition*, Academic Press, 2003.
- [29] Pattern Recognition Part II. Lecture Notes, 2006.  
<http://www.ee.cuhk.edu.hk/~tanlee/teaching/ele5410>.
- [30] James R. Wertz, *Spacecraft Attitude Determination and Control*, Kluwer Academic Publishers, Dordrecht, The Netherlands, 1991.
- [31] H. W. Sorenson, "Least-squares estimation: from Gauss to Kalman", *Kalman Filtering: Theory and Application*, IEEE Press, 1985.
- [32] Eric Robert Bachmann, Inertial and Magnetic Angle Tracking of Limb Segment Orientation for Inserting Humans into Synthetic Enviroments. Ph.D.'s Thesis, Naval Graduate School, 2000.
- [33] Markley, F. L., "Attitude Determination Using Vector Observations: Theory," *Journal of the Astronautical Sciences*, vol. 37, no. 1, January-March 1989, pp. 41-58.
- [34] Greg Welch, Gary Bishop, "An Introduction to the Kalman Filer," UNC-Chapel Hill, TR 95-041, 2004.
- [35] The Kalman Filter: Some Tutorials, References and Research on the Kalman Filter, 2006.  
<http://www.cs.unc.edu/~welch/kalman>.
- [36] R. E. Kalman, "A New Approach to Linear Filtering and Prediction Problems," *Transactions of the ASME—Journal of Basic Engineering*, vol. 82, no. Series D, pp. 35-45, 1960.
- [37] João Luís Marins, Xiaoping Yun, Eric R. Bachmann, Robert B. McGhee, and Michael J. Zyda, "An Extended Kalman Filter for Quaternion-Based Orientation Estimation Using MARG Sensors," *Proceedings of the 2001 IEEE/RJS International Conference on Intelligent Robots and Systems*, Hawaii, 2001.
- [38] A. H. Jazwinski, *Stochastic Processes and Filtering Theory*. San Diego, CA: Academic, 1970.
- [39] B. Friedland, "Treatment of Bias in Recursive Filtering," *IEEE Transactions on Automatic Control*, vol. AC-14, pp.359-367, 1969.
- [40] Foxlin, E., "Inertial Head-Tracker Sensor Fusion by a Complementary



- Separate-Bias Kalman Filter,” *Proceeding of VRAIS '96*, IEEE, 1996, pp. 185-194.
- [41] M. D. Shuster, S. D. Oh., “Three Axis Attitude Determination From Vector Observations,” *Journal of Guidance, Control and Navigation*, vol. 4, no. 1, pp. 70-77, January-February, 1981.
- [42] Markley, F. L., “Attitude Determination Using Vector Observations: a Fast Optimal Matrix Algorithm,” *Journal of the Astronautical Sciences*, vol. 41, no. 2, Apr-Jun. 1993, pp. 261-280.
- [43] Simon Julier, Jeffrey Uhlmann, Hugh F. Durrant-Whyte, “A New Method for the Nonlinear Transformation of Means and Covariances in Filters and Estimators,” *IEEE Transactions on Automatic Control*, vol. 45, no. 3, March 2000.
- [44] Simon Julier, Jeffrey K. Uhlmann, “A General Method for Approximating Nonlinear Transformations of Probability Distributions,” Technical report, Robotics Research Group, Department of Engineering Science, University of Oxford, 1996.
- [45] Eric A. Wan, Rudolph van der Merwe, Alex T. Nelson, “Dual Estimation and the Unscented Transformation,” *Advances in Neural Information Processing System 12*, pp. 666-672, MIT Press, 2000.
- [46] Eric A. Wan, Rudolph van der Merwe, “The Unscented Kalman Filter for Nonlinear Estimation,” *Proceedings of the IEEE Symposium 2000: Adaptive Systems for Signal Processing, Communications, and Control*, Lake Louise, Alberta, Canada, October 1-4, 2000.
- [47] John L. Crassidis, F. Landis Markley, “Unscented Filtering for Spacecraft Attitude Estimation,” *AIAA Journal of Guidance, Control, and Dynamics*, vol. 26, no. 4, July-August 2003, pp. 536-542.
- [48] Edgar Kraft, “A Quaternion-based Unscented Kalman Filter for Orientation Tracking,” *Proceedings of the Sixth International Conference on Information Fusion*, Cairns, Australia, July 2003.
- [49] Lefferts, E. J., Markley, F. L., Shuster, M. D., “Kalman Filtering for Spacecraft Attitude Estimation,” *Journal of Guidance, Control, and Dynamics*, vol. 5, no. 5, Sept.-Oct. 1982, pp.417-429.
- [50] Sanjeev Arulampalam, Simon Maskell, Neil Gordon, Tim Clapp, “A Tutorial on Particle Filters for On-line Non-linear/Non-Gaussian Bayesian Tracking,” *IEEE Transactions on Signal Processing*, vol. 50, no. 2, pp. 174-188, Feb. 2002.
- [51] Won-Chul Bang, Wook Chang, Kyeong-Ho Kang, Eun-Seok Choi, Alexey Potanin, Dong-Yoon Kim, “Self-contained Spatial Input Device for Wearable Computers,” *Proceedings of the Seventh IEEE International Symposium 2003*

## Schematics

- 1. Digital Writing Instrument (main board section)
- 2. Digital Writing Instrument (sensor board section 1)
- 3. Digital Writing Instrument (sensor board section 2)



# Appendix A

## Schematics

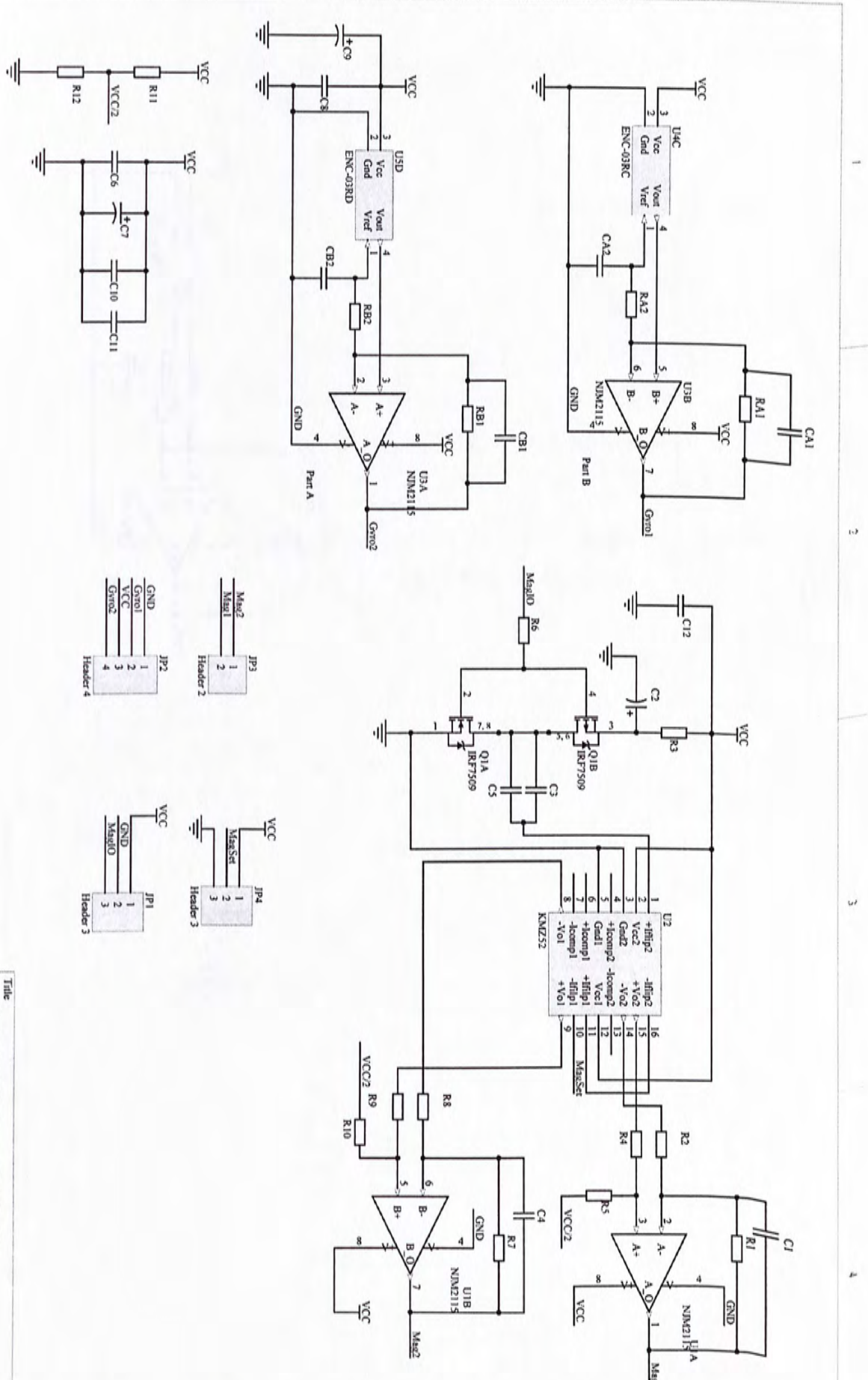
1. Digital Writing Instrument (main board section)
2. Digital Writing Instrument (sensor board section 1)
3. Digital Writing Instrument (sensor board section 2)



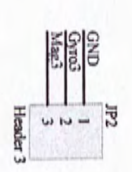
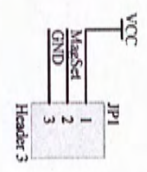
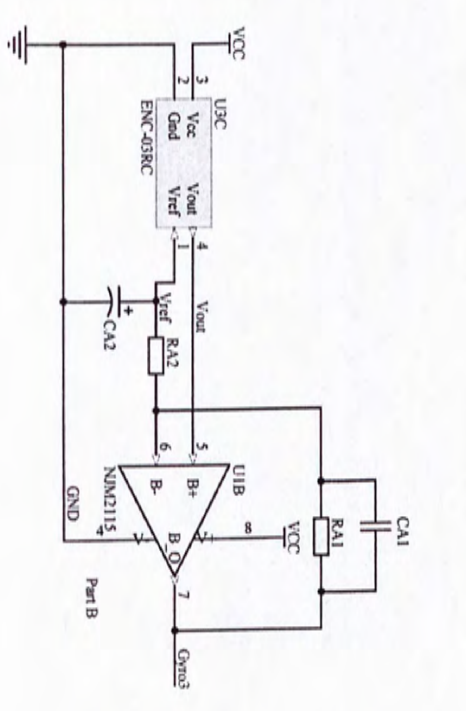
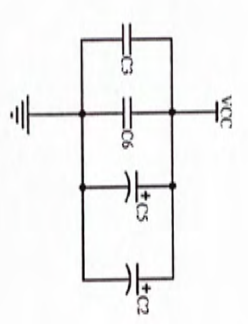
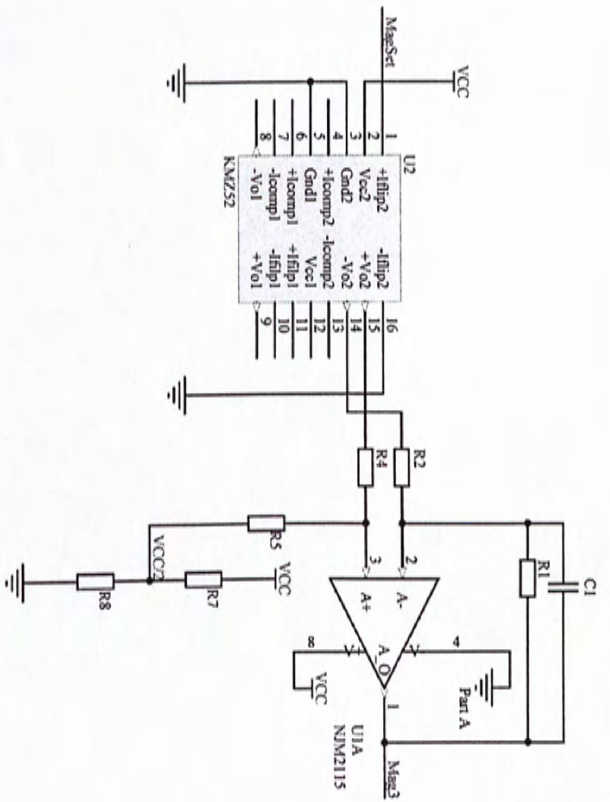


A B C D

1 2 3 4



Title		Revision	
Wireless Digital Writing Instrument Sensor Board (1)		Size	Number
		A4	1
Date:		9/15/2006	Sheet of
File:		D:\Program Files\3gsm\2img\1_print\Salibawa By...	1



Title: Wireless Digital Writing Instrument Sensor Board (2)

Size	Number	Revision
A	1	1.2

Date: 9/15/2006 Sheet of 2  
 File: D:\Program Files\img\Igorol\_1.prim.SCH.DOC





CUHK Libraries



004359199